The *Schizosaccharomyces pombe* bifunctional enzyme Asp1 regulates cellular levels of 1,5-bisdiphosphoinositol tetrakisphosphate

Inaugural dissertation

for the attainment of the title of doctor
in the Faculty of Mathematics and Natural Sciences
at the Heinrich Heine University Düsseldorf

presented by

Marina Pascual-Ortiz

from Alzira

Düsseldorf, October 2017

from the Institute for Functional Genome Research of Microorganisms, Eukaryotic Microbiology at the Heinrich Heine University Düsseldorf

Published by permission of the
Faculty of Mathematics and Natural Sciences at
Heinrich Heine University Düsseldorf

Supervisor: Prof. Dr. Ursula Fleig

Co-supervisor: Prof. Dr. Michael Feldbrügge

Date of the oral examination:

A mi yayo,
por mis ojos, por los tuyos

Table of contents

Summary

Inositol pyrophosphates are signalling molecules present in all eukaryotic cells. They are phosphate-rich molecules consisting of an inositol ring with at least one di-phosphate group (pyrophosphate). Although these molecules were discovered only 25 years ago, an extremely wide range of biological processes have already been defined to be controlled by inositol pyrophosphates. These include the phosphate starvation response in *Saccharomyces cerevisiae*, chromosome transmission fidelity in *Schizosaccharomyces pombe*, cell morphogenesis in a number of fungi, insulin secretion in mammals, and immune defense mechanisms in mammals and plants. Understanding how these molecules are synthesized, hydrolysed and their cellular concentration regulated is essential to understand how they modulate biological processes. In this context, the functional analysis of the *S. pombe* Asp1 protein is of a great interest as this protein controls intracellular pyrophosphate levels.

Asp1 belongs to the highly conserved Vip1 protein family. All members of this family present a dual domain structure: the N-terminal domain synthesizes inositol pyrophosphates and a C-terminal domain has homology to histidine acid phosphatases. Prior to this study, the function of the C-terminal domain of Vip1 proteins was unclear. Using different methods such as direct quantification of cellular inositol pyrophosphates with a HPLC-based approach and analysis of microtubule stability as an *in vivo* read-out of cellular inositol pyrophosphate production, I have demonstrated that the C-terminal domain of Asp1 is enzymatically active *in vivo* and identified the amino acids essential for this activity. I determined the *in vivo* substrate specificity of both domains of Asp1; the N-terminal domain synthesizes IP_8 (1,5-bisdiphosphoinositol tetrakisphosphate) using 5-IP_7 (5-diphosphoinositol pentakisphosphate) as a substrate and the C-terminal domain dephosphorylates IP_8 to 5-IP_7 (5-diphosphoinositol pentakisphosphate). Interestingly, the pyrophosphatase activity of Asp1 reduced 2-fold cellular IP_8 levels. Thus the C-terminal Asp1 pyrophosphatase domain controls intracellular IP_8 levels.

How the two opposing activities of Asp1 (synthesis and hydrolysis of IP_8) are regulated was another goal of my study. An interaction partner of Asp1, the mitochondrial-associated protein Met10, inhibited Asp1 pyrophosphatase activity *in vitro.* Interestingly, microscopical analysis showed that some Asp1 mutant variants can also associate with mitochondria, suggesting a spatial subcellular regulation of Asp1 bifunctional activity.

Previous studies showed that Asp1-generated IP_8 modulate polarized growth, a microtubule-regulated process in *S. pombe*. Microtubules regulate mitochondria distribution via the protein Mmb1. This work presents new data to understand how Asp1-generated IP_8 regulates the microtubule cytoskeleton possibly through association with the mitochondrial

network. *asp1*$^{+}$ and *mmb1*$^{+}$ genetically interact and strikingly Asp1-generated IP_8 are required for proper mitochondrial distribution.

Finally, I have uncovered a new function relationship between inositol pyrophosphates and phosphate homeostasis in *S. pombe*. Asp1-generated inositol pyrophosphates levels correlated directly with the accumulation of polyP (inorganic polyphosphate), suggesting a connection between Asp1 function and phosphate homeostasis.

1. Introduction

The combination of biological intrinsic and extrinsic signals is essential for cells to adapt to the changing environment. Different stimuli induce a cascade of intracellular pathways that allow cells to respond to different conditions. In particular, fungi can respond to external signals such as hormones, nutrients or different stresses by activating signal transduction pathways that sense and promote morphological adaptations.

Inositol pyrophosphates are signaling molecules required for the morphological response to different intracellular and extracellular cues in fungi (Lev et al., 2015; Pöhlmann and Fleig, 2010; Pöhlmann et al., 2014). In the fission yeast, *Schizosaccharomyces pombe,* attainment of a correct cell shape during normal physiological conditions as well as the cell shape change in response to some environmental challenges depends on the production of specific inositol pyrophosphates (Pohlmann and Fleig, 2010; Pöhlmann et al., 2014) . These molecules are important modulators of the microtubule cytoskeleton, which is crucial in the determination of fungal cell morphology (Fischer et al., 2008; Pöhlmann et al., 2014). Thus, in order to understand how the microtubule cytoskeleton is modulated by inositol pyrophosphates, it is essential to also understand how these molecules are synthesized and hydrolyzed.

1.1. Inositol pyrophosphates: description, significance and metabolism

1.1.1. What are inositol pyrophosphates?

Originally discovered in the amoeba *Dictyostelium discoideum* (Europe-Finner et al., 1991), inositol pyrophosphates are present in all eukaryotic organisms tested, the main characteristic of these signaling molecules is their high concentration of phosphate groups. The structure of **i**nositol **p**yrophos**p**hates (IPPs) consists of a six-carbon ring inositol in which the hydroxyl groups are substituted by monophosphates and at least one di-phosphate group (pyrophosphate), resulting in a molecule with more phosphates than carbons (Fig1). The most used abbreviation of inositol pyrophosphates species, and also the one used in this study, is **IPx**, where “I” stands for inositol, “P” stands for phosphate and “x” represents the number of phosphates attached to the inositol ring.

The best studied inositol pyrophosphates are the two diphosphoinositol pentakisphosphate isoforms, 1-IP_7 and 5-IP_7 (pyrophosphate bond at position 1 or 5 of the inositol ring, respectively) and bis-diphosphoinositol tetrakisphosphate 1,5-$InsP_8$ (two pyrophosphate bonds, one at position 1 and the other at position 5 of the inositol ring) (Fig1). However, further phosphorylation of inositol pyrophosphates is possible and results in the

generation of molecules with more than two pyrophosphates or even with a tri-phosphate group (Draskovic et al., 2008; Losito et al., 2009). Inositol pyrophosphates are commonly described as high energy molecules due to the presence of pyrophosphate bonds. The energy released from the hydrolysis of the pyrophosphate bond present in 1,5-IP_8 (bis-diphosphoinositol tetrakisphosphate) (Fig1) has been estimated to be higher than that of ATP (Laussmann et al., 1996).

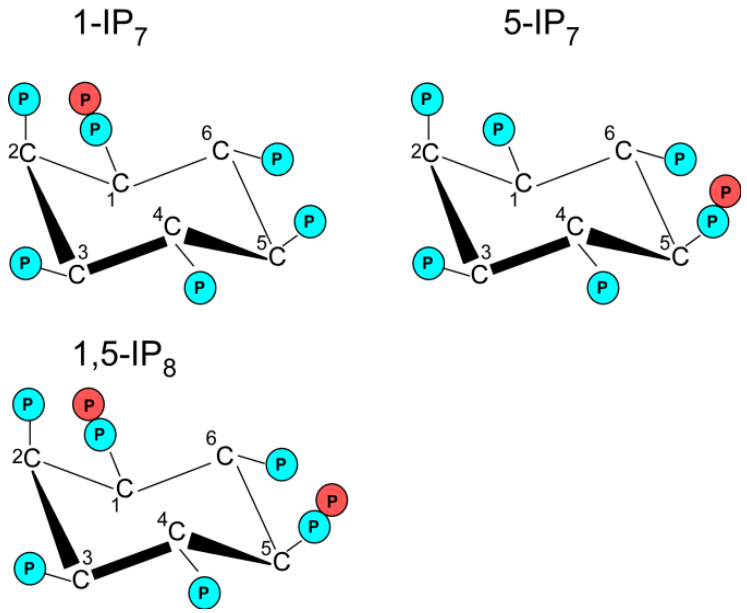

Fig1. Structure of inositol pyrophosphates. The fully phosphorylated inositol ring can be pyrophosphorylated at positions 1 and 5 (counterclockwise numbering system). As a result, the inositol pyrophophosphates 1-IP_7, 5-IP_7 and 1,5-IP_8 are generated. Monophosphate groups are shown in blue and diphosphate groups (pyrophosphates) in red.

1.1.2. Synthesis and catabolism of cellular inositol pyrophosphates

Molecules resulting from the phosphorylation of the inositol ring are named inositol **poly**phosphates. This group includes IP_2, IP_3, IP_4, IP_5 and IP_6 but also inositol **pyro**phosphates IP_7 and IP_8. In this work, IP_7 and IP_8 are called inositol pyrophosphates to differentiate these molecules from the other inositol polyphosphates. However when IP_6, IP_7 and IP_8 are presented together, the term will be inositol polyphosphates.

The precursor of inositol polyphosphate metabolism is phosphatidylinositol 4,5-biphosphate, $PI(4,5)P_2$, which is located at the plasma membrane. Upon extracellular stimuli, the phospholipase C hydrolyzes $PI(4,5)P_2$ to IP_3 and diacylglycerol (DAG)(Berridge, 1993). In *S. cerevisiae*, once released from the membrane, IP_3 is further phosphorylated by the inositol polyphosphate multikinase Arg82 at positons 6 and 3 to generate IP_4 and IP_5, respectively (Odom et al., 2000; Saiardi et al., 2001). Phosphorylation of IP_5 by Ipk1 at position 2 generates inositol hexakisphosphate IP_6 (also known as phytic acid) (York et al., 1999).

Most important for the purpose of my study is the synthesis of inositol pyrophosphates. These molecules are synthesized from inositol hexakisphosphate (IP_6) by two classes of enzyme families with positional specificity: the IP_6 kinases (IP6Ks), named Kcs1 in *S. cerevisiae* and in *S. pombe,* and the diphosphoinositol pentakisphosphate kinases (PPIP5Ks), named Vip1 in *S. cerevisiae* and Asp1 in *S. pombe*. Synthesis of 5-IP_7 is carried out by the 5-kinase activity of IP6Ks/Kcs1 (Draskovic et al., 2008; Saiardi et al., 1999) while the 1-kinase activity of PPIP5Ks/Vip1 can convert IP_6 to 1-IP_7 and is predicted to convert 5-IP_7 to 1,5-IP_8 as proposed from *in vitro* evidence (Fridy et al., 2007; Lin et al., 2009; Mulugu et al., 2007; Wang et al., 2011) (Fig2). Whether the kinase activity PPIP5Ks/Vip1 preferentially generates 1-IP_7 or 1,5-IP_8 under physiological *in vivo* conditions was unclear prior to my study. In *S. cerevisiae*, Vip1 was proposed to be an IP_6 kinase, however its activity was assayed in a strain where the *KCS1* gene was deleted and thus 5-IP_7 was not available as a substrate (Mulugu et al., 2007). A later study, in which inositol polyphosphates were analyzed in a *S. cerevisiae VIP1* deletion strain, suggested that Vip1 kinase activity generated IP_8 (Onnebo and Saiardi, 2009). During the progress of my study, other publications have demonstrated that the PPIP5Ks/Vip1 family members in *Cryptococcus neoformans*, *Arabidopsis thaliana* and humans cells are responsible for the cellular synthesis of IP_8. (Gu et al., 2016; Laha et al., 2015; Lev et al., 2015).

Although, the specific kinases that synthesize inositol pyrophosphates are intensely studied and have helped to a better understanding of how these molecules are synthesized, the role of (pyro)phosphatases which regulate the catabolism of inositol pyrophosphates is understood poorly. Previous to my study, only one group of proteins were known to dephosphorylate inositol pyrophosphates, the DIPPs/Ddp1 from the Nudix hydrolase family (Safrany et al., 1998). Members of this family show phosphohydrolase activity and cleave diphosphate groups. However, these proteins lack specificity towards inositol pyrophosphates and they prefer to dephosphorylate inorganic polyphosphate (polyP) (Lonetti et al., 2011) and diadenosine polyphosphates (Fisher et al., 2002). Only one specific enzyme with pyrophosphatase activity towards 5-IP_7 has been recently described: Siw14 is a specific inositol pyrophosphate phosphatase which has been identified in *S. cerevisiae*. Siw14 specifically dephosphorylates 5-IP_7 to IP_6 *in vitro* and *in vivo* (Steidle et al., 2016).

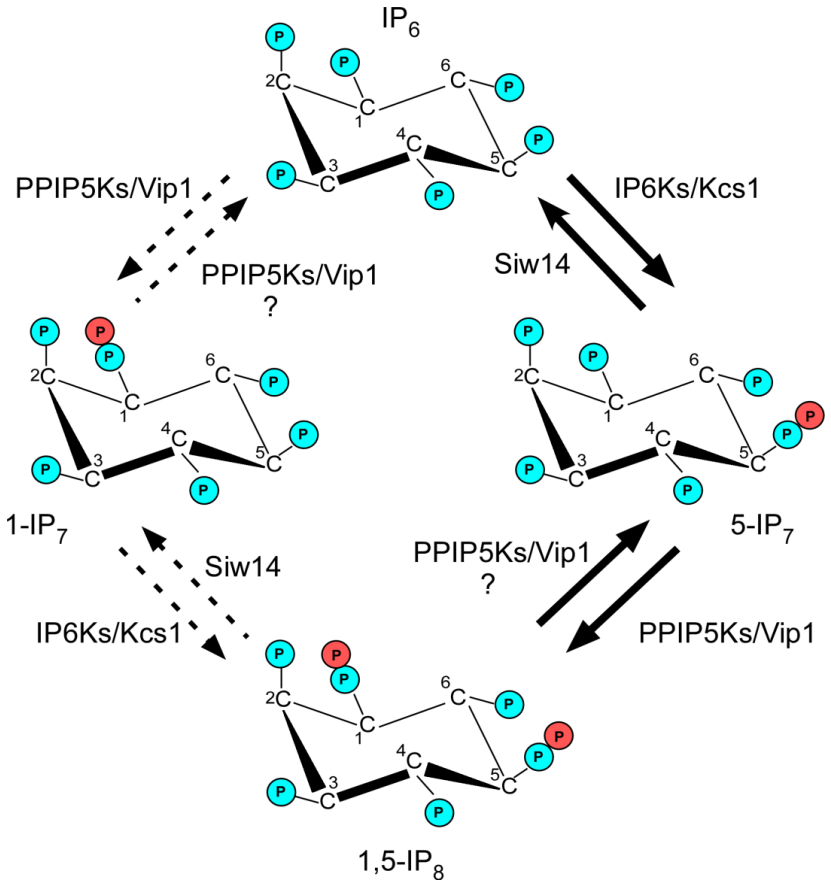

Fig2. Inositol pyrophosphates synthetic pathway. Proposed pathway for the generation of 1,5-IP_8**:** the 5-kinase activity of IP6Ks/Kcs1 generates 5-IP_7 from IP_6 which is then probably used by the 1-kinase activity of PPIP5Ks/Vip1 to generate 1,5-IP_8. The alternative pathway (broken arrows) appears to be unlikely due to the higher affinity that PPIP5Ks/Vip1 show towards 5-IP_7 than to IP_6 *in vitro (Choi et al., 2007)*. Catabolism of 5-IP_7 is carried out by the specific activity Siw14. The purpose of my study was to determine the specific substrate of the Vip1 member, Asp1 kinase activity (IP_6 or 5-IP_7) *in vivo* and furthermore, investigate if Asp1 could also participate in the catabolism of inositol pyrophosphates (question marks).

The intracellular relative abundance of inositol pyrophosphates can be modified under specific conditions. It was shown for *Arabidopsis thaliana* that the jasmonate-mediated wound response causes an specific increase of IP_8 (Laha et al., 2015). In the amoeba *Dictyostelium discoideum* inositol pyrophosphates are increased during chemotactic response (Luo et al., 2003) and in mammalian cells IP_8 levels can be elevated upon hyperosmotic stress (Choi et al., 2007; Pesesse et al., 2004). Thus, mechanisms which regulate the activity either of the kinases responsible for the production of IPPs and/or the possible pyrophosphatases involved in their catabolism must exist.

Inositol pyrophosphates, IP_7 (both 1-IP_7 and 5-IP_7) and IP_8 (1,5-IP_8) are only present between 2-5% of their precursor IP_6 in mammalian and yeast cells under physiological conditions (Bennett et al., 2006). Despite this low cellular abundance of inositol pyrophosphates in comparison to IP_6, a large number of cellular processes are regulated by these high energy molecules. Interestingly, the conversion of IP_5 to IP_6 is extremely slow in

comparison to the conversion of IP_6 to inositol pyrophosphates. It has been estimated that 50% of the IP_6 pool is converted every hour to inositol pyrophosphates (Menniti et al., 1993). Thus, in order to understand their importance as signaling molecules it is fundamental to study how their rapid turnover is modulated and which enzymes are involved in the hydrolysis of inositol pyrophosphates.

1.1.2. Biological roles of inositol pyrophosphates

Many examples of processes regulated by inositol pyrophosphates have been described in fungi, mammals, and plants. 1-IP_7 mediates the phosphorylation of the interferon regulatory factor IRF3 and stimulates innate immune response in mammalian cells (Pulloor et al., 2014). Insulin secretion is impaired in mice lacking the IP_6 kinase 1 (Bhandari et al., 2008; Chakraborty et al., 2010). In yeast, inositol pyrophosphates produced by Kcs1 are involved in telomere length maintenance and DNA recombination (Luo et al., 2002; Saiardi et al., 2005; York et al., 2005). Inositol pyrophosphates are also involved in the response to external environmental signals. In *Arabidopsis,* it has been described that the jasmonate-regulated defense against wound induces an increase of IP_8 levels(Laha et al., 2015). Upon phosphate limitation Vip1-generated inositol pyrophosphates mediate the *S. cerevisiae* phosphate starvation response (Lee et al., 2007) and in *Dictyostelium discoideum* these molecules are greatly increased during the chemotaxis response (Luo et al., 2003).

Our lab has shown that inositol pyrophosphates are key elements in the regulation of the microtubule cytoskeleton and cell morphogenesis in fungi (Pöhlmann and Fleig, 2010; Pohlmann et al., 2014; Topolski et al., 2016). The Vip1 homolog in *S. pombe* is named Asp1. Mutation of the key catalytic residue of Asp1 kinase domain (D333), and thus presumably no generation of inositol pyrophosphates 1-IP_7 or 1,5-IP_8 *in vivo* led to an aberrant microtubule cytoskeleton.

During mitosis, duplicated sister chromosomes must be correctly distributed between the two daughter cells. The correct segregation of chromosomes is vital to avoid severe phenotypes such as aneuploidy. Lack of Asp1-generated inositol pyrophosphates increased chromosome segregation mistakes and affected the function of the spindle (microtubule structure) (Topolski et al., 2016). In interphase cells, the microtubule cytoskeleton is essential to determine cell shape during physiological conditions as well as to modulate the dimorphic switch upon adverse environmental conditions. In fact, *S.pombe* cells require the Asp1 kinase function to correctly establish and maintain their shape and to change their morphology in response to external cues (Pöhlmann and Fleig, 2010; Pöhlmann et al., 2014).

Accordingly, our laboratory also showed that the resistance to the microtubule poison thiabendazole (TBZ) is an effective tool to predict intracellular levels of Asp1-generated

inositol pyrophosphates. Asp1 proteins which show a higher-than-wild type inositol pyrophosphates production *in vitro* induce higher TBZ resistance i.e, more stable microtubules *in vivo*. On the other hand, Asp1 proteins with no kinase activity *in vitro* cause higher TBZ sensitivity, i.e, less stable microtubules, when were expressed in cells (Pöhlmann et al., 2014). Thus, the cellular production of inositol pyrophosphates by Asp1 correlates with a reliable phenotype based on the microtubule fitness i.e. the resistance to TBZ.

1.1.3. Modes of action of inositol pyrophosphates

In general, inositol pyrophosphates have the ability to modulate their targets via two different mechanisms: direct binding to the target or pyrophosphorylation (Wu et al., 2016). However, although inositol pyrophosphates are crucial for many biological processes, their specific targets have not been identified due to technical difficulties *in vivo*. To date, strong yet only indirect evidences exist.

One well characterized example exits, that demonstrates the ability of inositol pyrophosphates to regulate a target protein by direct binding, is the Pho80/Pho85/Pho81 complex in *S. cerevisiae.* During phosphate starvation, *S. cerevisiae* activates a signaling response named the PHO pathway. The *PHO* genes are regulated by the transcription factor Pho4. Upon phosphorylation of Pho4 by the Cdk complex Pho80-Pho85 under phosphate-rich conditions, Pho4 localized to the cytoplasm. When phosphate is limiting, the Cdk inhibitor Pho81 inhibits the kinase activity of Pho80-Pho85, thus Pho4 is not phosphorylated, enters the nucleus and induces transcription of the *PHO* genes (O'Neill et al., 1996). It was found that IP_7 was required for the inactivation of Pho80-Pho85 kinase activity. This inositol pyrophosphate molecule is able to bind and induce additional interactions between Pho80/Pho85/Pho81 complex *in vitro* which obstructs the entry of substrates (Lee et al., 2008; Lee et al., 2007).

Regarding the regulation of target molecules via pyrophosphorylation, inositol pyrophosphates can transfer the β-phosphate to a pre-phosphorylated serine flanked by acidic residues in the target protein (Bhandari et al., 2007; Saiardi et al., 2004). Pyrophosphorylation of the interferon regulatory factor IRF3 by inositol pyrophosphates has been demonstrated *in vitro* using cell-free phosphorylation assays. IRF3 phyrophosphorylation was reduced in extracts from PPIP5K silenced cells and interestingly, it was rescued after addition of 1-IP_7 or 1,5-IP_8 but not when 1-IP_7 or 1,5-IP_8 analogs, unable to transfer their β-phosphates, were added (Pulloor et al., 2014). Other studies have also proposed that inositol pyrophosphates enzymatically modulate their targets: the pyrophosphorylation of the protein subunit AP3B1 involved in HIV-1 released by 5-IP_7 (Azevedo et al., 2009), pyrophosphorylation of RNA polymerase I subunits in *S. cerevisiae* by 5-IP_7 (Thota et al., 2015) and pyrophosphorylation of dynein by IP_7 which promotes the

interaction with dynactin (Chanduri et al., 2016). However, the relevance of pyrophosphorylation by IPPs *in vivo* remains unclear.

1.1.4. Interplay between inositol pyrophosphates and phosphate metabolism

Intracellular levels of inositol pyrophosphates can be modulated in response to external signals as described in chapter 1.1.3. Among all these different signals, inorganic phosphate is of a major importance. Inositol pyrophosphates act as sensing molecules which react to variations of extracellular phosphate (Gu et al., 2017; Lee et al., 2007; Lonetti et al., 2011). In *S. cerevisiae,* the PHO pathway is responsible of sensing and responding to fluctuations of external phosphate and interestingly, the activity of an essential component of this pathway is modulated by Vip1-generated inositol pyrophosphates (Lee et al., 2008). But, in addition to sense extracellular phosphate, inositol pyrophosphate regulate other aspects of phosphate homeostasis

Cellular phosphate is stored in the form of inorganic polyphosphate (also called polyP). This molecule is a linear polymer of phosphates (Fig3) which contains more than four phosphate residues linked by phosphoanhydride covalent bonds (Kornberg et al., 1999). PolyP is found in all organisms and its main function is to buffer cellular phosphate (Azevedo and Saiardi, 2017). In *S. cerevisiae*, polyP is synthesized and transported into the vacuoles by the vacuolar transporter chaperone complex VTC (Hothorn et al., 2009). Degradation of polyP to produce free phosphate is carried out by the exo- and endo-polyphosphatases, Ppx1 and Ppn1, respectively (Sethuraman et al., 2001; Wurst et al., 1995).

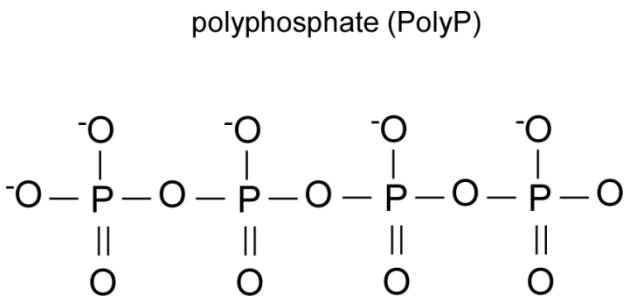

Fig3. Inorganic polyphosphate. Schematic representation of inorganic polyphosphate chain (polyP).

PolyP metabolism and inositol pyrophosphates seem to be interconnected. Studies performed in *S. cerevisiae* have shown that cells lacking inositol pyrophosphates do not accumulate polyP (Auesukaree et al., 2005; Lonetti et al., 2011). Furthermore, inositol pyrophosphates are able to promote the synthesis of polyP in purified vacuoles possibly via direct binding and activation of the polymerase activity of the VTC complex (Gerasimaite et al., 2017). The later study proposed that the 5-IP_7 isomer was more efficient promoting polyP synthesis than other inositol pyrophosphates. In line with this, lack of 1-kinase activity in a *S.*

cerevisiae VIP1 deletion strain, and therefore no synthesis of 1-IP_7 and 1,5-IP_8, does not affect cellular polyP levels, while the KCS1 deletion strain (no 5-IP_7 synthesis) results in the loss of polyP accumulation (Lonetti et al., 2011).

Another phosphate-rich molecule, ATP, is also influenced by inositol pyrophosphates. Cells with lower than wild-type inositol pyrophosphates show an increase of ATP (Szijgyarto,2011)

Thus, there are multiple connections between phosphate availability, inositol pyrophosphate metabolism, ATP and accumulation of inorganic polyphosphate in which the abundance of the different components influence each other (Azevedo and Saiardi, 2017).

1.2. The PPIP5K/Vip1 family

This work focuses on the role of the *S. pombe* Asp1 protein. Asp1 belongs to the highly conserved family of proteins called Vip1. Members of this family can be found in all tested organisms from yeast to mammals (Mulugu et al., 2007). Representatives of this family in *S. cerevisiae* and *S. pombe* are Vip1 and Asp1, respectively, and show 55% sequence identity and 68% similarity (Feoktistova et al., 1999). Humans have two Vip1-like proteins: PPIP5K1 and PPIP5K2. The main characteristic of the Vip1 family is the dual-domain structure of the proteins that will be described in the following section.

1.2.1. Domain structure and function

All members of the Vip1 family have a dual-domain structure (Fig4). The **N-terminal** domain contains an ATP-grasp domain found in enzymes which catalyze ATP-dependent reactions (reviewed in (Fawaz et al., 2011)). In fact, the N-terminal domain of all tested Vip1 members holds a kinase activity responsible of the synthesis of inositol pyrophosphates in an ATP-dependent reaction (Fridy et al., 2007; Lin et al., 2009; Mulugu et al., 2007; Pöhlmann et al., 2014). A catalytic aspartic residue, D333 (Asp1 numbering) is present in all Vip1 family members and is required for the kinase activity of the N-terminal domain (Fridy et al., 2007; Mulugu et al., 2007). The **C-terminal** domain of Vip1-like proteins represents the biggest part of the protein. In Asp1 this domain contains 60% of the total number of amino acids and it contains the typical signature of histidine-acid-phosphatases. However, the function of this domain remained controversial at the time of the starting of my PhD thesis and thus deserves its own section (1.2.2).

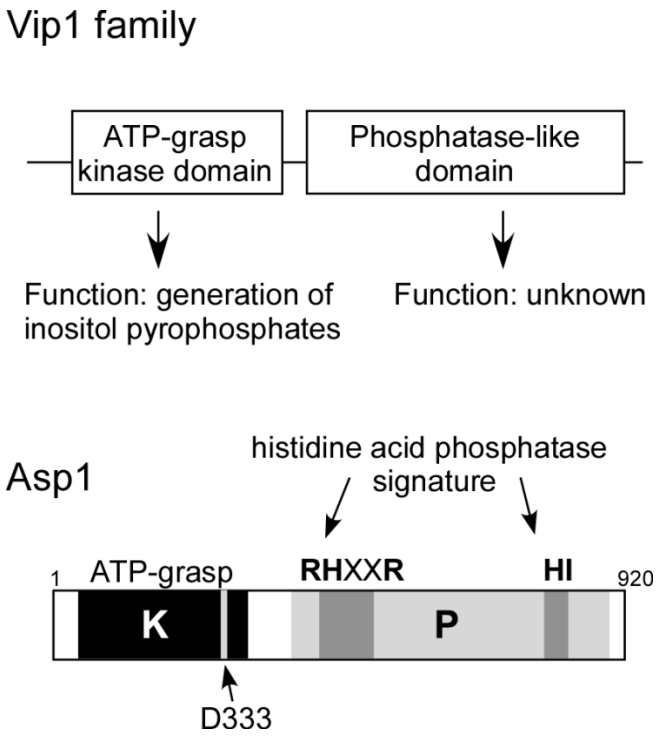

Fig4. Dual-domain structure of the Asp1 protein. Top: Diagrammatic representation of the general dual-domain structure of the Vip1-like proteins. Bottom: Diagrammatic representation of Asp1 domains. The N-terminal kinase domain (K, black box) showing the catalytic residue D333. The C-terminal phosphatase-like domain (P, light grey box) showing the conserved signature of histidine-acid-phosphatases (dark-grey boxes).The function of C-terminal domain was unknown at start of my thesis.

1.2.2. Function of the C-terminal domain of PPIP5K/Vip1 proteins?

The active site signature of histidine-acid-phosphatases consists of two histidine motifs, namely RHxxR and HD, review in (Rigden, 2008). Intriguingly, in Asp1 and all members of the Vip1 family the aspartate next to the second histidine (H**D**) is replaced either by isoleucine, valine or alanine, thus the motif in Asp1 is H**I** (Fig4 bottom)(Fridy et al., 2007). This important amino acid change led, for years, to the idea that the C-terminal domain of Vip1-like proteins was enzymatically inactive (Gokhale et al., 2011). There were two main reasons for this idea: the publication of a paper claiming that C-terminal domain of PPIP5K/Vip1 proteins was enzymatically inactive (Gokhale et al., 2011) and the reaction mechanism of histidine acid phosphatases which is described below.

For the catalytic mechanism of **histidine acid phosphatases** two histidine motifs are required, RHxxR and HD. The first histidine is surrounded by two arginines (RHxxR) which together form the phosphate pocket. During the phosphatase reaction this histidine residue is phosphorylated and the two arginines help to stabilize the phospho-group via electrostatic interactions (Rigden, 2008). The second histidine also contributes to the phosphate pocket

and is commonly accompanied by an aspartate residue (HD) which is required to donate a proton to the released phosphate group (Rigden, 2008). Although the two motifs are localized away from each other in the protein sequence, in the 3-dimensional structure the second motif must be in proximity to the first motif as shown in Fig5.

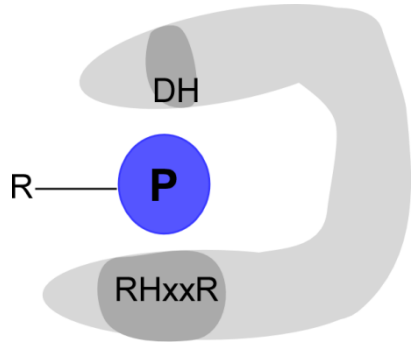

Fig5. Catalytic mechanism of histidine acid phosphatases. Representation of the phosphatase reaction performed by histidine acid phosphatases. Conserved signature motifs are shown in dark grey areas in which the residues are written. Note that the HD motif is turned 180º, therefore is represented as DH. The phosphate group is shown in blue and R represents the dephosphorylated leaving substrate.

Hence, the apparent lack of a residue capable of donating a proton in Vip1-like proteins led scientists to consider the C-terminal domain as catalytically inactive. Actually, a quite different role was assigned to the C-terminal domain of Vip1 proteins. The human PPIP5K was described wrongly to be enzymatically inactive and the authors proposed that the function of this domain was to spatially separate the synthesis of inositol pyrophosphates in the cell (Gokhale et al., 2011; Yong et al., 2015). The localization role of the human PPIP5Ks C-terminal domains was shown in two different studies: PPIP5K1 was specialized in binding lipids of the plasma membrane (Gokhale et al., 2011) while PPIP5K2 showed a functional nuclear translocation sequence (Yong et al., 2015).

Our group showed that Asp1 C-terminal domain influenced the inositol pyrophosphate output of the N-terminal kinase domain in an *in vitro* assay. This influence was proved to be enzymatic since the exchange of the first histidine residue by alanine abolishes the effect of the C-terminal domain. Thus, contrary to previous publications showing that the C-terminal domain of PPIP5K/Vip1 was enzymatically inactive, our laboratory was the first to demonstrate that the C-terminal domain of Asp1 is enzymatically active and uses as a substrate the inositol pyrophosphates produced by the N-terminal domain *in vitro* (Pöhlmann et al., 2014).

1.3. Function of Asp1-generated inositol pyrophosphates in microtubule-dependent growth.

We identified a new role for Asp1-generated inositol pyrophosphates as modulators of the microtubule cytoskeleton and cell morphogenesis (Pöhlmann and Fleig, 2010; Pöhlmann et al., 2014). Cell morphogenesis depends on the correct positioning of the growth machinery

by the microtubule cytoskeleton. We showed that Asp1 kinase activity is required to stabilize microtubules and, consistently, is required for growth zone selection. Interestingly this new role of PPIP5K/Vip1-generated inositol pyrophosphates is conserved in other fungi as similar phenotypes were observed in *Aspergillus nidulans* and *Ustilago maydis* (Pöhlmann et al., 2014). In this chapter the role of the microtubule cytoskeleton in the regulation of cell morphogenesis is described, as well as the implications of Asp1-generated inositol pyrophosphates in such processes.

1.3.1. Polarized growth: description and significance

The shape of a cell is critical to achieve its function. Multiple examples exist in biology which show that different cell shapes have evolved to fulfill specific tasks. Many microorganisms such as filamentous fungi, can adapt their growth and cell shape to the environment in order to survive or increase their biological efficiency (Fischer et al., 2008; Vollmeister et al., 2012). Also, higher eukaryotes have specialized cells that need to adapt their shape to execute sometimes very complex tasks. In plants, growth and shape of the pollen tube is directed towards the ovule during fertilization and in mammals neurons the axon growth towards the proper target and dendrites differentiation require shape change (Bedinger et al., 1994; da Silva and Dotti, 2002; Dent et al., 2011). Importantly, loss of cell polarity is often observed in epithelial tumors (Coradini et al., 2011). But, how do cells control their shape? A certain cellular shape is attained by directing cellular growth. To build and maintain specific cell shapes and structures, eukaryotic cells need to spatially organize intracellular components. The term "polarized growth" refers to the restriction of growth to specific areas within the cell in order to build spatially organized structures or control the direction of growth.

S. pombe it is rod-shaped organism which grows in a highly polarized manner during the entire cell cycle (Martin, 2009). Thus, the yeast *Schizosaccharomyces pombe* is a perfect model organism to study cell polarity establishment and maintenance.

1.3.2. Polarized growth in *Schizosaccharomyces pombe*

The fission yeast *S. pombe* is an unicellular organism with 7-14μm length and 3-4μm in diameter in its yeast form. *S. pombe* keeps its cylindrical shape by restricting growth to the opposite ends of the cell (Fig6A). Polarized growth is controlled temporally during the cell cycle. During mitosis, the growth machinery is localized to the middle of the cell where the medial contractile ring is form and will separate the two daughter cells (Fig6B). After cytokinesis, each daughter cell initiates monopolar growth at the end which was present before division in the previous cell cycle, thus it is called the “old end” (Fig6B). Growth at the old end continues until the completion of S-phase. Once cells have duplicated their DNA and

attained a critical cell size of 8-9μm, growth at the opposite cell end (new end) is initiated in a process called NETO (**n**ew **e**nd **t**ake **o**ff) (Mitchison and Nurse, 1985).

Thus, understanding the mechanisms that regulate NETO is a useful tool to discover how cell establish a new growing site and, in general, cell polarity. Several pathways involved in the NETO transition have been identified. Some of the molecules involved are Rho GTPases such as Cdc42, protein kinases, membrane proteins, actin and microtubule -related proteins, reviewed in (Martin, 2009). Among all these molecules, our laboratory found that Asp1 kinase activity was also essential for the NETO transition in *S. pombe*. 84% of *asp1*^{D333A} (kinase dead Asp1 variant, absence of Asp1-generated inositol pyrophosphates) cells do not activate growth at the new end and grow exclusively monopolar (Pohlmann and Fleig, 2010). Interestingly, the function of Asp1 in growth zone selection is conserved in other fungi. The kinase activity of the Vip1 family member in *Aspergillus nidulans VlpA,* is required for the correct positioning of the second germ tube and in *Ustilago maydis* UmAsp1 is required for normal cell shape (Pohlmann et al., 2014).

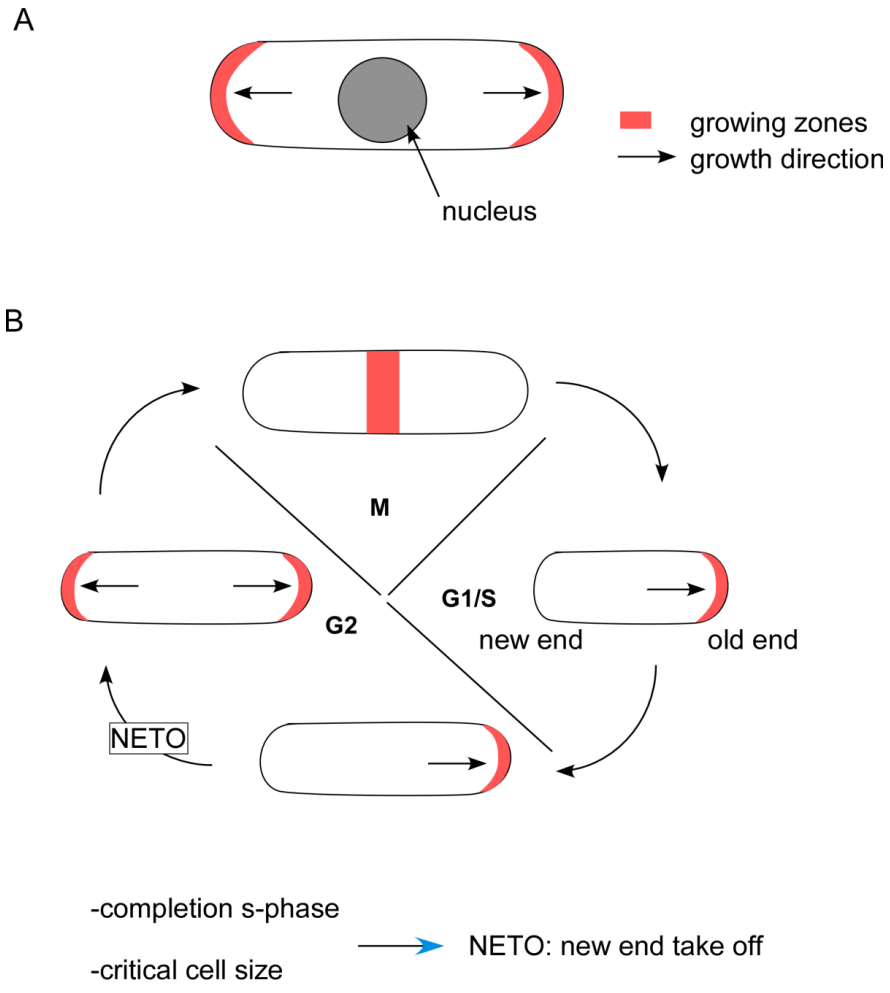

Fig6. *S. pombe* polarized growth is cell-cycle regulated. A) Schematic representation of a typical *S. pombe* rod-shaped cell. Polar growth at the cell tips (marked in red) triggers cell shape. B) Schematic representation of different stages of polar growth during the cell cycle. Switch from monopolar to bipolar growth is termed NETO (new end take off) occurs only when S-phase is completed and cells reach a critical cell length.

1.3.3. Modulation of polarized growth by the microtubule cytoskeleton

In *S. pombe*, the growth machinery needs to be directed to different localizations within the cells at different moments during the cell cycle. These dynamic growing sites are marked by proteins called polarity factors. These proteins are transported to the cell ends by the microtubule cytoskeleton (Mata and Nurse, 1997). How do microtubules transport polarity factors? During interphase, *S. pombe* microtubules are packed in bundles of 4-5 microtubules which are organized along the long cell axis (Marks et al., 1986). Microtubules are polar structures with one slow-growing minus end and a fast growing plus end. The minus ends of antiparallel microtubules overlap in the cell center close to the nuclear envelope while their plus ends dynamically grow towards the cell end transporting polarity factors. Once microtubules reach the cell end, they pause generally for 1-2 min and then undergo catastrophe and depolymerize (Drummond and Cross, 2000).

Microtubule dynamics at the plus end is controlled by the proteins called +TIPs. Representatives of +TIPs are, Mal3 (EB1 family member), the kinesin Tea2 and Tip1 (CLIP-170 family member).+TIPs are also essential for the microtubule recruitment of polarity factors (Beinhauer et al., 1997; Browning et al., 2000; Brunner and Nurse, 2000). The Tip1 protein is required for the binding of the polarity factor Tea1 to the plus end of the microtubules (Fig7). Tea1 forms a complex with Tea4 and both proteins are transported and delivered to the cell ends by microtubules. At the cell ends, Tea1 is anchored by the prenylated protein Mod5 and Tea4 promotes the recruitment of the formin For3, which is an actin nucleator required for the actin assembly machinery (Fig7)(Martin et al., 2005; Snaith et al., 2005; Snaith and Sawin, 2003).

Thus, microtubule cytoskeleton and polarity factors are essential in the correct positioning of growing zones and therefore cell polarity. Absence of Tea1 or Tea4 leads to abnormal cell shape in which the growing sites are ectopically localized and NETO is defective. *S. pombe* cells with an aberrant microtubule cytoskeleton are often curved or bent, showing that polar growth is possible in absence of microtubules but mis-positioned.

Interestingly, a previous study from our group showed that cells which do not undergo NETO in absence of Asp1 kinase activity also exhibit an unequal distribution of Tea1 between the two cells ends (Jennifer Pöhlman, unpublished observations). Microtubule dynamics are also altered in absence of Asp1-generated inositol pyrophosphates. *asp1*^{D333A} cells show highly dynamic microtubules which grow faster, have a shorter pausing time at the cell ends and increased number of catastrophe events in comparison to the wild-type (Pohlmann et al., 2014). In contrast, microtubules are more stable and grow for a longer time in *asp1*^{H397A} cells, which lack one of the conserved histidines of the histidine acid phosphatase signature. This protein variant Asp1^{H397A} generates double the amount of IP_7 *in vitro* in comparison to wild type protein (Pöhlmann et al., 2014).

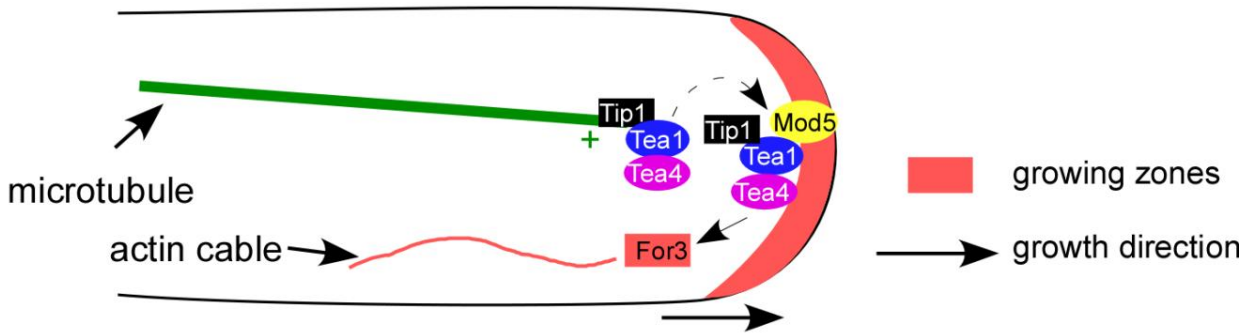

Fig7. Microtubules transport polarity factors to the cell ends. Main components of the polarity machinery in *S. pombe*. The Tea1-Tea4 complex binds to Tip1 and is deposited at the cell ends by microtubules. Tea1/Tea4 complex is anchored at the cell end by the membrane protein Mod5 and recruits For3 which promotes actin cable assembly.

1.4. Objectives of the study

This work focuses on two different aspects of Asp1 biology. The first and major aim was to elucidate the function of Asp1 C-terminal domain. In particular I wanted to elucidate the role of the conserved histidine acid phosphatase signature. As part of this aim, the objectives were to define if the Asp1 C-terminal domain has *in vivo* enzymatic activity, find its substrate and dissect its possible contribution to intracellular inositol pyrophosphate levels. The second aim of this PhD thesis was a better understanding of how Asp1-generated inositol pyrophosphates modulate the microtubule-dependent polarized growth.

2. Materials and Methods

2.1. Reagents

Reagent	**Source**
4-(2-hydroxyethyl)-1-piperazineethanesulfonic acid (HEPES)	ROTH
Acrylamid solution Rotiphorese-Gel	ROTH
Adenine, Glutamic acid, Histidine, Lysine, Uracil	Sigma Aldrich
Adenosin-5'-triphosphate-Mg-Salt (ATP)	Sigma Aldrich
Agarose	Biozym
Alanine	AppliChem
Ammoniumpersulfate (APS)	Sigma Aldrich
Ammonium sulfate $(NH_4)_2SO_4$	ROTH
Ampicillin	Sigma Aldrich
Arginine, Leucine	AppliChem
Aspartic acid, Cysteine, Glutamine, Isoleucine, Methionine, Proline, Serine, Threonine, Tryptophane, Tryosine, Valine	ROTH
Bacto Agar, Bacto Malt extract	BD
BCIP (5-Bromo-4-chloro-3-indolyl phosphate) / NBT (nitroblue tetrazolium chloride)	Sigma Aldrich/ Serva
β-glycerophosphate	AppliChem
Biotin	Sigma Aldrich
Boric acid (H_3BO_3)	Sigma Aldrich
Calcium chloride dihydrate ($CaCl_2$ x 2 H_2O)	Grüssing
Calcium pantothenate	ROTH
Calcium sulphate dihydrate ($CaSO_4$ x 2 H_2O)	ROTH
Calcofluor white	Sigma Aldrich
Carrier DNA	Sigma Aldrich
Chloramphenicol (CAM)	ROTH
Complete protease inhibitor	Roche
Coomassie Brilliant Blue	Serva
Copper sulfate pentahydrate ($CuSO_4$ x 5 H_2O)	Sigma Aldrich
Dimethylsulfoxide (DMSO)	Merck
Dithiothreitol (DTT)	ROTH
Disodium hydrogen phosphate (Na_2HPO_4)	ROTH
Ethanol, Isopropanol, Methano	Chemical storage HHU

Ethylenediaminetetraacetic acid (EDTA	AppliChem
Ethylene glycol bis-(aminoethyl ether) (EGTA)	Sigma Aldrich
Genetecin sulfate (G418)	Merck
Glucose	ROTH
Glutathion Agarose	Sigma
Glycerol	Fisher
Glycine	VWR
HisPur^{TM} Ni NTA Resin	Thermo Scientific
Hydrochloric acid (HCl)	Sigma Aldrich
Inositol	Sigma Aldrich
Iron chloride hexahydrate ($FeCl_3$ x $6H_2O$)	Sigma Aldrich
Isopropyl-β-D-thiogalactopyranoside (IPTG)	ROTH
Kanamycin	Life Technologies
L- Glutathion, reduced	Sigma
Lithium acetate (LiAc)	ROTH
Lithium chloride (LiCl)	Merck
Manganese sulphate ($MnSO_4$)	Sigma Aldrich
Magnesium chloride hexahydrate ($MgCl_2$ x 6 H_2O)	ROTH
Magnesium sulphate ($MgSO_4$)	Sigma Aldrich
Magnesium sulphate heptahydrate ($MgSO_4$ x 7 H_2O)	Grüssing
Milk powder	ROTH
Nicotinic acid	Sigma Aldrich
OrangeG	Sigma Aldrich
Peptone	BD
Phenylalanine	TCI
Phenylmethylsulfonyl fluoride (PMSF)	Serva
Phytic acid (IP_6)	ROTH
Phosphocreatine	Sigma Aldrich
p-nitrophenylphosphate	Sigma Aldrich
Polyethylene glycol (PEG)	Sigma Aldrich
Potassium acetate (KAc)	Grüssing
Potassium chloride (KCl)	ROTH
Potassium hydroxide (KOH)	Grüssing
Potassium iodide (KI)	Sigma Aldrich

Potassium phthalate monobasic	Sigma Aldrich
Sodium chloride (NaCl)	Fisher
Sodium citrate	AppliChem
Sodium deoxycholate	Sigma Aldrich
Sodium fluoride (NaF)	Sigma Aldrich
Sodium hydroxate (NaOH)	AppliChem
Sodium lauryl sulfate (SDS)	Sigma Aldrich
Sodium orthovanadate	Sigma Aldrich
Sodium pantothenic acid	Sigma Aldrich
Sodium phosphate	Sigma Aldrich
Sodium sulfate (Na_2SO_4)	Merck
Sorbitol	ROTH
Tetramethylethylene diamine (TEMED)	Merck
Thiabendazole (TBZ)	Sigma Aldrich
Thiamine	Sigma Aldrich
Toluidine Blue	Sigma Aldrich
Tris(hydroxymethyl)aminomethane (Tris)	Honeywell
Triton	AppliChem
Tryptone	BD
Tween	AppliChem
Yeast extract	BD
Yeast nitrogen base	BD
Zinc sulfate heptahydrate ($ZnSO_4$ x 7 H_2O)	Sigma Aldrich

2.2. Enzymes

Enzyme	**Source**
Creatinphosphokinase (CPK)	Sigma Aldrich
Lysozym	Sigma Aldrich
Taq DNA polymerase	U. Fleig
Q5 High-Fidelity DNA polymerase	New England Biolabs
QuikChange II Site-Directed Mutagenesis Kit	Agilent
EcoRI, HindIII, SmaI, XhoI, NotI, PstI	Thermo Scientific
PacI, SexAI	England Biolabs

Proteinase K	AppliChem
β-Glucoronidase	Roche
Zymolyase	Seikagaku

2.3. Antibodies

Antibody	**Source**
monoclonal α-GFP (from mouse)	Roche
γ-tubulin (from mouse)	Sigma Aldrich
α-Asp1 (from rabbit)	K. Gould
α-mouse IgG (from rabbit)	Promega
α-rabbit (from mouse)	Promega
Anti-GST (from rabbit)	Santa Cruz
Anti-His(6) (from mouse)	Quiagen

2.4. Commercial kits

Kit	**Source**
PCR purification Kit	Qiagen
Plasmid Midi Kit	Qiagen
Gel Extraction Kit	Qiagen

2.5. Oligonucleotides

Lab. number	**Description**	**Sequence 5´→3´**
98	Sequencing integration in pJR2-3XL	GATAATGGACCTGTTAATCGA
99	Sequencing integration in pJR2-3XL	ATCGTAATATGCAGCTTGAAT
198	Verification *kanMX6* integration	TCGAGTAGATATTTCAGCATCATTG
347	Sequencing *asp1*$^{+}$ ORF	TAGATGATTCTAATGCTGCC

373	Sequencing *GBP*	CGGATCCCTGGGTTAATT
423	Verification *kanMX6* integration	TCGCGAATCATTTTGGCGCC
519	Sequencing *asp1*$^{+}$ ORF	CGAAAGTTTGGAATAGAAATC
520	Sequencing *asp1*$^{+}$ ORF	GACTCTGAGGCAATTTGAGA
605	Determination mating type *S. pombe*	AAAGAGAGTGAGAAGAAGGG
606	Determination mating type *S. pombe*	AAATTGTATTGGTGTTACTAACC
607	Determination mating type *S. pombe*	GTAGGTGTAGAGTGTGGAGGG
608	Sequencing *asp1*$^{+}$ ORF/cloning *asp1* variants in pKM36	CCTCTAAGATATCAATTGCG
681	Sequencing *asp1*$^{+}$ ORF/ cloning *asp1* variants in pKM36	CCTGGTGAGAGTGTGATACG
675	Sequencing *asp1*$^{+}$ ORF	GTGATCTTCACCATAGACTG
681	Sequencing *asp1*$^{+}$ ORF	CCTGGTGAGAGTGTGATACG
777	Verification *kanMX6* integration	CACCGGATTCAGTCGTCACTC
843	Cloning *asp1* variants in pJR2-3XL	GAAAAACCCTAGCAGTACTGGCAAGGGAGACATTCCTTTTATTAATTAATGTTAACAGG
846	Cloning *asp1* variants in pJR2-3XL	CAATCTCATTCTCACTTTCTGACTTATAGTCGCTTTGTTAAATGATTCAAAATGCAAGTCATC
850	Cloning asp1 variants in pJR2-3XL	CTCATTCTCACTTTCTGACTTATAGTCGCTTTGTTAAATGAGACGGAATCGTGTACCTTCAG
884	Sequencing *asp1*$^{+}$ ORF	GTATTCTGGGCCTCCATGTCG
1005	Cloning *asp1-gfp* variants in pJR2-3XL	AAAAACCCTAGCAGTACTGGCAAGGGAGACATTCCTTTTATTATTTGTATAGTTCATCCA
1006	Cloning *asp1-gfp* variants in pJR2-3XL	TCGAATTTTGAAACAAATGTTTCATGTTGCCGAACGTCATCGGATCCCCGGGTTAATTAA
1292	Sequencing *asp1*$^{+}$ ORF	CTCAAATTGCCTCAGGCTCCAAGCTTGATTGCC
1420	Sequencing *asp1*$^{+}$ ORF/ cloning *asp1* variants in pJR2-3XL	TAAGTCTCCATGCCTCAC
1421	Cloning *asp1-GFP* variants in pJR2-3XL	AGTTCATCTTCCCAAAAGGTTTATTCCTGTTAACATTAATCGGATCCCCGGGTTAATTAA
1423	Sequencing *asp1*$^{+}$ ORF/ cloning *asp1* variants in pJR2-3XL	TTATGATAATGCTGCTCG

1486	Verification *kanMX6* integration	CGAAAACCGAGGACCTCTGC
1770	Site directed mutagenesis *asp1* ^{I808D}	CTTTACTAAAGAGTCTCATGACTATACCTTG CTTAATTG*
1771	Site directed mutagenesis *asp1* ^{I808D}	CAATTAAGCAAGGTATAGTCATGAGACTCTT TAGTAAAG*
1786	Site directed mutagenesis *asp1* ^{R400A}	GGAGTCCTGCGTCACGCGGATGCTACACC TAAACAAAAGTTT*
1787	Site directed mutagenesis *asp1* ^{R400A}	AAACTTTTGTTTAGGTGTAGCATCCGCGTG ACGCAGGACTCC*
1788	Site directed mutagenesis *asp1* ^{H807A}	ATGTACTTTACTAAAGAGTCTGCTATCTATA CCTTGCTTAAT*
1789	Site directed mutagenesis *asp1* ^{H807A}	ATTAAGCAAGGTATAGATAGCAGACTCTTTA GTAAAGTACAT*
1875	Sequencing integration in pKM36	TACTTGAAATCCAGCAAGTAT
1916	Cloning *asp1* variants in pJR2-3XL	AGACGGAATCGTGTACCTTCAGTCCAAGAA GTTTTAAATC
1917	Cloning *asp1* variants in pJR2-3XL	TCGAATTTTGAAACAAATGTTTCATGTTGCC GAACGTCATATCTTTTACCCATACGATG
1918	Cloning *asp1* variants in pJR2-3XL	GATTTAAAACTTCTTGGACTGAAGGTACAC GATTCCGTCTGCACTGAGCAGCGTAATCTG
1919	Cloning *asp1* variants in pJR2-3XL	CAGCGTATGATTGCTTTTAAATATTTAATTTT CATCGTTTTTAATTAATGTTAACAGGAA
2026	Cloning *asp1-gfp* variants in pJR2-3XL	GATTTAAAACTTCTTGGACTGAAGGTACAC GATTCCGTCTTTTGTATAGTTCATCCATGC
2071	Site directed mutagenesis *asp1* ^{I808V}	CTTTACTAAAGAGTCTCATGTCTATACCTTG CTTAATTGT*
2072	Site directed mutagenesis *asp1* ^{I808V}	ACAATTAAGCAAGGTATAGACATGAGACTC TTTAGTAAAG*
2152	Cloning *SPCC584.01c* in pKM36	TCCTCCAAAATCGGATCTGATCGAAGGTCG TGGGATCCCCATGGTTGCTACTGATTCTTC
2153	Cloning *SPCC584.01c* in pKM36	ACGCGCGAGGCAGATCGTCAGTCAGTCAC GATGAATTCCCCTAGTAAACTTCGATGACAA
2179	Site directed mutagenesis *asp1* ^{C607S}	CAGAAAACATGCCCAAGCCTTCTGAAGTAA TGCAACAAGTTGTT
2180	Site directed mutagenesis *asp1* ^{C607S}	AACAACTTGTTGCATTACTTCAGAAGGCTTG GGCATGTTTTCTG

*Mutated nucleotides are underlined

2.6. Plasmids

Lab number	Description	Source
177	*GFP:: kan^R , Amp^R*	U.Fleig
179	*(HA)$_3$::kan^R, Amp^R*	U.Fleig
270	pJR2-*3XL LEU2, Amp^R,* pREP3X, *nmt1$^+$*Promoter	U.Fleig
648	pKM36 *Amp^R*, pGEX-3X (GE-Healthcare), *tac* Promoter, *lac* Operator, *GST, TRP*	K. Mölleken
649	pKM36-*GST-asp1$^{1-364aa,}$ Amp^R*, pGEX-3X (GE-Healthcare), *tac* Promoter, *lac* Operator, *TRP*	U.Fleig
650	pKM36-*GST-asp1$^+$ Amp^R*, pGEX-3X (GE-Healthcare), *tac* Promoter, *lac* Operator, TRP	U.Fleig
672	pJR2-3XL *-asp1$^{1-364aa}$, LEU2, Amp^R*, pREP3X, *nmt1$^+$*Promoter	U.Fleig
875	pBsk+-*asp1$^+$::kan^R*	U.Fleig
882	pJR2-3XL-*asp1$^+$, LEU2, Amp^R,* pREP3X, *nmt1$^+$*Promoter	U.Fleig
883	pJR2-3XL-*asp1^{D333A,} , LEU2, Amp^R,* pREP3X, *nmt1$^+$*Promoter	U.Fleig
884	pJR2-3XL-*asp1^{H397A,} , LEU2, Amp^R*, pREP3X, *nmt1$^+$*Promoter	U.Fleig
885	pJR2-3XL-*asp1$^{365-920}$-GFP*, *LEU2*, *Amp^R,* pREP3X, *nmt1$^+$*Promoter	U.Fleig
887	pJR2-3XL-*asp1$^+$-GFP, LEU2, Amp^R*, pREP3X, *nmt1$^+$*Promoter	U.Fleig
889	pJR2-3XL-*asp1^{H397A}-GFP*, *LEU2, Amp^R*, pREP3X, *nmt1$^+$*Promoter	U.Fleig
890	pJR2-3XL-*asp1$^{1-794}$, LEU2, Amp^R*, pREP3X, *nmt1$^+$*Promoter	U.Fleig
916	pJR2-3XL-*asp1$^{365-920aa}$, LEU2, Amp^R,* pREP3X, *nmt1$^+$*Promoter	U.Fleig
917	pJR2-3XL-*asp1$^{365-920/H397A}$, LEU2, Amp^R,* pREP3X, *nmt1$^+$*Promoter	U.Fleig
946	pKM36-*GST-asp1$^{365-920aa}$*, *Amp^R*, pGEX-3X (GE-Healthcare), *tac* Promoter, *lac* Operator, *TRP*	U.Fleig
947	pKM36-*asp1$^{365-920/H397A}$, Amp^R,* pGEX-3X (GE-Healthcare), *tac* Promoter, *lac* Operator, *TRP*	U.Fleig
948	pKM36-a*sp1$^{365-920/R396A}$, Amp^R,* pGEX-3X (GE-Healthcare), *tac* Promoter, *lac* Operator, *TRP*	U.Fleig
1029	pFT25-*asp1$^{365-920aa}$, Amp^R, tac* Promoter, *lac* Operator His(6) (N-terminal)	U.Fleig
1048	pBsk+-*asp1^{I808D}::kan^R*	This work
1052	pKM36-*GST-asp1^{I808D}, Amp^R,* pGEX-3X (GE-Healthcare), *tac* Promoter, *lac* Operator, *TRP*	This work
1059	pJR2-3XL-*asp1^{I808D} LEU2, Amp^R,* pREP3X, *nmt1$^+$*Promoter	This work
1060	pBsk+-*asp1^{H807A}::kan^R*	This work

1061	pBsk+-*asp1*^{R400A}*::kan*^{R}	This work
1062	pKM36-*GST-asp1*^{H807A} *Amp*^{R}, pGEX-3X (GE-Healthcare), *tac* Promoter, *lac* Operator*, TRP*	This work
1063	pKM36-*GST-asp1*^{R400A} *Amp*^{R}*,* pGEX-3X (GE-Healthcare), *tac* Promoter, *lac* Operator, *TRP*	This work
1071	pJR2-3XL-*asp1*^{H807A} *, LEU2, Amp*^{R}*,* pREP3X, nmt1+Promoter	This work
1072	pJR2-3XL-asp1^{R400A}, LEU2, Amp^{R}, pREP3X, *nmt1*$^{+}$Promoter	This work
1074	pKM36-*GST- DDP1*$^{+}$*, Amp*^{R}*,* pGEX-3X (GE-Healthcare), *tac* Promoter, l*ac* Operator, *TRP*	U.Fleig
1076	pJR2-3XL-*asp1*^{I808D}*-GFP*, *Amp*^{R}, pREP3X, *nmt1*$^{+}$Promoter	This work
1080	pKM36-*GST-asp1*$^{365\text{-}920,I808D}$*, Amp*^{R}*,* pGEX-3X (GE-Healthcare), *tac* Promoter, *lac* Operator, *TRP*	U.Fleig
1087	pJR2-3XL-*asp1*^{H807A}*-GFP, LEU2, Amp*^{R}*,* pREP3X, *nmt1*$^{+}$Promoter	This work
1092	pKM36-*GST-asp1*$^{365\text{-}920/R400A}$*, Amp*^{R}, pGEX-3X (GE-Healthcare), *tac* Promoter, *lac* Operator, *TRP*	U.Fleig
1097	pJR2-3XL-*asp1*$^{365\text{-}920/I808D}$*, LEU2, Amp*^{R}*,* pREP3X, *nmt1*$^{+}$Promoter	This work
1102	pKM36-*GST-asp1*$^{365\text{-}920/H807A,}$*, Amp*^{R}, pGEX-3X (GE-Healthcare), *tac* Promoter, l*ac* Operator, *TRP*	U.Fleig
1169	pBsk+-*asp1*^{I808V}*::kan*^{R}	This work
1180	pJR2-3XL-*asp1*^{I808V}, *LEU2, Amp*^{R}, pREP3X, *nmt1*$^{+}$Promoter	This work
1183	pJR2-3XL-*asp1*^{I808V}*-GFP , LEU2, Amp*^{R}, pREP3X, *nmt1*$^{+}$Promoter	This work
1188	pJR2-3XL-*SPAC1071, LEU2, Amp*^{R}, pREP3X, *nmt1*$^{+}$Promoter	This work
1189	pJR2-3XL-*asp1*^{R400A}*-GFP, LEU2, Amp*^{R}, pREP3X, *nmt1*$^{+}$Promoter	This work
1208	pJR2-3XL-*SPCC584.01c, LEU2, Amp*^{R}, pREP3X, *nmt1*$^{+}$Promoter	U.Fleig
1210	pJR2-3XL-*asp1*$^{365\text{-}920/H807A}$*, LEU2, Amp*^{R}, pREP3X, *nmt1*$^{+}$Promoter	This work
1212	pJR2-3XL-*asp1*$^{365\text{-}920/H397A}$*-GFP, LEU2, Amp*^{R}, pREP3X, *nmt1*$^{+}$Promoter	This work
1213	pJR2-3XL-*asp1*^{R396A}*-GFP, LEU2, Amp*^{R}, pREP3X, *nmt1*$^{+}$Promoter	This work
1214	pJR2-3XL-*asp1*$^{365\text{-}920/I808D}$*-GFP, LEU2, Amp*^{R}*,* pREP3X, *nmt1*$^{+}$Promoter	This work
1219	pKM36-*GST-SPCC584.01c, Amp*^{R}, pGEX-3X (GE-Healthcare), *tac* Promoter, *lac* Operator, *TRP*	This work
1222	pBsk+-*asp1*^{C607S}*::kan*^{R}	This work
1225	pJR2-3XL-*asp1*^{C607S}*, LEU2, Amp*^{R}, pREP3X, *nmt1*$^{+}$Promoter	This work

1226	pJR2-3XL-*asp1*^{C607S}*-GFP, LEU2, Amp*^{R}, pREP3X, *nmt1*$^{+}$Promoter	This work
1236	pJR2-3XL-*asp1*$^{365\text{-}920/R396A}$*, LEU2, Amp*^{R}, pREP3X, *nmt1*$^{+}$Promoter	This work
1237	pJR2-3XL-*asp1*$^{365\text{-}920/R400A}$*, LEU2, Amp*^{R}, pREP3X, *nmt1*$^{+}$Promoter	This work

2.7. Strains and growth conditions

2.7.1. *Schizosaccharomyces pombe* strains and media

Lab number	**Genotype**	**Source**
40	*ade6-M210, leu1-32, h*$^{-}$	U. Fleig
605	*his3-D1, ade6-M210, leu1-32, ura4-D18, h*$^{-}$	K. Gould
771	*asp1-pk-gfp::ura4+, ade6-M210, ura4-D18, his3-D1, leu1-32, h*$^{-}$	U. Fleig
1156	*asp1Δ::kan*^{R}*, his3-D1, ade6-M216, leu1-32, ura4-D18, h*$^{-}$	U. Fleig
1157	*asp1Δ::kan*^{R}*, his3-D1, ade6-M216, leu1-32, ura4-D18, h*$^{+}$	U. Fleig
1511	*asp1*^{D333A}*::kan*^{R}*, his3-D1, ade6-M210, leu1-32, ura4-D18, h*$^{+}$	U. Fleig
1579	*asp1*^{H397A}*::kan*^{R}*, his3-D1, ade6-M210, leu1-32, ura4-D18, h*$^{+}$	U. Fleig
1764	*pef1Δ::ura4*$^{+}$*, leu1-32, ura4-D18, his3D1, ade6-M210, h*$^{-}$	U. Fleig
1776	*asp1*^{H397A}*::kan*^{R}*, pef1Δ::ura4*$^{+}$*, ade6-M210, leu1-32, ura4-D18, his3-D1, h*$^{+}$	U. Fleig
1782	*asp1*^{D333A}*::kan*^{R}*, pef1Δ::ura4*$^{+}$*, ade6-M210, leu1-32, ura4-D18, his3-D1, h*$^{-}$	U. Fleig
2079	*asp1*^{H397A}*-gfp::ura4*$^{+}$*, ade6-M210, his3-D1, leu1-32, ura4-D18, h*$^{+}$	U. Fleig
2134	*asp1*^{D333A}*::kan*^{R}*, tea1-gfp::ura4*$^{+}$*, crn1-tdtomato::kan*^{R}*, ura4-D18, leu1-32, his3-*	U. Fleig
2135	*asp1*^{H397A}*::kan*^{R}*, tea1-gfp::ura4*$^{+}$*, crn1-tdtomato::kan*^{R}*, ura4-D18,*	U. Fleig
2136	*tea1-gfp::ura4*$^{+}$*, crn1-tdtomato::kan*^{R}*, ura4-D18,*	U. Fleig
2156	*leu1-32::SV40::atb2*$^{+}$*-gfp[LEU2], his3-D1,h*$^{-}$	U. Fleig
2294	*asp1*$^{1\text{-}364}$*::kan*^{R}*, ura4-D18, leu1-32, his3-D1, ade6-M21x, h*$^{+}$	U. Fleig
2467	*cdc10-129, crn1-gfp-HA::kan*^{R}*, leu1-32, ura4-D18, his3-D1, ade6-M216, h*$^{-}$	This study
2469	*cdc10-129, asp1*^{D333A}*::kan*^{R}*, crn1-gfp-HA::kan*^{R}*, leu1-32, ura4-D18, h*$^{-}$	This study
2471	*cdc10-129, asp1*^{H397A}*::kan*^{R}*, crn1-gfp-HA::kan*^{R} *, leu1-32, ura4-D18, his3-D1, ade6-M210*	This study

2475	*cdc10-129, crn1-gfp-HA::kan^{R}, tea1Δ::ura4^{+}, leu1-32, ura4-D18, his3-D1, ade6-M216, h^{+}*	This study
2518	*asp1^{I808D}::Kan^{R}, ade6-M210, leu1-32, h^{-}*	This study
2553	*asp1^{I808D}::kan^{R}, his3-D1, ade6-M210, leu1-32, ura4-D18, h^{-}*	This study
2641	*asp1^{D333A}::kan^{R}, leu1-32::SV40::atb2^{+}-gfp[LEU2], h^{+}*	This study
2758	*SPCC584.01c::Kan^{R}, his3-D1, ade6-M210, leu1-32, ura4-D18, h^{-}*	U. Fleig
2795	*SPCC584.01c-gfp::kan^{R}, his3-D1, ade6-M210, leu1-32, ura4-D18, h^{-}*	U. Fleig
2805	*SPCC584.01c::Kan^{R}, asp1^{D333A}:: Kan^{R}, his3-D1, ade6-M210, leu1-32, ura4-D18, h^{-}*	U. Fleig
2807	*SPCC584.01c::Kan^{R}, asp1^{H397A}:: KanR, his3-D1, ade6-M210, leu1-32, ura4-D18, h^{-}*	U. Fleig
2940	*cox4-rfp:LEU2, asp1^{D333A}-gfp::ura4^{+}, ade6-m210, leu1-32, ura4-D18, his3-D1 h^{-}*	This study
2941	*asp1-pk-gfp::ura4^{+}, cox4-rfp:LEU2, ade6-M21X, leu1-32, ura4-D18, his3-D1, h^{+}*	This study
2943	*asp1^{H397A}-gfp::ura4^{+}, cox4-rfp:LEU2, ade6-M210, his3-D1, leu1-32, ura4-D18,*	This study
2945	*asp1$^{1-364}$-gfp::kan^{R}, cox4-rfp:LEU2 , ura4-D18, leu1-32, ade6-M21x, h^{-}*	This study
2947	*mmb1Δ:Kan^{R}, ade6-m210, leu1-32 ura4-D18, his3-D1 h^{+}*	This study
2651	*asp1Δ::kan^{R}, cox4-rfp:LEU2 , ura4-D18, leu1-32, ade6-M21x, h^{-}*	This study

Full medium (YE5S) 2 L

10 g Yeast extract

20 ml Histidine (7.5 mg/ ml)

20 ml Leucine (7.5 mg/ ml)

150 ml Adenine (2.7 mg/ ml adenine hemisulfate)

75 ml Uracil (2 mg/ ml)

20 ml Lysine (7.5 mg/ ml)

1515 ml dH_2O

Media was autoclaved. For solid media 20 g/ L Bacto agar was added.

Separately autoclaved glucose was added to an end concentration of 3 % after autoclavation.

Minimal medium (MM) 2L

5.5 g Na_2HPO_4 x $2H_2O$

6 g Potassium phthalate monobasic

2 g Glutamic acid

40 ml Salt stock*

2 ml Vitamine stock**

0.2 ml Mineral stock***

1760 ml dH_2O

Media was autoclaved. For solid media 20 g/ L Bacto agar was added.

Separately autoclaved glucose was added to an end concentration of 4 % after autoclavation. Selective media was prepared by adding the required amino acids to an end concentration of 75 µg/ ml.

Salt stock*: 21.4 g $MgCl_2$ x $6H_2O$, 0.29 g $CaCl_2$ x $2H_2O$, 20 g KCl, 0.8 g Na_2SO_4, 400 ml dH_2O. Stored at 4ºC.

Vitamine stock**: 1 g sodium pantothenic acid, 10 g nicotinic acid, 10 g inositol, 10 mg Biotin, 1 L dH_2O. Stored at 4ºC.

Mineral stock***: 5 g H_3BO_3, 4 g $MnSO_4$, 4 g $ZnSO_4$ x $7H_2O$, 2 g $FeCl_2$ x $6H^2O$, 4 g MoO_3, 1 g KI, 4 g $CuSO_4$ x $5H_2O$, 10 g citric acid, 1 L dH_2O. Stored at 4ºC.

To prepare **MM inositol-poor media** a different vitamine stock without inositol was prepared and added. After autoclavation of the MM inositol free media, different volumes from a stock solution of 50 mM inositol were added depending on the concentration required.

ADDITIONAL COMPONENTS FOR *S. pombe* MEDIA IF REQUIRED:

To grow *met10Δ* strain in MM: 330 µM cysteine and 140 µM methionine.

To regulate the expression of the genes under control of $nmt1^+$ promoter: 5 µg/ ml thiamine (stock 10 mg/ ml in ddH2O)

To test microtubule stability: TBZ (stock 10 mg/ ml in DMF)

To select kanamycin resistance: 100 µg/ ml G418 (Geneticin disulfate in ddH2O)

Malt medium 1L

30 g Bacto malt extract

75 mg Histidine

75 mg Leucine

75 mg Adenine

75 mg Uracil

1 L dH_2O

The pH was adjusted with 10 M NaOH to 5.5 before autoclavation.
Media was autoclaved. For solid media 20 g/ L Bacto agar was added.

1000x Minimal Sporulating Liquid MSL-N (1 L) (Fennessy et al., 2014)

10 g Glucose
2 g Arginine
1 g KH_2PO_4
0.1 g NaCl
0.2 g $MgSO_4$ x 7 H_2O
0.1 g $CaSO_4$ x 2 H_2O
500 µg Boric acid
50 µg $CuSO_4$ x 5 H_2O
100 µg KI
200 µg $FeCl_3$ x 6 H_2O
500 µg $MnSO_4$ x 4 H_2O
150 µg MoO_3
400 µg $ZnSO_4$ x 7 H_2O
10 µg Biotin
100 µg Calcium pantothenate
1 mg Nicotinic acid
1 mg Meso-inositol
1 L dH_2O

2.7.2. *Saccharomyces cerevisiae* strains and media

Name	Genotype	Source
CenPK	*Mata, leu2-3, 112, ura3-52, trp1-289,his3Δ1, MAL2-8c, SUC2*	J.Hegemann

Full medium (YPD) 1 L

20 g peptone
10 g Bacto yeast extract
2 ml Adenine (2.7 mg/ ml adenine hemisulfate)
4 ml Tryptophane (5 mg/ ml)
1 L dH_2O

For solid media 27 g/ L Bacto agar was added. After autoclavation separately autoclaved glucose was added to an end concentration of 4 %.

Synthetic defined media (SD) 1 L

1.7 g Yeast nitrogen base

5 g Ammonium sulfate

2 g Drop-out mix*

900 ml dH_2O

The pH was adjusted with 10 M NaOH to 5.5 before autoclavation.

Media was autoclaved. For solid media 20 g/ L Bacto agar was added. Separately autoclaved glucose was added to an end concentration of 4 % after autoclavation.

Drop-out mix*: 0.2 g para amino benzoic acid, 0.5 g adenine, 2 g alanine, 2 g arginine, 2 g aspartic acid, 2 g cysteine, 2 g lysine, 2 g methionine, 2 g phenylalanine, 2 g proline, 2 g glutamine, 2 g glutamic acid, 2 g histidine, 2 g inositol, 2 g isoleucine, 2 g serine, 2 g threonine, 2 g tyrosine, 2 g uracil, 2 g valine

2.7.3. *Escherichia coli* strains and media

Name	Genotype	Source
Rosetta (DE3)	F– *ompT hsdS*$_B$ (r_B– m_B–) *gal dcm* (DE3) pRARE *(*Cam^R)	Novagen
XL1-blue	*recA1, lac*$^-$*, endA1, gyrA46, thi, hsdR17,supE44, relA1, F' [proAB*$^+$*, lacI*^{q}*, laczΔM15,Tn (tet*^{r}*)]*	Stratagene

Lysogeny broth medium (LB) 1 L

10 g Tryptone

5 g Bacto yeast extract

5 g NaCl

1 L dH2O

For solid media 20 g/ L Bacto agar was added. After autoclavation separately autoclaved glucose was added to an end concentration of 4 %.

Depending on the application the media was supplemented with ampicillin (50 µg/ ml) kanamycin (12.5 µg/ ml) or chloramphenicol (20 µg/ml).

2.8. DNA manipulation

2.8.1. Site directed mutagenesis

Asp1 variant were generated following the protocol " QuikChange II Site-Directed Mutagenesis Kit" from Agilent.

2.8.2. *In vivo* recombinational cloning

PCR fragments generated by directed mutagenesis were cloned into different vectors via homologous recombination in *S. cerevisiae* (Jakopec et al., 2011)

***Saccaromyces cerevisiae* transformation protocol:** (Gietz R.D., 2006)

1. Overnight cultures grown in 5 ml YPD at 30°C.
2. Dilution of cultures to an OD_{600} of 0.1-0.2. in 50 ml YPD.
3. 4-5 h incubation at 30°C.
4. OD_{600} measurement.
5. Centrifugation at 3500 rpm for 5 min.
6. 1x wash with 25 ml dH_2O and resuspension in 1 ml 0.1 M LiAc pH 8.4-8.9.
7. Centrifugation for 10 sec at 13000 rpm.
8. Cell pellet resuspension at a concentration of 2 x 10^9 cells/ ml in 0.1 M LiAc pH 8.4-8.9.
9. Pipette 50 µl per transformation and centrifugation for 10 sec at 13000 rpm. Discard supernatant
10. Addition of:
    - 240 µl 50 % PEG_{3350}
    - 36 µl 1 M LiAc pH 8.4-8.9
    - 50 µl boiled cold carrier DNA (2 mg/ ml)
    - 34 µl DNA diluted in dH_2O
11. Vortex until pellet dissolved.
12. Incubation at 30°C for 30 min.
13. Heat-shock at 42°C for 30 min.
14. Centrifugation for 10 sec at 13000 rpm. Discard supernatant.
15. Pellet resuspension in 200 µl dH2O. 10 % and 90 % volume on plasmid-selective plates.

2.8.3. *Schizosaccharomyces pombe* transformation

General protocol (Okazaki et al., 1990):

1. Overnight cultures were grown in 100-200 ml YE5S at 25°C or 30°C.
2. Centrifugation of 1x 10^8 cells/ transformation for 3 min at 3500 rpm.
3. 1 wash with 0.1 M LiAc pH 4.9. Centrifugation for 3 min at 3500 rpm.
4. Cells resuspension in 70 µl 0.1 M LiAc/ transformation.
5. 1 h incubation at 25°C or 30°C.
6. Addition of 0.5 µg plasmid DNA or PCR-product + 2 µl carrier DNA (10 mg/ ml)
7. Addition of 290 µl 50% PEG_{4000}. Resuspend carefully.
8. 1 h incubation at 25°C or 30°C.
9. Heat-shock for 15 min at 43°C.
10. Samples cooled down for 2 min at RT.
11. Centrifugation for 5 min at 3500 rpm.
12. Cells resuspension in 1 ml YE5S*****
13. 1 h incubation at 25°C or 30°C******
14. 2x washes with 1 ml dH_2O.
15. Cells resuspension in 1 ml dH_2O.
16. 1x 50 µl and 1x 100 µl plated on selective plates.

*****: MSL-N for endogenous homologous recombination

******: 16 h for endogenous homologous recombination (Fennessy et al., 2014)

***asp1Δ* transformation protocol:**

1. Overnight cultures were grown to1x 10^7 cells/ ml in 100-200 ml MM at 25°C or 30°C.
2. Transfer 50 ml of culture to a falcon tube and incubate 15 min on ice
3. Centrifugation for 5 min at 3500 rpm.
4. 3 x wash with 50 ml ice-cold water.
5. Cell resuspension with 5 ml of 0.6 M sorbitol, 25 mM DTT, 20 mM HEPES.
6. 15 min incubation at 30ºC.
7. Centrifugation for 5 min at 3500 rpm.
8. Wash with 5 ml 1 M ice-cold sorbitol.
9. Cell resuspension with 500 µl of 1 M ice-cold sorbitol.
10. Pre-chill electroporation cuvettes.
11. Place 100 ng DNA in an eppendorf tube and add 50 µl of compentent cells.
12. Transfer DNA-cell mix into pre-chilled electroporation cuvettes
13. Electroporation at 2.1 kV, 200 Ω, 25 µF.

14. Addition of 0.9 ml of ice-cold 1 M sorbitol and transfer to eppendorf.
15. 10 min incubation at 30ºC.
16. Plate 100 µl cells on selective media

2.8.4. *Escherichia coli* transformation

Electroporation *in E. coli*

1. Addition of 1-5 µl plasmid DNA to 40 µl electro-competent cells.
2. Transfer sample to electroporation cuvette.
3. Electroporation at 2.1 kV, 200 Ω, 25 µF
4. Addition of 1 ml LB.
5. Transfer to tube.
6. 1 hour incubation at 37°C.
7. Centrifugation for 2 min at 13000 rpm. Discard supernatant.
8. Pellet resuspension in 200 µl LB. Vortex.
9. Plate 10 % and 90 % on selective media.

2.8.5. DNA isolation from *S. pombe*

S. pombe genomic DNA was isolated following this protocol (Hoffman and Winston, 1987):

1. Overnight cultures grown in 8 ml YE5S at 30ºC.
2. Centrifugation for 5 min at 3000 rpm.
3. Cell pellet resuspension in 1 ml SP1 (1.2 M sorbitol, 50 mM sodium citrate, 50 mM sodium phosphate, 40 mM EDTA , pH 5.6) with 25 mg freshly added Zymolyase.
4. Incubation for 45 min at 37°C. Spheroplasts formation checked under the microscope.
5. Centrifugation for 5 min at 6000 rpm.
6. Pellet resuspension in 450 µl 5x TE (50 mM Tris pH 8, 5 mM EDTA)
7. Addition of 50 µl 10 % SDS. 5 min incubation at RT.
8. Addition of 150 µl 5 M KAc. Incubation for 10 min on ice
9. Centrifugation for 10 min at 13000 rpm. Transfer supernatant to fresh tube.
10. Addition of 1 V isopropanol. Centrifugation for 3 min at 13000 rpm.
11. Wash with 500 µl 70 % EtOH. Pellet resuspension in 250 µl 5x TE with 2 µl freshly added RNase (10 mg/ ml).
12. Incubation for 20 min at 37°C.
13. Addition of 2 µl 10 % SDS and 2 µl 5 mg/ ml Proteinase K.
14. Incubation for 1 h at 55°C.
15. Phenol-chloroform extraction (1:1 V) followed by chloroform-extraction (1:1 V).

16. Centrifugation for 8 min at 13000 rpm. Transfer upper fraction to fresh tube.
17. Addition of 1:10 V 3 M NaAc pH 5.1 and 2.5:1 V 96 % EtOH.
18. Centrifugation for 30 min at 13000 rpm.
19. Wash with 500 µl 70 % EtOH.
20. Centrifugation for 10 min at 13000 rpm.
21. Pellet resuspension in 30 µl 1x TE.

2.8.6. Plasmid isolation from *S. cerevisiae*

S. cerevisiae plasmid DNA was isolated following this protocol (Birnboim and Doly, 1979):

1. Overnight culture grown in 5 ml SD at 30°C.
2. Centrifugation of 2 ml of culture for 5 min at 3500 rpm.
3. 2x washes with 2 ml dH_2O.
4. Pellet resuspension in 0.5 ml P1 (50 mM Tris/ HCl pH 8, 100 mM EDTA, 100 µg/ ml RNase).
5. Addition of 0.5 ml P2 (200 mM NaOH, 1 % SDS).
6. Mix by inverting the tubes 4-6 times.
7. Addition of ~ 2/3 volume glass beads.
8. Lysis of cells in Precellys (2x 2000 U for 20 sec). Cells kept on ice.
9. Centrifugation for 2 min at 2000 rpm.
10. Transfer 1 ml supernatant into fresh tube.
11. Addition of 0.5 ml P3 (3 M potassium acetate pH 5.5).
12. Mix by inverting the tube 4-6 times.
13. Incubation on ice for 10 min.
14. Centrifugation for 15 min at 13000 rpm.
15. Transfer 750 µl supernatant into a fresh tube, addition of 1 volume isopropanol and vortex.
16. Centrifugation for 30 min at 13000 rpm.
17. Wash with 70 % EtOH. Pellet air-dried.
18. DNA resuspended in 20 µl dH_2O.

2.8.7. Plasmid isolation from *E. coli*

Plasmid isolation from E. coli was performed following the alkaline lysis method (Maniatis et al., 1989).
For higher DNA yields a Qiagen Midi Kit was used according to Qiagen instructions.

2.9. Serial dilution patch test

1. Overnight cultures grown in 5 ml YE5S or plasmid-selective MM media
2. Dilutions of every culture to 2x 10^6 cells/ ml. Dilution series with 2x 10^5, 2x 10^4, 2x 10^3 cells/ ml were prepared and 5 µl of each dilution patched on the required media.

2.10. Live-cell microscopy

Live-cell imaging of *Met10-gfp* cells stained with Mito-tracker or *Cox4-rfp* cells expressing different *asp1* variants was performed using a Zeiss spinning-disk confocal microscope equipped with a Rolera EM-C^2 (QImaging). A z-stack of 25 z slices with a distance of 0.5 µm was recorded and a maximum-intensity projection (MIP) image created. All imaging was carried out at 25 °C in a temperature controllable chamber.

2.10.1. Preparation of samples

Cultures were grown in filter-sterilized MM media (LFM). Depending on the application the cells were grown in volumes between 5 ml and 50 ml of LFM and slides were prepared as the protocol below:

1. 2x centrifugation of 1 ml of exponentially growing cultures for 1 min at 3500 rpm. Tubes turned 180°C in between the two centrifugation steps.
2. Discard 980 µl supernatant. Cells resuspension with the remaining volumen.
3. 50 µl 100°C warm MM medium containing agarose was pipetted on an object slide to generate an agarose pad.
4. Drop of 2 µl of cell suspension on the agarose pad.
5. After several minutes a cover slip was placed on the agarose pad and it was sealed with VALAP (pre-heated at 100°C).

2.10.2. Calcofluor staining. Visualization of cell wall

Cultures were grown in filter-sterilized MM media (LFM) were stained with calcofluor white in order to visualize the cell wall.

1. 1 ml of exponentially growing cultures for 1 min at 3500 rpm. Tubes turned 180°C in between the two centrifugation steps.
2. Discard 960 µl supernatant. Cells resuspension with the remaining 40 µl.
3. Add 10 µl of calcofluor white (stock solution: 50 µg/ ml).
4. 3 min incubation in the dark
5. Wash with 50 µl dH_2O

6. Preparation slides as described in 2.10.1.

2.11. Protein analysis

2.11.1. Protein extraction from *S. pombe* cultures

Protocol:

1. Cultures were grown overnight in YE5S or plasmid-selective MM with the required supplements.
2. $2x10^8$ cells were centrifuged for 5 min at 3500 rpm.
3. Pellet resuspended in 5 ml STOP buffer (150mM NaCl, 10mM EDTA, 1mM NaN_3, 50mM NaF, pH 8)
4. Centrifugation for 5 min at 3500 rpm.
5. Pellet resuspended in the remaining STOP buffer.
6. Centrifugation for 5 min at 10000 rpm. Discard supernatant.
7. Addition of 500 µl HB15 buffer (25mM MOPS, 60 mM β-glycerophosphate, 15 mM p-nitrophenylphosphate, 15 mM $MgCl_2$, 15 mM EGTA, 1 mM DTT, 0.1 mM Sodium orthovanadate, 1 % Triton X 100, 1 mM PMSF, complete protease inhibitot) and add glass beads below liquid meniscus.
8. Cell lysis with Precellys instrument (1x5000 U for 10 sec) x 2. Samples on ice.
9. Eppendorf tubes were pierced with a heated needle and placed on a new eppendorf tubes.
10. Centrifugation for 30 sec at 3000 rpm. Pierced eppendorf tubes discarded.
11. Centrifugation for 30 min at 13000 rpm. Supernatant recovered.
12. Centrifugation for 30 min at 13000 rpm. Supernatant recovered.
13. Samples were used for Western blot analysis or stored at -20°C.

2.12.2. Determination of protein concentration

The Bradford assay was used to measure the concentration of total protein in the samlples.

1. Protein extracts were diluted 1:800 in ddH_2O in a total volume of 800 µl.
2. Addition of 200 µl Bradford solution. Vortex.
3. 10 min of incubation at RT.
4. Measurement of the OD_{595}.
5. Protein samples were diluted to the lowest OD at 595 nm to normalize the protein amount.

2.12.3. Western blot analysis and Coomassie staining

32,5 µl of protein samples were mixed with 12.5 µl 4x SDS loading buffer and 5 µl 1 M DTT. After boiling for 10 min at 100°C, same volume of the samples was loaded on two 10 % SDS-gels and separated by PAGE at 100 V until the SDS loading buffer reached the resolving gel. Afterwards the voltage was increased to 200 V.

After PAGE, one of the gels was stained with Coomassie blue and the protein content of other one was transferred onto a PVDF blotting membrane for 30 min at 300 mA using a blotting instrument.

Afer transfer proteins were detected using the following protocol:

1. Block the PVDF membrane for 1 h in 3 % milk powder in PBS + 0.1 % Tween at RT.
2. Incubation with primary antibody overnight at 4°C.
3. Membrane washed 2x briefly, 1x 15 min and 3x 5 min with PBS + 0.1 % Tween.
4. Incubation with secondary antibody for 4-6 h at RT.
5. Membrane washed 2x briefly, 1x 15 min and 3x 5 min with PBS + 0.1 % Tween.
6. Detection with DIG P3 + NBT/BCIP until signals appeared.

2.13. *In vitro* enzymatic activity of Asp1 variants

S. pombe recombinant proteins *Asp1*$^{1-364}$*, Asp1*$^{365-920}$ and *Asp1*$^{365-920/H397A}$ were previously generated.
1751 bp PCR fragments containing *asp1*$^{365-920/R396A}$*, asp1*$^{365-920/H397A}$*, asp1*$^{365-920/R400A}$*, asp1*$^{365-920/H807A}$, *asp1*$^{365-920/I808D}$*,* 3101 bp fragment containing the entire met10^{+} ORF or 649 bp fragment containing the entire Sc*DDP1* ORF were cloned into *E. coli* expression vector pKM36 to generate GST-tagged proteins or into *E. coli* expression vector pFT25 to generate His-tagged proteins. Proteins were expressed and purified from *E.coli* Rosetta (DE3) strain. GST-tagged proteins were purified following the protocol from Sigma-Aldrich. His-tagged proteins were purified following the protocol from Quiagen. Protein concentration was determined using a Bradford assay. Western blot analysis was carried out using GST or His antibodies. For the kinase reaction, 4 µg of purified Asp1$^{1-364}$ protein was incubated for 16 h at 37°C with 300 µM IP_6. Inactivation of Asp1$^{1-364}$ was achieved by incubation at 65°C for 20 min. Inactivation was verified by performing a kinase assay with the treated Asp1$^{1-364}$ protein. 30µl of the mix generated by the Asp1$^{1-364}$ kinase reaction containing IP_7 were incubated with 8 µg of Asp1$^{365-920}$ variants for 16 h at 37°C, followed by PAGE analysis. In Fig 21 (page 62) 6 or 8 µg of GST-Met10, 2 µg of GST-Ddp1 and 4µg of Asp1$^{365-920}$ were used in the assay.

2.14. Spectrometry

2.14.1. Determination of Fe-S clusters by UV-visible spectroscopy

Protein samples used to determine *in vitro* enzymatic activity of Asp1$^{365-920}$ were subjected to spectroscopic analysis. UV-visible absorbance measurements were made using JASCO V-650 spectrophotometer in 10 mm quartz cuvettes at room temperature. After data collection, the ratio A410/A280 nm was calculated to determine the % of protein molecules bound to an iron-sulfur cluster.

2.15. Extraction and detection of inositol polyphosphates

Labelling, extraction, separation and detection of inositol polyphosphates were performed as previously described (Azevedo and Saiardi, 2006). Equipment and reagents were kindly provided by Prof. Dr. Adolfo Saiardi.

2.15.1. Radioactive labelling of inositol polyphosphates

1. *S. pombe* cells were grown at 30ºC in 5 ml MM + 10 µM inositol overnight in a falcon tube.
2. Dilution of cultures to OD $_{600}$ 0,05 (total volume 5 ml) and addition of + 6µl H^3-inositol/ml (total 30µl).
3. Overnight incubation at 30ºC.
4. Check turbidity of cultures. Ideally cells must have completed 4-5 divisions. Incubate longer if necessary.

2.15.2. Inositol polyphosphates extraction

1. Centrifugation of cultures at 3000 rpm for 3 min and discard supernatant
2. Resuspension in 1 ml MM + 10 µM inositol and transfer to eppendorf tube
3. Spin down for 3 min at 3000 rpm, 10°C
4. Discard supernatant and wash 2 times with 1 ml media MM 10 µM inositol
5. Resuspension pellet in 200 µl 1M Percloric acid + 3 mM EDTA.
6. Addition of glass beads 200µl (with glass dispenser) to a level just below the meniscus and vortex 5 min 4°C.
7. Spin down 5 min 4°C 13000 rpm.
8. Transfer 200 µl in new eppendorf tube (keep sediment*)

9. Add of 92 µl of 1M potassium carbonate (K_2CO_3) and 3 mM EDTA. Measure pH, take 2 µl and pipette on a pH strip (pH must be between 6-8) Leave the tubes open, CO_2 bubles will form.
10. Keep samples couple of hours on ice. Every 30 min flick gently the tubes
11. Centrifuge for 10 min 13000 rpm at 4°C and collect supernatant

    * it is used to measure lipid inositol (quantity of lipid inositol/soluble fraction)

2.15.3. Inositol polyphosphates separation by High Performance Liquid Chromatography

Prepare HPLC instrument (partisphere SAX 4.6 × 125 mm column; Whatman) by running a buffer containing 1 mM EDTA. Prepare the cartridge holder and set the fraction collector to collect 1 ml fractions.

1. Inject supernatant from step 11 (section 2.15.2).
2. Each HPLC run takes about 2 hours. 90 fractions (1 per minute) are collected by the end of each run.

2.15.4. Inositol polyphosphates detection by radioactivity

1. mix vigorously each fraction with 4 ml of Ultima-Flo AP
2. quantify radioactivity (cpm) of each eluted fraction in the scintillation counter for 3-5 min (total counting time 5 hours)

2.16. Extraction and detection of Poly-P

Poly-P was extracted from logarithmic growing cultures as described (Lonetti et al., 2011). Equipment and reagents were kindly provided by Prof. Dr. Adolfo Saiardi.

1. 10 ml of cultures were centrifuged at 3500 rpm for 5 min at 10 °C.
2. Cells were resuspended in one volume of LETS buffer (100 mM LiCl, 10 mM EDTA, 10 mM Tris·HCl, pH 8.0, 0.5% SDS).
3. After addition of one volume of phenol, glass beads were added and samples were vortexed at 4 °C for 5 min.
4. Samples were centrifuged at 13000 rpm for 5 min at 4 °C and aqueous phase was collected.
5. Two volumes of chloroform were added and samples were vortexed at 4 °C for 5 min.
6. After spinning at 5,000 rpm for 5 min, the aqueous phase was collected.
7. Precipitation of nucleic acid was done by adding 2.5 volumes of ethanol, vortexing and incubating at −80 °C for 1–2 h.

8. Samples were spun at 13000 rpm for 10 min, pellets were resuspended in 100µl 10 mM Tris·HCl, pH 8, 1 mM EDTA, and 0.1% SDS.
9. RNA concentration was measured by reading the absorbance at 260 nm with Nanodrop.
10. All samples were normalized to RNA content before loading the gel. Detection of polyP was done by Toluidine staining.

Malachite green was used to quantify poly-P levels as described (Van Veldhoven and Mannaerts, 1987):

1. Dilute the samples to 0.3 µg/µl.
2. Take 5µl from each (1.5µg) and add 200 µl H_2O +50 µl 7,7% sulfuric acid.
3. Incubate for at least 30° min 100°C.
4. Spin down and 5 min RT.
5. Add 500 µl of malachite green solution.
6. Vortex and wait 1 min RT.
7. Add 500 µl 7.7% sulfuric acid.
8. Vortex and incubate 60 min RT.
9. 200µl of each sample will be read in duplicates in a microtiter plate $A_{650nm.}$

3. Results

3.1. Study of Asp1 catalytic function

Vip1-like proteins harbor two distinct domains: an N-terminal kinase domain which synthesizes inositol pyrophosphates and a C-terminal domain which contains the conserved signature motif of histidine acid phosphatases (Fridy et al., 2007). In the following section, a thorough analysis of the catalytic function of these domains will be presented using biochemical, genetic and molecular biology approaches.

3.1.1. *In vivo* analysis of Asp1 N-terminal domain kinase activity

The N-terminal kinase domain of all tested Vip1-like proteins synthesizes inositol pyrophosphates; 1-IP_7 and 1,5-IP_8 (Fridy et al., 2007; Mulugu et al., 2007; Pohlmann et al., 2014; Wang et al., 2011). Accordingly, *in vitro* studies performed in our laboratory showed that the kinase domain of Asp1 phosphorylates IP_6 to 1-IP_7 (Pöhlmann et al., 2014).

To define the substrate of the Asp1 kinase activity *in vivo*, *S. pombe* cells were cultured in presence of [^{3}H]inositol in order to label inositol polyphosphates which were then extracted and separated by HPLC. Inositol polyphosphates were analyzed in three different strains: wild-type, *asp1^{D333A}* in which the catalytic amino acid of the kinase domain has been replaced by alanine (Mulugu et al., 2007) and in the asp1 deletion strain, *asp1Δ*.

S.pombe is a natural inositol auxotroph and requires a minimum concentration of 10µM inositol in the media (Fig1) as already described (Fernandez et al., 1986; Ridgway and Douglas, 1958). Thus, in order to avoid phenotypical consequences, wild-type, *asp1^{D333A}* and *asp1Δ* strains were radiolabeled with [^{3}H]inositol in presence of 10µM cold inositol. Next, soluble inositol polyphosphates were extracted, fractions separated by HPLC and quantified by scintillation counting (Azevedo and Saiardi, 2006).

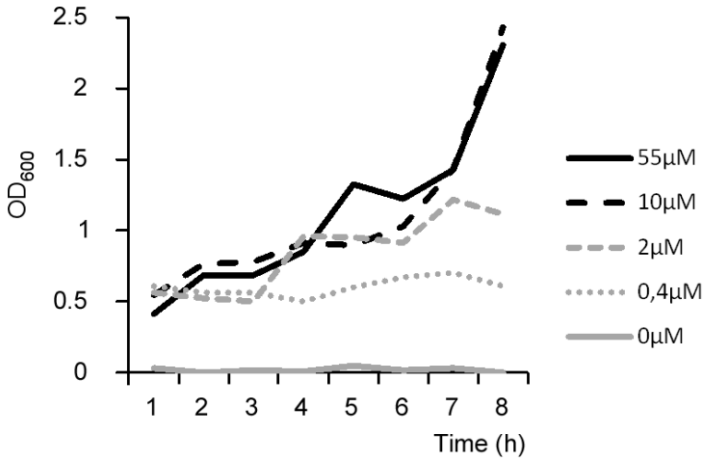

Fig1. Inositol auxotrophy of *S. pombe*. Growth of *S.pombe* wild-type cells in minimal media containing 55, 10, 2, 0.4 or 0 µM inositol. OD_{600} of each culture was measured in duplicates every hour during 8 hours.

The inositol polyphosphate profile of the wild-type strain showed three major peaks which

corresponded to IP_6, IP_7 and IP_8 (Fig2A, black line). Identification of the peaks was done by running PP-IP_4 (IP_6 isomer) and IP_7 standards (FigS1). The IP_8 peak was absent in the profile of the *asp1*^{D333A} strain (Fig2A, grey line), showing only two prominent peaks corresponding to IP_6 and IP_7. Levels of IP_8 were undetectable and IP_7 was increased in *asp1*^{D333A} in comparison to the wild-type (Fig2A and 2B)

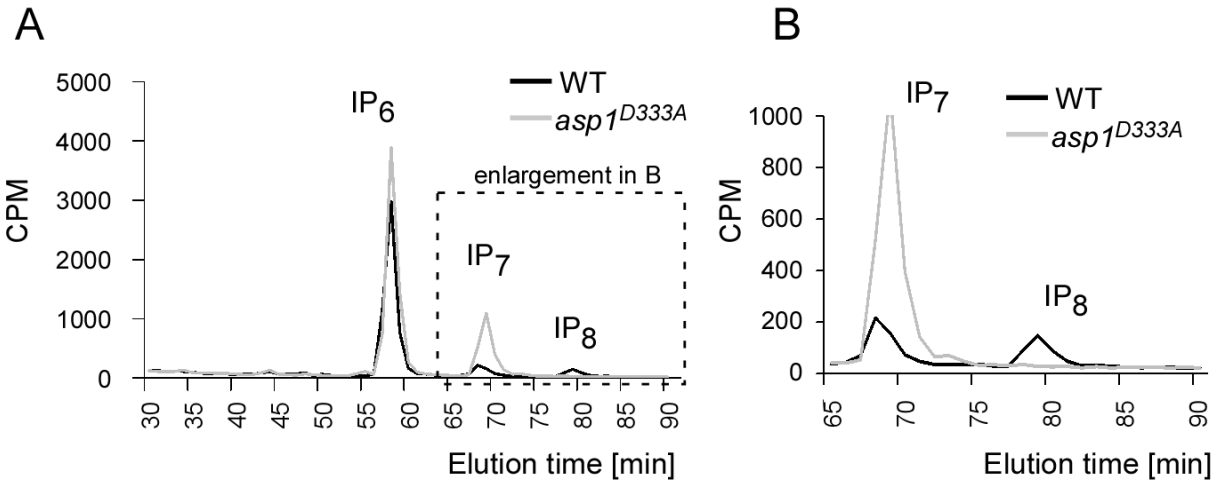

Fig2. Inositol polyphosphate profiles of wild-type and *asp1*^{D333A} strains. A) HPLC elution profile of inositol polyphosphates of the wild-type (black) and *asp1*^{D333A} strain (grey). B) Enlargement of IP_7 and IP_8 peaks from the HPLC elution profile of the *wild-type* strain (black) and *asp1*^{D333A} strain (grey). *S.pombe* cells were radiolabeled with [^{3}H] inositol in minimal media and cell lysates were separated using anion-exchange HPLC. Representative inositol polyphosphate profiles of two independent experiments.

Inositol polyphosphates of the *asp1Δ* strain were also analyzed. Similar to the *asp1*^{D333A} strain, the most abundant inositol polyphosphate species in *asp1Δ* were IP_6 and IP_7, with no detectable levels of IP_8 (Fig3A, enlargement of IP_7 and IP_8 peaks in B).

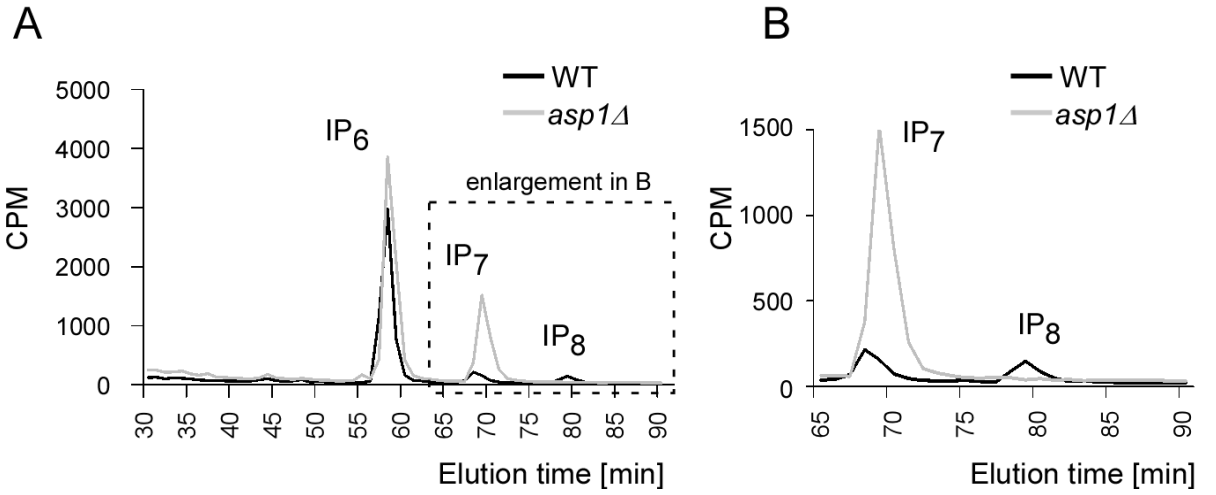

Fig3. Inositol polyphosphate profiles of wild-type and *asp1Δ* strains. A) HPLC elution profile of inositol polyphosphates of the wild-type (black) and *asp1Δ* strain (grey). B) Enlargement of IP_7 and IP_8 peaks in the HPLC elution profile of the wild-type strain (black) and *asp1Δ* strain (grey). *S.pombe* cells were radiolabeled as in Fig2. Representative examples of inositol polyphosphate profiles of two independent experiments.

Thus, in absence of Asp1 kinase activity, IP_7 levels increase and IP_8 levels decrease whereas IP_6 levels remain invariable. These results demonstrate that the preferable substrate for the Asp1 kinase reaction is IP_7 which is then converted to IP_8 under physiological conditions.

Next I assessed if an increase of Asp1 kinase activity beyond that of a wild-type strain had the opposite effect, i.e. an increase of IP_8 levels. Either a vector control or a plasmid coding for *asp1*$^{1-364}$ were transformed in a wild-type strain and inositol polyphosphates were analyzed. In comparison to the wild-type control, plasmid-borne expression of *asp1*$^{1-364}$ led to an increase of the two detectable inositol pyrophosphates species, IP_7 and IP_8 (Fig4A). However, the accumulation of IP_7 was about 2-fold higher than the one of IP_8 (Fig4B). This result proves that, as expected, an increase of Asp1 kinase activity leads to higher IP_8 levels. However, under non-physiological conditions, it appears that IP_6 can be used as a substrate by Asp1$^{1-364}$ to generate IP_7 as has been shown *in vitro*. (Pöhlmann et al., 2014).

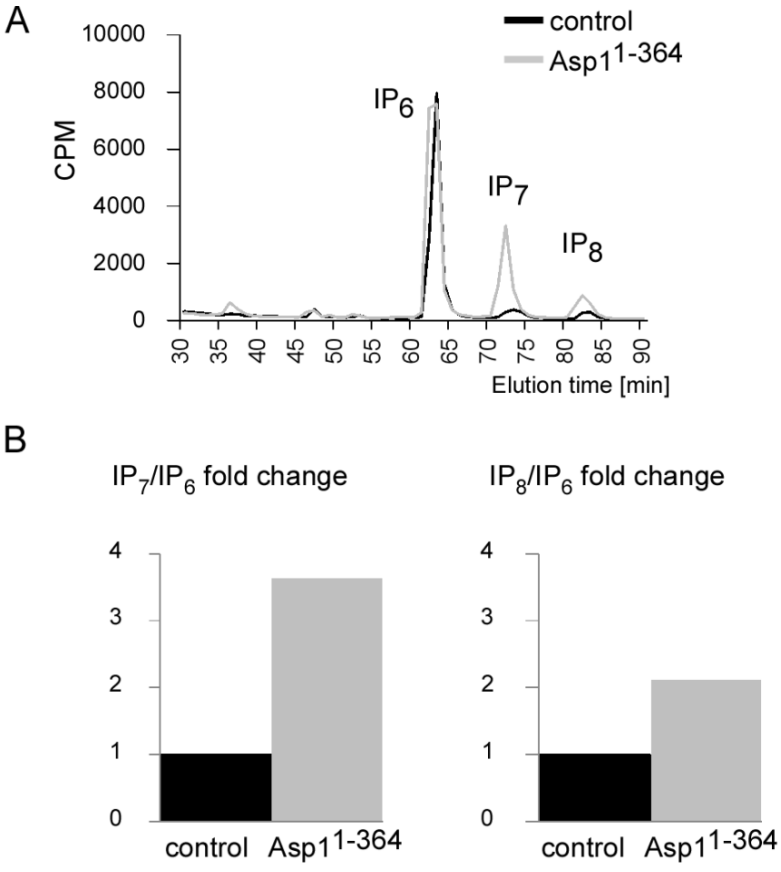

Fig4. Plasmid-borne expression of *asp1*$^{1-364}$ increases inositol pyrophosphates levels. A) HPLC elution profile of inositol polyphosphates of a wild-type strain transformed with vector control (black) or expressing the *asp1*$^{1-364}$ from the thiamine-repressible promoter *nmt1*$^{+}$ (grey). B) Results represented as IP_7/IP_6 or IP_8/IP_6 ratios. Ratios were calculated relative to IP_6 and normalized to the vector control. *S.pombe* cells were radiolabeled with [^{3}H] inositol in thiamine-less minimal media and cell lysates were separated using anion-exchange HPLC. Representative inositol polyphosphate profiles of two independent experiments. Figure and figure legend modified from (Pascual-Ortiz et al, 2017 submitted manuscript)

3.1.2. *In vitro* analysis of Asp1 C-terminal domain enzymatic activity

The C-terminal domain of Vip1-like family members contains the conserved signature of the Histidine Acid Phosphatase superfamily (HAP) (Fridy et al., 2007). However prior to the beginning of my study, no enzymatic function for this domain had been reported for any member of the Vip1-like family, as a matter of fact a publication from 2011 stated categorically that Vip1 proteins had no phosphatase activity (Gokhale et al., 2011). In contrast, studies from our group had described that *in vitro* the C-terminal domain of Asp1 negatively regulates the inositol pyrophosphate output (IP_7) of the N-terminal kinase domain, suggesting a pyrophosphatase activity of Asp1 C-terminal domain (Pohlmann et al., 2014).

To elucidate the function of Asp1 C-terminal domain, a mutagenesis analysis of the conserved signature of Asp1 C-terminal domain was performed. Five conserved amino acids conform the HAP signature (**RH**AD**R** and **HI**) (Rigden, 2008). In my study, each of the amino acids was replaced by alanine with the exception of the amino acid at position 808 where isoleucine was replaced by aspartate (Fig5).

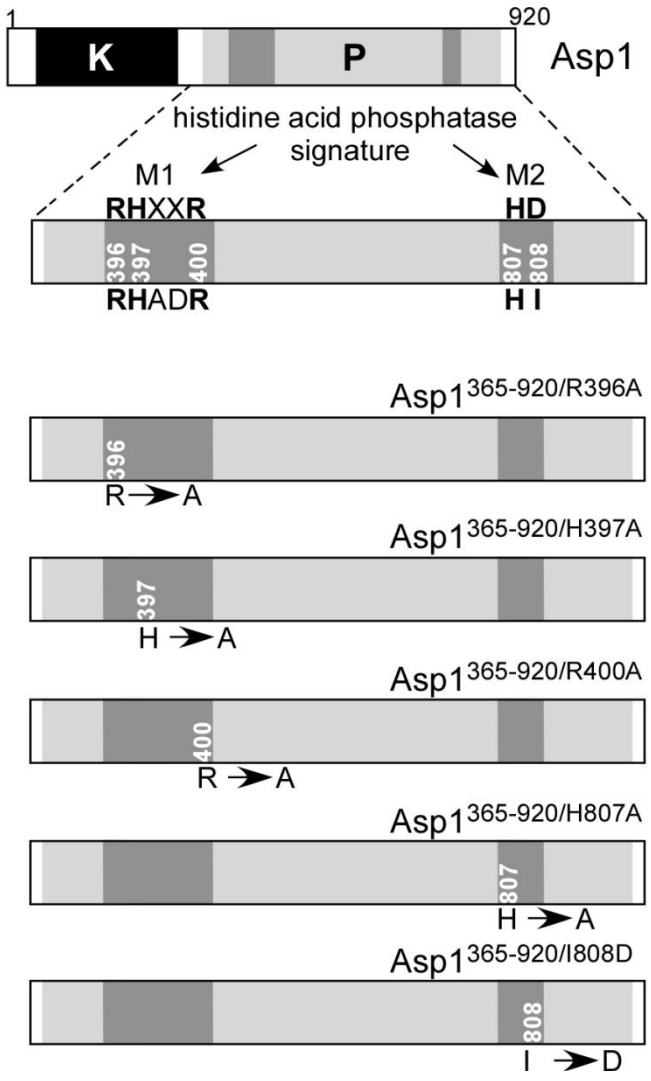

Fig5. Recombinant Asp1$^{365-920}$ variants used in this study. Top: full-length Asp1 shows the N-terminal kinase domain (K black) and the C-terminal pyrophosphatase domain (P grey). M1 and M2 (dark grey) represent the two conserved motifs part of the histidine acid phosphatase signature. **RH**AD**R** and **HI**, respectively. Bottom: Asp1 C-terminal mutants are depicted with the corresponding amino acid changes. Figure and figure legend modified from (Pascual-Ortiz et al, 2017 submitted manuscript).

During the process of my study, a publication reported that bacterially expressed Asp1 protein could associate with an iron-sulfur cluster which inhibits the pyrophosphatase activity (Wang et al., 2015). In order to examine whether the mutations of the conserved histidine acid phosphatase signature affected the assembly of an iron-sulfur cluster into Asp1 C-terminal domain, the presence of an iron-sulfur cluster in bacterially expressed Asp1$^{365\text{-}920}$ variants was determined. Proteins which contain iron-sulfur clusters show an absorption distinct feature at a wavelength of 420 nm, thus Asp1$^{365\text{-}920}$ protein samples were subjected to spectroscopic analysis in ultraviolet and visible (UV/VIS) range (Fig6).

The absorption spectra of Asp1$^{365\text{-}920}$ revealed that no significant iron-sulfur clusters were present in the protein sample (Fig6A). The same was observed when either Asp1$^{365\text{-}920/H397A}$, Asp1$^{365\text{-}920/R396A}$, Asp1$^{365\text{-}920/R400A}$, Asp1$^{365\text{-}920/H807A}$ or Asp1$^{365\text{-}920/I808D}$ proteins were analyzed (Fig6B-F). These results proved that the protein samples to be used to determine Asp1$^{365\text{-}920}$ pyrophosphatase activity contain no iron-sulfur clusters.

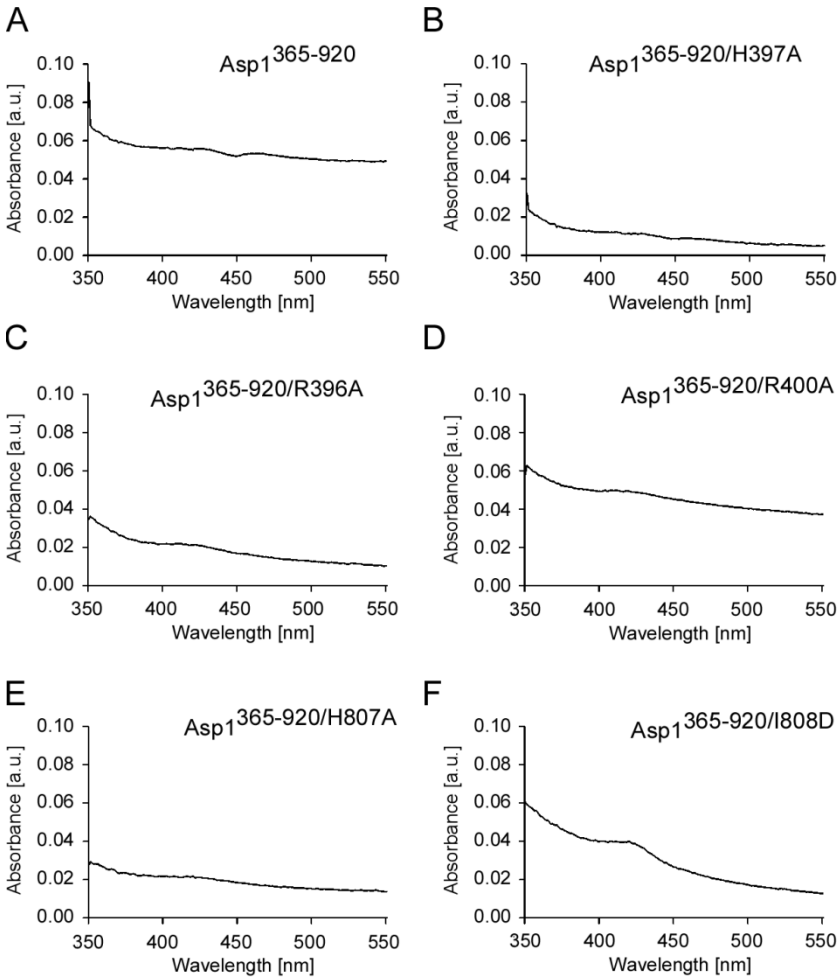

Fig6. Determination of possible iron-sulfur clusters in Asp1$^{365\text{-}920}$ variants. UV–visible absorption spectra of recombinant Asp1$^{365\text{-}920}$, Asp1$^{365\text{-}920/H397A}$, Asp1$^{365\text{-}920/R396A}$, Asp1$^{365\text{-}920/R400A}$, Asp1$^{365\text{-}920/H807A}$ and Asp1$^{365\text{-}920/I808D}$ are shown. ~1 µg/µl protein concentration used. Figure and figure legend modified from (Pascual-Ortiz et al, 2017 submitted manuscript).

To examine the Asp1 C-terminal domain function, recombinant GST-tagged constructs containing solely the C-terminal domain of Asp1, Asp1$^{365-920}$, were generated and their enzymatic activity was analyzed *in vitro* using Asp1-generated IP_7 as a substrate (Fig7). The products of the enzymatic reaction were separated by PAGE and detected by Toluidine blue staining (Loss et al., 2011).

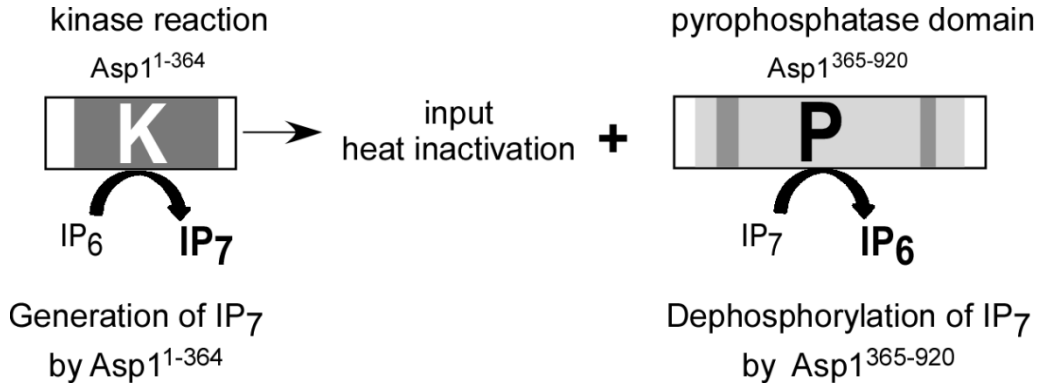

Fig7. Representation of the experimental design to measure *in vitro* Asp1 pyrophosphatase activity. After *in vitro* generation of IP_7 by the Asp1$^{1-364}$ (kinase domain), the protein was heat inactivated. To this (input) Asp1 C-terminal domain was added and incubated at 37°C during 16 hours. The resulting inositol polyphosphates were resolved on a 35.5% PAGE and stained with Toluidine. Figure and figure legend modified from (Pascual-Ortiz et al, 2017 submitted manuscript).

Changes in the mobility of the Toluidine stained bands on the polyacrylamide gel revealed dephosphorylation of IP_7. The absence of the IP_7 band and the stronger toluidine blue staining of the IP_6 band in comparison to the input control, demonstrated an enzymatic dephosphorylation of IP_7 by Asp1$^{365-920}$ (Fig8, second lane).Thus, Asp1$^{365-920}$ is enzymatically active and uses IP_7 generated by the kinase domain of Asp1 as a substrate. The IP_7 and IP_6 bands corresponding to the assay using Asp1$^{365-920/H397A}$, Asp1$^{365-920/R400}$ or Asp1$^{365-920/R396A}$ (Fig8, lanes 3,4 and 5 respectively) showed no difference in intensity in comparison to the input control (Fig8, lane 1). These results confirmed that these variants are catalytically inactive, and that the three residues within the first conserved motif, **RH**AD**R,** are essential for the pyrophosphatase activity of Asp1.

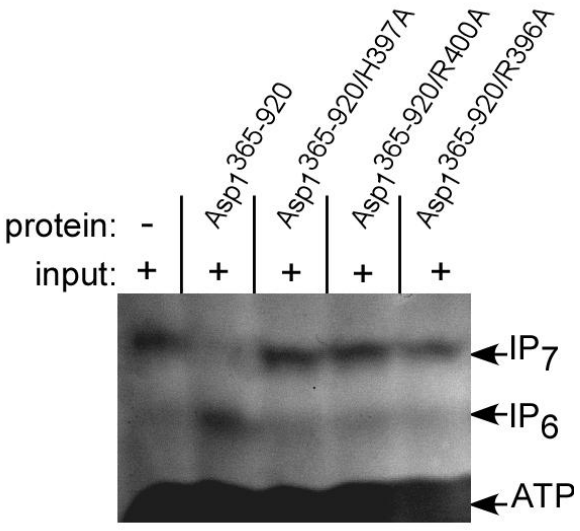

Fig8. Asp1$^{365-920}$ has pyrophosphatase activity. *In vitro* pyrophosphatase assay using Asp1$^{365-920}$, Asp1$^{365-920/H397A}$, Asp1$^{365-920/R400A}$, or Asp1$^{365-920/R396A}$. 8 µg of the indicated proteins were incubated with IP_7 generated by the Asp1 kinase domain (first lane shows input), incubated for 16 hours and the resulting inositol polyphosphates resolved on a 35.5% PAGE and stained with Toluidine Blue; - component not added , + component added. Assay performed by E. Walla. Figure and figure legend modified from (Pascual-Ortiz et al, 2017 submitted manuscript).

The results shown in Fig8 demonstrated that Asp1 dephosphorylates IP_7 *in vitro.* Furthermore, analysis of H397, R396 and R400 residues demonstrated that these conserved amino acids are essential for the pyrophosphatase activity of Asp1. In the general catalytic mechanism of histidine acid phosphatases, the first conserved motif **RH**xx**R** must be, in a three dimensional structure, in proximity to the second motif **HD**, where the aspartate residue acts as a proton donor during the reaction (Rigden, 2008). Thus, the second conserved motif of Asp1 pyrophosphatase domain **HI** was analyzed. Proteins Asp1$^{365\text{-}920/H807A}$ and Asp1$^{365\text{-}920/I808D}$ were tested in the *in vitro* pyrophosphatase assay and the resulting inositol polyphosphates were analyzed by PAGE.

Similar to wild-type Asp1 protein, IP_7 was reduced after incubation with Asp1$^{365\text{-}920/H807A}$, indicating that this variant displayed pyrophosphatase activity towards IP_7 (Fig9, broken box). Thus, this finding suggested that Histidine 807 is not essential for the pyrophosphatase reaction.

However, the protein Asp1$^{365\text{-}920/I808D}$ which now harbored the correct signature of histidine acid phosphatases, possessed no pyrophosphatase activity (Fig9, black box). This result revealed that isoleucine 808 is essential for Asp1 pyrophosphatase activity.

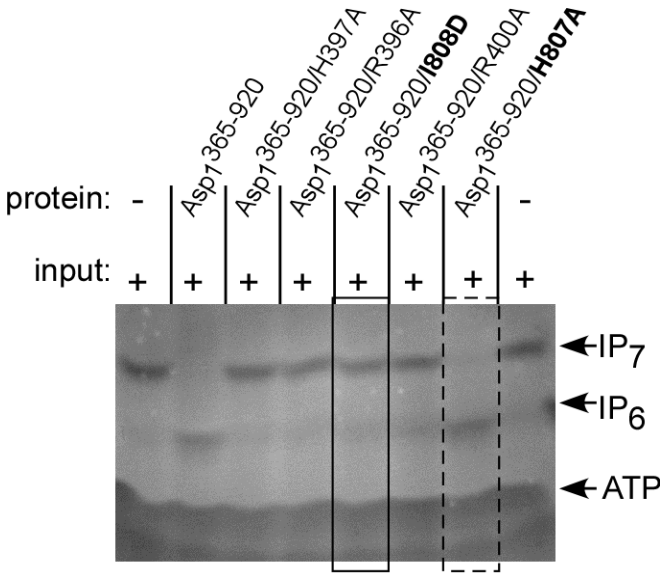

Fig9. Function of the HI domain of Asp1. *In vitro* pyrophosphatase assay using Asp1$^{365\text{-}920}$, Asp1$^{365\text{-}920/H397A}$, Asp1$^{365\text{-}920/R400A}$, Asp1$^{365\text{-}920/R396A}$, Asp1$^{365\text{-}920/H807A}$ or Asp1$^{365\text{-}920/I808D}$. 8 µg of the indicated proteins were incubated with IP_7 generated by the Asp1 kinase domain (input shown in lane 1), as described in Fig8: - component not added , + component added. Assay performed by E. Walla. Figure and figure legend modified from Pascual-Ortiz et al, 2017 (submitted manuscript).

It had been shown by another laboratory that Histidine 807 was essential for Asp1 pyrophosphatase function *in vitro* (Wang et al., 2015). In order to evaluate whether the enzymatic activity of Asp1$^{365\text{-}920/H807A}$ protein was comparable to the wild-type activity, an *in vitro* pyrophosphatase assay was performed using decreasing amounts of protein. Variant Asp1$^{365\text{-}920/R400A}$ was included in the assay as a control of inactive pyrophosphatase activity. (Fig10).

As already shown in Fig9, using 8µg of the protein Asp1$^{365\text{-}920/H807A}$ was sufficient to dephosphorylate IP_7 and no difference in activity was seen in comparison to the wild-type Asp1$^{365\text{-}920}$ (Fig10). However, when 4µg of protein were used in the assay, the activity of Asp1$^{365\text{-}920/H807A}$ was lower compared to the wild-type. Addition of 2µg of protein to the assay was sufficient to observe the pyrophosphatase activity of the wild-type protein but no activity was detected for Asp1$^{365\text{-}920/H807A}$. The control Asp1^{R400A} showed no activity regardless of the protein amount used. These results demonstrated that Asp1$^{365\text{-}920/H807A}$ has residual pyrophosphatase activity.

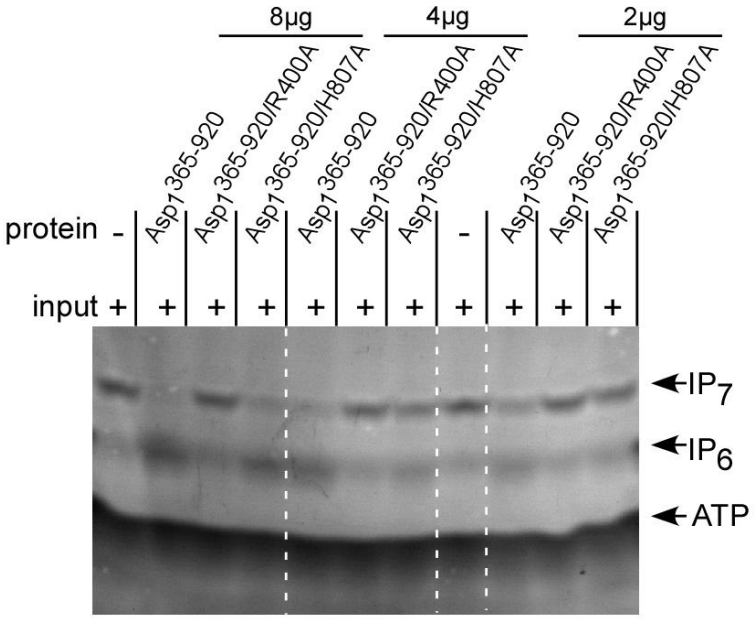

Fig10. Residual pyrophosphatase activity of Asp1$^{365\text{-}920/H807A}$. *In vitro* pyrophosphatase assay using Asp1$^{365\text{-}920}$, Asp1$^{365\text{-}920/R400A}$ or Asp1$^{365\text{-}920/H807A}$. Either 8, 4 or 2 µg of Asp1$^{365\text{-}920}$, Asp1$^{365\text{-}920/R400A}$ or Asp1$^{365\text{-}920/H807A}$ were incubated with IP_7 generated by the Asp1 kinase domain (first lane shows input), incubated for 16 hours and the resulting inositol polyphosphates resolved on a 35.5% PAGE and stained with Toluidine Blue; - component not added , + component added. Assay performed by E.Walla. Figure and figure legend modified from (Pascual-Ortiz et al, 2017 submitted manuscript).

The results obtained from the *in vitro* analysis of Asp1 pyrophosphatase activity revealed that the conserved domains are essential for enzymatic reaction. The differences observed in activity are not due to defects of iron-sulfur cluster incorporation among the Asp1$^{365\text{-}920}$ variants tested. All residues within the first domain of the conserved histidine acid phosphatase signature **RH**AD**R** (amino acids 396 to 400) are essential. However, histidine 807 in the second motif (HI) is not essential and, surprisingly, isoleucine 808 is required for the enzymatic activity of Asp1. The later finding points to a difference in the catalytic mechanism of Vip1 proteins in comparison to other members of the histidine acid phosphatase superfamily.

3.1.3. *In vivo* read-out of Asp1 C-terminal domain enzymatic activity

As previously shown by our group, modification of the ratio between Asp1 kinase/pyrohosphatase activities affected the microtubule cytoskeleton (Pöhlmann and Fleig, 2010; Pöhlmann et al., 2014; Topolski et al., 2016). Variant Asp1^{D333A} (kinase-dead) was unable to generate IP_7 *in vitro* whereas Asp1^{H397A} (pyrophosphatase-dead) increased two fold the IP_7 output of the kinase in comparison to the wild-type protein (Pöhlmann et al., 2014). In line with this, the *in vivo* sensitivity to the microtubule poison thiabendazole (TBZ) of the strain *asp1^{D333A}* was increased while it was reduced in the strain *asp1^{H397A}*, demonstrating that the sensitivity to microtubule poisons is a reliable indicator of Asp1 generation of inositol pyrophosphates *in vivo* (Pohlmann et al., 2014).

Hence, to study *in vivo* function of Asp1 C-terminal domain, the sensitivity to TBZ was used as an *in vivo* read-out of Asp1-generated inositol pyrophosphates. The sensitivity to TBZ would be increased in cells with reduced IPPs levels as a result of Asp1 pyrophosphatase activity.

A wild-type strain expressing either *asp1$^{365-920}$* or *asp1$^{365-920/H397A}$* on a plasmid from the thiamine-repressible promoter, *nmt1^{+}* was grown with or without TBZ (Fig11A). High expression of *asp1$^{365-920}$* reduced growth and increased TBZ sensitivity suggesting that *asp1$^{365-920}$* reduced cellular inositol pyrophosphate levels. The mutant *asp1$^{365-920/H397A}$* did not affect TBZ sensitivity indicating that, Asp1$^{365-920/H397A}$ was enzymatically inactive and did not have an effect on cellular inositol pyrophosphates (Fig11A). This result indicated that extra Asp1$^{365-920}$ reduces the level of inositol pyrophosphates produced by the kinase domain (Fig11B).

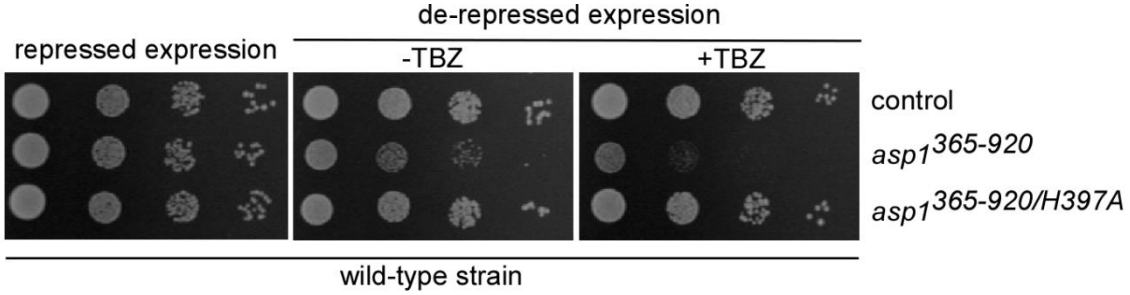

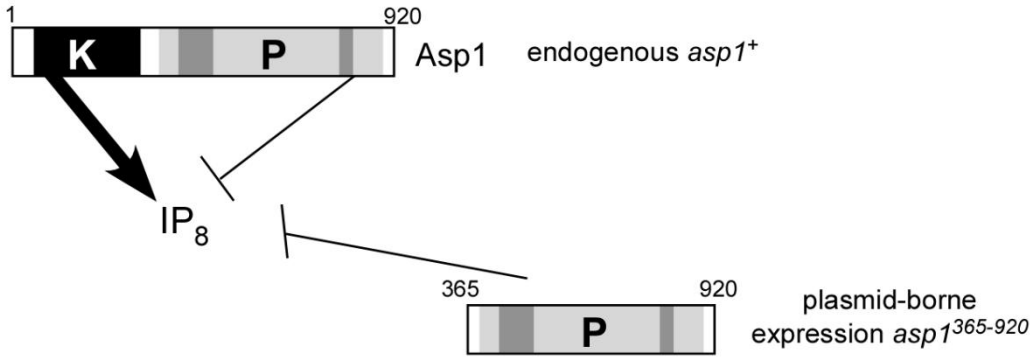

Fig11. *In vivo* function of Asp1$^{365-920}$. Top: Serial dilution patch tests (10^4 to 10^1cells) of a wild-type strain transformed with vector (control), or plasmids expressing *asp1*$^{365–920}$ or *asp1*$^{365–920/H397A}$ from the thiamine-repressible promoter *nmt1*$^+$. Transformants were grown under plasmid selective conditions in absence or presence of 7µg/ ml thiabendazole (TBZ) at 25°C for 7 days. Bottom: Model of Asp1 C-terminal domain function. Plasmid expression of *asp*$^{365-920}$ dephosphorylates inositol pyrophosphates produced by the kinase domain.

To determine the role of the other conserved residues part of the histidine acid phosphatase domain of Asp1 *in vivo*, the TBZ sensitivity of a wild-type strain expressing *asp1*$^{365-920}$, *asp1*$^{365–920/R396A}$, *asp1*$^{365–920/H397A}$, *asp1*$^{365–920/R400A}$, *asp1*$^{365-920/H807A}$ *or asp1*$^{365-920/I808D}$ on a plasmid from the thiamine-repressible promoter, *nmt1*$^+$ was analyzed.

Compared to the vector control, expression of *asp1*$^{365–920/R396A}$ and *asp1*$^{365–920/R400A}$ did not have an effect on TBZ sensitivity (Fig12), suggesting that, as *asp1*$^{365–920/H397A}$, these proteins had no pyrophosphatase activity. In contrast, Asp1$^{365-920/H807A}$ reduced growth upon higher plasmid expression and increased TBZ sensitivity of the wild-type strain. This effect was similar to the one caused by the wild-type protein and indicated that both proteins were enzymatically active *in vivo* (Fig12). Asp1$^{365-920/I808D}$ showed no effect on TBZ sensitivity, indicating that it had no pyrophosphatase activity (Fig12).

As the expression levels of all proteins were similar (FigS2), these findings are consistent with our *in vitro* data and provide strong support that Asp1$^{365-920}$ enzymatic activity modulates the levels of inositol pyrophosphates *in vivo*. Furthermore the increased TBZ sensitivity caused by Asp1$^{365-920/H807A}$ was also in accordance with the residual enzymatic activity that this protein exhibited *in vitro* (Fig9 and Fig10).

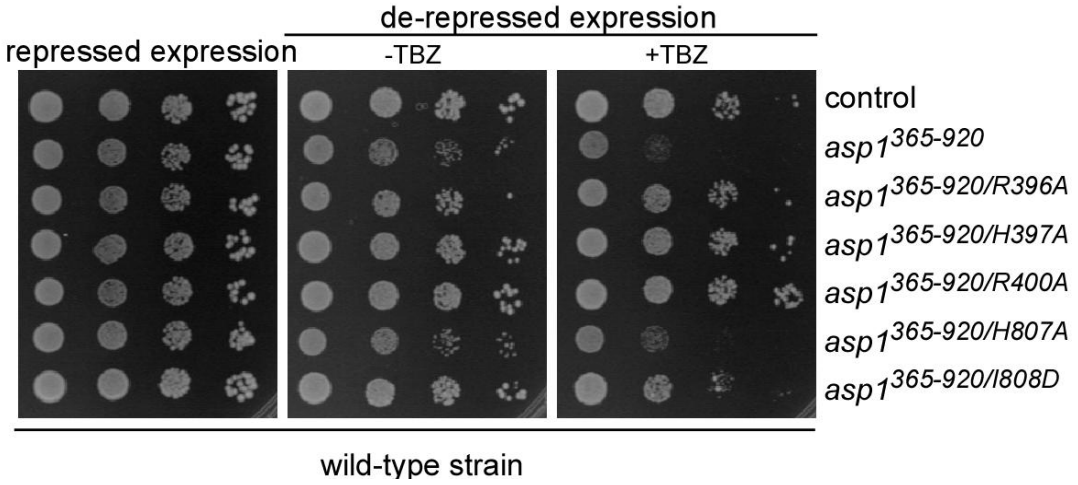

Fig12. *In vivo* function of Asp1$^{365-920}$ variants. A)Serial dilution patch tests (10^4 to 10^1cells) of wild-type strain transformed with vector (control) or plasmids expressing *asp1*$^{365-920}$, *asp1*$^{365–920/R396A}$, *asp1*$^{365–920/H397A}$, *asp1*$^{365–920/R400A}$, *asp1*$^{365-920/H807A}$ *or asp1*$^{365-920/I808D}$ from the thiamine-repressible promoter *nmt1*$^+$. Transformants were grown under plasmid selective conditions in absence or presence of thiamine and 7µg/ ml thiabendazole (TBZ) at 25°C for 7 days.

Next, to determine whether the Asp1 pyrophosphatase function was functional independently of the kinase activity *in vivo*, the TBZ sensitivity of a wild-type strain expressing either *asp1*$^{365-920}$ or the full-length *asp1*^{D333A} on a plasmid was analyzed.

Asp1$^{365\text{-}920}$ and the variant Asp1^{D333A} reduced growth and increased the TBZ sensitivity of the wild-type strain (Fig13A). This result suggested that, as Asp1$^{365\text{-}920}$, the Asp1^{D333A} protein harbors only pyrophosphatase activity capable of dephosphorylating inositol pyrophosphates *in vivo* (Fig13B).

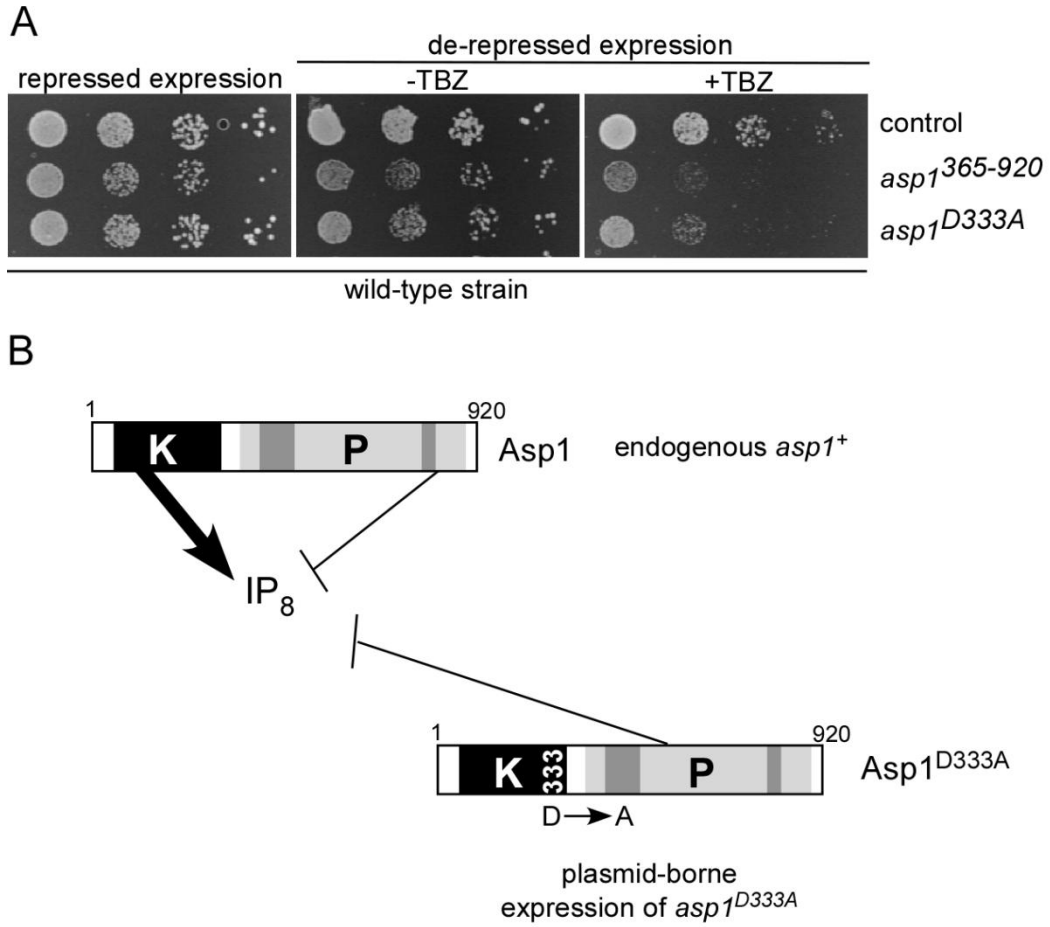

Fig13. *In vivo* function of Asp1^{D333A} variant. A)Serial dilution patch tests (10^4 to 10^1cells) of wild-type strain transformed with vector (control) or plasmids expressing *asp1*$^{365\text{-}920}$ or *asp1*^{D333A} from the thiamine-repressible promoter *nmt1*$^{+}$. Transformants were grown under plasmid selective conditions in absence or presence of thiamine and 8µg/ ml thiabendazole (TBZ) at 25°C for 7 days. B) Model of Asp1^{D333A} function. Plasmid expression of *asp*^{D333A} alters the levels of inositol pyrophosphates produced by the kinase domain by dephosphorylation.

Next, to confirm that the *in vivo* TBZ phenotype caused by plasmid-borne expression of asp1$^{365\text{-}920}$ did not require the presence of the endogenous *asp1* C-terminal domain function, a plasmid encoding *asp1*$^{365\text{-}920}$ was expressed in the strains *asp1*^{H397A} and *asp1*$^{1\text{-}364}$, in which the pyrophosphatase domain is inactive or absent, respectively. In the *asp1*^{H397A} strain the first highly conserved histidine residue had been replaced by alanine affecting the function of the C-terminal domain, and in *asp1*$^{1\text{-}364}$ the entire C-terminal domain containing the pyrophosphatase domain of Asp1 was deleted, thus it was possible to study the effect that the plasmid expression of *asp1*$^{365\text{-}920}$ could cause in absence of functional endogenous C-terminal domain.

In comparison to vector control, plasmid-borne expression of *asp1*$^{365–920}$ in the *asp1*^{H397A} strain massively reduced growth and increased TBZ sensitivity while expression of *asp1*$^{365–920/H397A}$ showed only a slight increase (Fig14A). Same phenotype was observed in the *asp1*$^{1-364}$ strain in where plasmid-borne expression of *asp1*$^{365–920}$ also reduced growth and increased TBZ sensitivity while Asp1$^{365–920/H397A}$ had only slight effect (Fig14B).

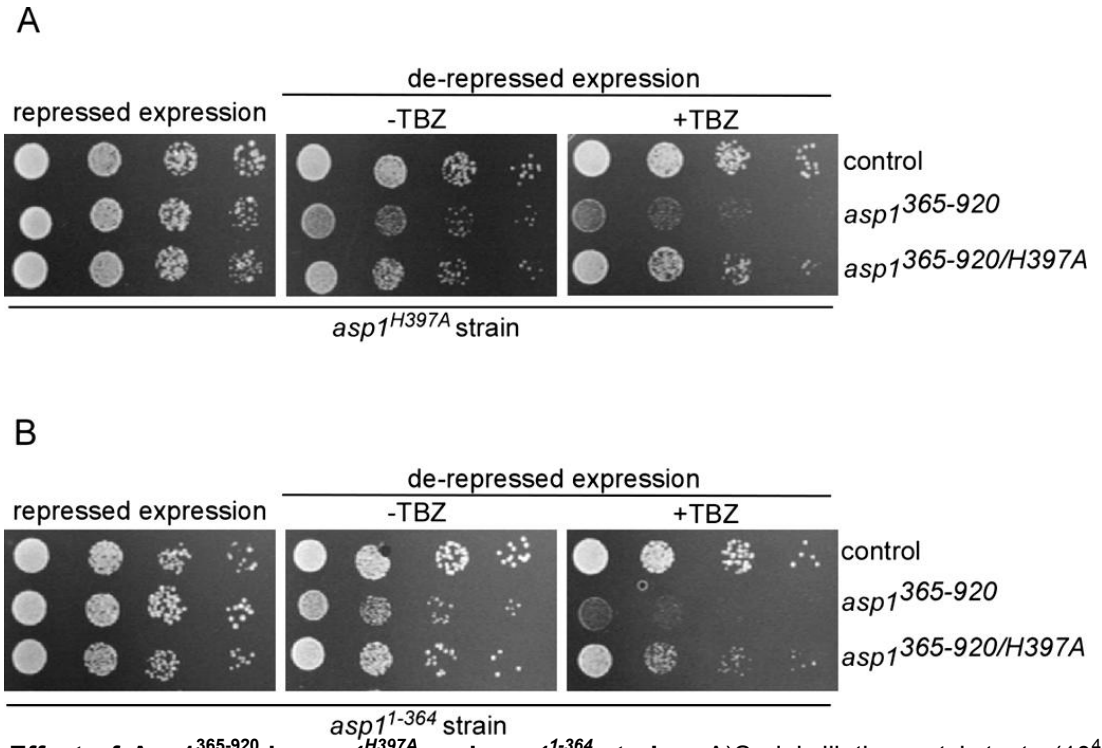

Fig14. Effect of Asp1$^{365-920}$ in *asp1*^{H397A} and *asp1*$^{1-364}$ strains. A)Serial dilution patch tests (10^4 to 10^1cells) of *asp1*^{H397A} strain transformed with vector (control) or plasmids expressing *asp1*$^{365-920}$ or *asp1*$^{365-920/H397A}$ from the thiamine-repressible promoter *nmt1*$^+$. B) Serial dilution patch tests (10^4 to 10^1cells) of the *asp1*$^{1-364}$ strain transformed with vector (control) or plasmids expressing *asp1*$^{365-920}$ or *asp1*$^{365-920/H397A}$ from the thiamine-repressible promoter *nmt1*$^+$. Transformants were grown under plasmid selective conditions in absence or presence of thiamine and 8µg/ ml thiabendazole (TBZ) at 25°C for 6 days.

Taken together, the phenotype observed strongly supported that Asp1$^{365-920}$ is enzymatically active *in vivo* and reduces the levels of Asp1-generated inositol pyrophosphates. In addition the conserved amino acids R396, H397, R400, and I808 were essential for the function of Asp1$^{365-920}$, with the exception of the second conserved histidine, H807. My finding implies that differences in the enzymatic mechanism between Asp1 pyrophosphatase domain and other members of the histidine acid phosphatase family exist.

To formally demonstrate if *in vivo* inositol pyrophosphates levels were altered upon plasmid-borne expression of *asp1*$^{365-920}$, inositol polyphosphates were radiolabeled in growing *S. pombe* cells.

A wild-type strain transformed with vector control showed three main peaks in the HPLC profile; IP_6, IP_7 and IP_8 (Fig15A). In comparison to the vector control, plasmid expression of *asp1*$^{365-920}$ decreased IP_8 levels and caused an increase of the IP_7 signal

(Fig15B). The inositol polyphosphate profile of Asp1$^{365\text{-}920/H397A}$ was similar to the wild-type control (Fig15C). A quantitative analysis of cellular inositol pyrophosphates relative to the precursor IP_6 is shown in Fig15D. IP_8 was greatly reduced in cells expressing *asp1*$^{365\text{-}920}$, while it remained invariable with *asp1*$^{365\text{-}920/H397A\ compared}$ to control cells. The opposite effect was observed for IP_7, which increased only when *asp1*$^{365\text{-}920}$ was expressed.

The results obtained, demonstrated that the Asp1$^{365\text{-}920}$ was enzymatically active *in vivo* and that the preferable cellular substrate of Asp1 pyrophosphatase activity is IP_8.

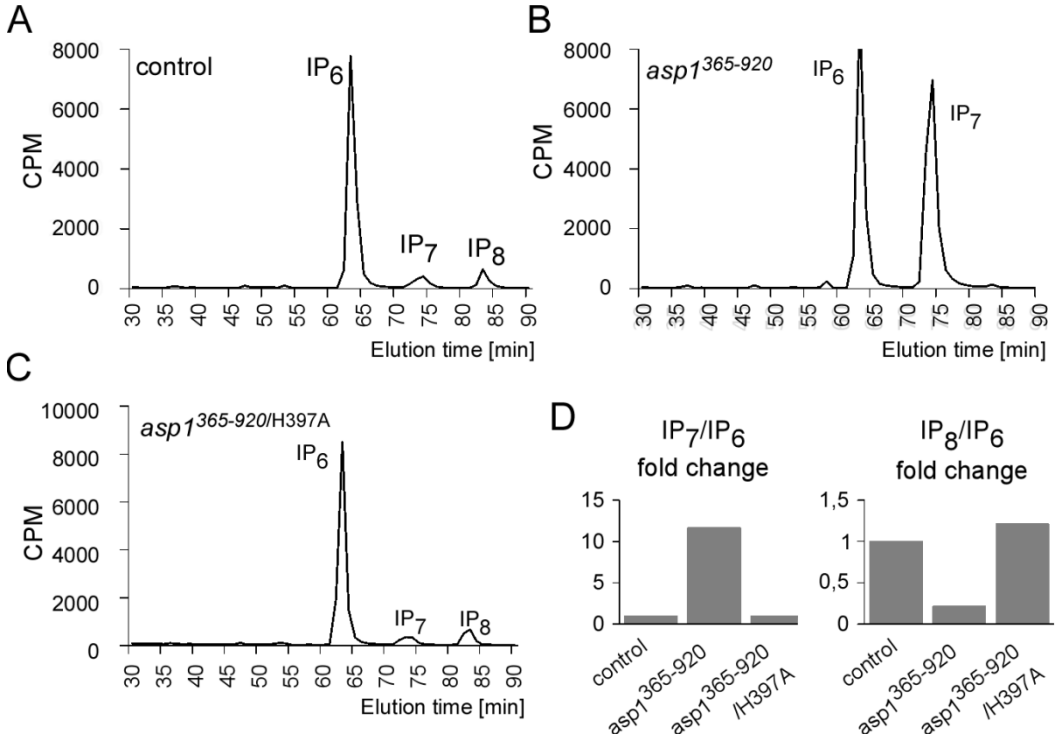

Fig15. Plasmid-borne expression of asp1$^{365\text{-}920}$ affects IPPs levels. A) HPLC elution profile of inositol polyphosphates of the wild-type strain transformed with vector control. B) HPLC elution profile of inositol polyphosphates of the wild-type strain expressing *asp1*$^{365–920}$ from the thiamine-repressible promoter *nmt1*$^{+}$. C) HPLC elution profile of inositol polyphosphates of the wild-type strain expressing asp1$^{365–920/H397A}$ from the thiamine-repressible promoter *nmt1*$^{+}$. D) Left: diagrammatic representation of IP_7 levels relative to IP_6 and normalized to the vector control using data from A, B and C. Right: diagrammatic representation of IP_8 levels relative to IP_6 and normalized to vector control using data from A, B and C . Figure and figure legend modified from Pascual-Ortiz et al. 2017 (submitted manuscript).

To better understand the contribution of the Asp1 C-terminal pyrophosphatase activity to the overall Asp1 enzymatic function in the context of full-length proteins in physiological conditions, strains in which the endogenous *asp1*$^{+}$ had been replaced by *asp1*^{H397A}, *asp1*^{I808D} or *asp1*$^{1\text{-}364}$ were analyzed.

Firstly, the resistance to TBZ was analyzed. A wild-type, *asp1*^{H397A}, *asp1*^{I808D} and *asp1*$^{1\text{-}364}$ strains were grown in full media, YE5S, with or without 12 µg/ml TBZ. Growth on the control plate was not affected in any of the strains tested (Fig16). However, upon addition of TBZ to the media, the strains *asp1*^{H397A} and *asp1*^{I808D} showed an increased resistance to

TBZ in comparison to the wild-type. Interestingly, *asp1*$^{1-364}$ exhibited a TBZ resistance comparable to the one of *asp1*^{H397A} and *asp1*^{I808D} strains (Fig16).

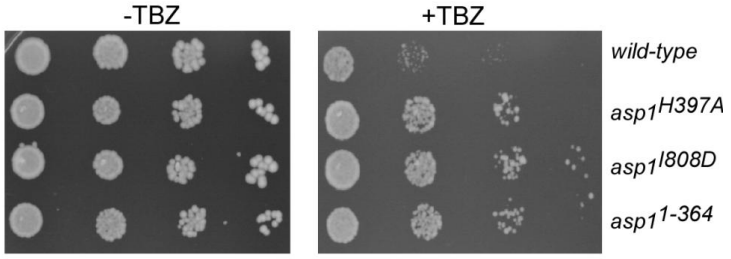

Fig16. *In vivo* TBZ resistance of endogenous *asp1* C-terminal domain mutants, *asp1*^{H397A}, *asp1*^{I808D} and *asp1*$^{1-364}$. Serial dilution patch tests (10^4 to 10^1cells) of wild-type, *asp1*^{H397A}, *asp1*^{I808D} and *asp1*$^{1-364}$ strains. Cells were grown in full media at 25°C for 5 days with or without 12µg/ml TBZ. Figure and figure legend modified from (Pascual-Ortiz et al., 2017 submitted manuscript).

Next, cellular inositol polyphosphates of the *asp1*^{H397A}, *asp1*^{I808D} and *asp1*$^{1-364}$ strains were analyzed. As already shown in Fig3, the inositol polyphosphate profile of the wild-type strain had three abundant peaks corresponding to IP_6, IP_7 and IP_8 (Fig17A). Inositol polyphosphates profiles of *asp1*^{H397A} *and asp1*^{I808D} strains showed an increased IP_8 peak in comparison to wild-type strain (Fig17B and C). The same effect was observed for the profile of the *asp1*$^{1-364}$ strain(Fig17D).

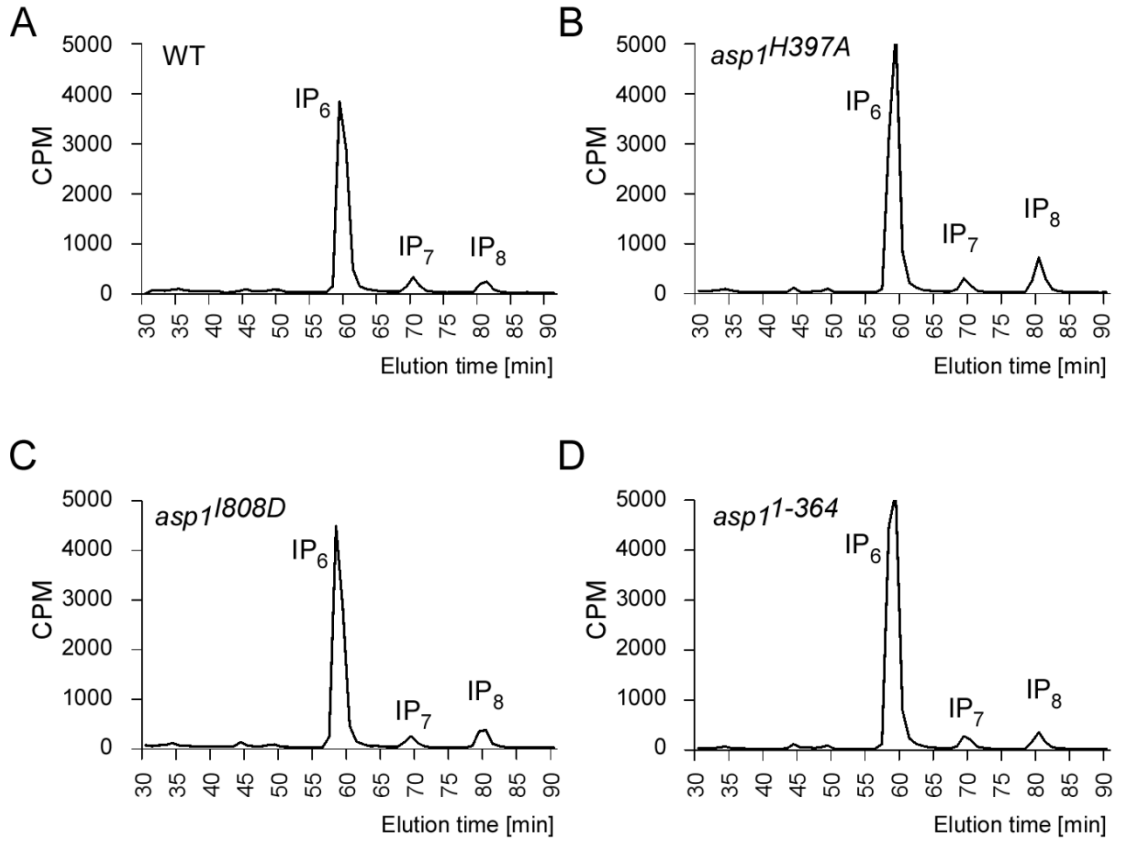

Fig17. IPP profiles of wild-type, *asp1*^{H397A}, *asp1*^{I808D} and *asp1*$^{1-364}$ strains. A) HPLC elution profile of inositol polyphosphates of the wild-type strain. B) HPLC elution profile of inositol polyphosphates of the *asp1*^{H397A} strain. C)HPLC elution profile of inositol polyphosphates of the *asp1*^{I808D} strain. D) HPLC elution profile of inositol polyphosphates of the *asp1*$^{1-364}$ strain. Figure and figure legend modified from Pascual-Ortiz, 2017 (submitted manuscript).

An enlargement of part of the HPLC elution profiles of *asp1*^{H397}, *asp1*^{I808D} and *asp1*$^{1-364}$ is shown in Fig18. Representation of the results shown as IP_8 to IP_7 ratio normalized to the wild-type showed that IP_8 levels were increased in the three strains analyzed (Fig18, right panels).

Together, these findings demonstrated that the endogenous pyrophosphatase activity of Asp1 modulates cellular pools of IP_8 in a dose-dependent manner. Extra Asp1 pyrophosphatase activity reduces the wild-type levels of IP_8 while lower Asp1 pyrophoshpatase activity increases wild-type IP_8 levels. Furthermore, the results showed that there is a correlation between intracellular levels of IP_8 and resistance to the microtubule poison TBZ.

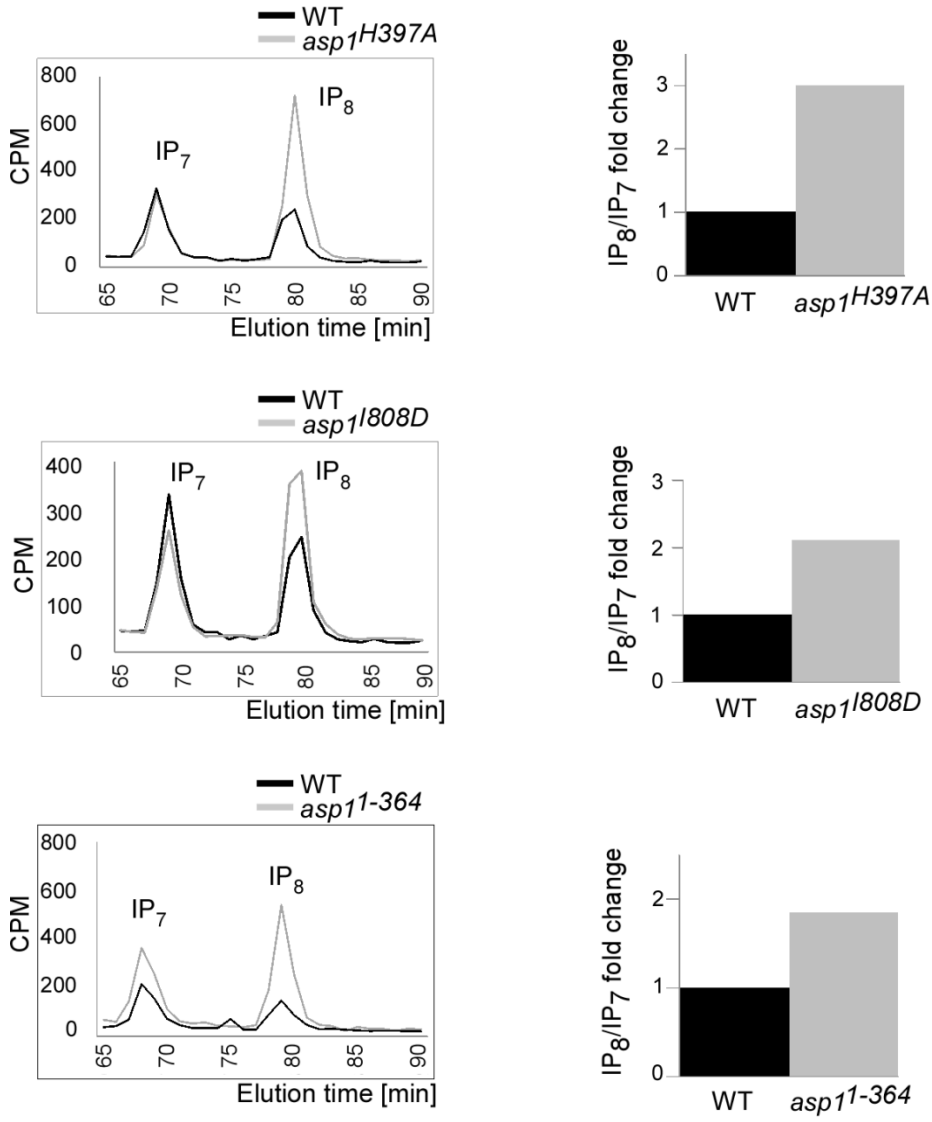

Fig18. Increase of IP_8 in *asp1*^{H397A}, *asp1*^{I808D} and *asp1*$^{1-364}$ strains. A)Left: Enlargement of IP_7 and IP_8 peaks in the HPLC elution profile of the *asp1*^{H397A} *and* wild-type strains using data from Fig17 A-B. Right: quantification of IP_8 levels relative to IP_7 and normalized to wild-type**.** B)Left: Enlargement of IP_7 and IP_8 peaks in the HPLC elution profile of the *asp1*^{I808D} and wild-type strain using data from Fig17A and C. Right: quantification of IP_8 levels relative to IP_7 and normalized to wild-type**.** C)Left: Enlargement of IP_7 and IP_8 peaks in the HPLC elution profile of the *asp1*$^{1-364}$ and wild-type strain using data from Fig17A and D. Right: quantification of IP_8 levels relative to IP_7 and normalized to wild-type**.** Figure and figure legend modified from (Pascual-Ortiz, 2017 submitted manuscript)

3.1.4. Analysis of the two Asp1 enzymatic activities

Asp1 N-terminal kinase domain and C-terminal pyrophosphatase domain have opposing enzymatic functions, namely synthesis and dephosphorylation of IP_8. However, the results shown in this chapter demonstrated that under physiological conditions, the pyrophosphatase activity dephosphorylates only a part of the IP_8 produced by the kinase domain.

To learn more about these two opposing activities, wild type *asp1*$^{+}$ was expressed on a plasmid in the *asp1Δ* strain and the TBZ sensitivity analyzed in comparison to the one caused by the expression of *asp1*$^{1\text{-}364}$ or *asp1*$^{365\text{-}920}$. Transformants were grown under plasmid selective conditions with or without TBZ. Wild-type Asp1 protein rescued the TBZ sensitivity of the strain (Fig19. *asp1*$^{+}$ *versus* control), although the rescue caused by expression of *asp1*$^{1\text{-}364}$ was stronger. Plasmid-borne expression of *asp1*$^{365\text{-}920}$ had a very slight effect on growth (Fig19). Comparison of the TBZ phenotypes caused by Asp1, Asp1$^{1\text{-}364}$ and Asp1$^{365\text{-}920}$ suggested that under high expression conditions the wild type protein favors the kinase activity.

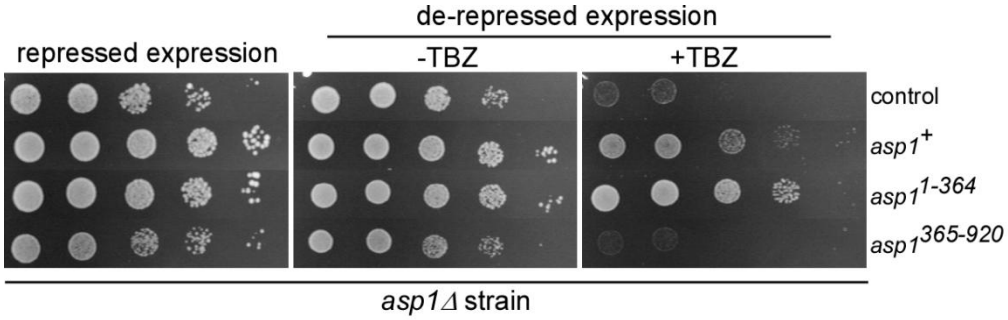

Fig19. Effect of full-length Asp1 in *asp1Δ* strain. Serial dilution patch tests (10^5 to 10^1cells) of *asp1Δ* strain transformed with vector (control) or plasmids expressing *asp1*$^{+}$, *asp1*$^{1\text{-}364}$ or *asp1*$^{365\text{-}920}$ from the thiamine-repressible promoter *nmt1*$^{+}$. Transformants were grown under plasmid selective conditions in absence or presence of thiamine and 10µg/ ml thiabendazole (TBZ) at 25°C for 7 days.

This and previous studies reported that plasmid expression of full-length pyrophosphatase mutants, *asp1*^{H397A} and *asp1*^{R400A} led to cell lysis, suggesting that higher than wild-type levels of inositol pyrophosphates, caused by an increased Asp1 kinase output, were toxic for the cell (FigS3) (Mulugu et al., 2007; Pöhlmann et al., 2014). Thus, if the kinase activity is favored in the wild type Asp1 protein, overexpression of wild type *asp1*$^{+}$ would also trigger cell lysis. Therefore, growth and TBZ phenotype of a wild-type, a*sp1*^{H397A} or *asp1*$^{1\text{-}364}$ strains expressing *asp1*$^{+}$ on a plasmid from the *nmt1*$^{+}$ promotor was analyzed. Plasmid expression of *asp1*$^{+}$ did not affect the growth of the wild-type strain but increased the resistance to TBZ (Fig20 top). However, when *asp1*$^{+}$ was expressed in the *asp1*^{H397A} strain, the growth of the colonies on thiamine-less plates was reduced and almost no growth was observed when TBZ was present in the media. Similar phenotype was exhibited by *asp1*$^{1\text{-}364}$

strain expressing *asp1*$^{+}$ on a plasmid (Fig20 bottom). Examination of the colonies by ocular microscopy confirmed that Asp1 overexpression caused cell lysis in *asp1*^{H397A} and *asp1*$^{1-364}$ strains but not in the wild-type strain.

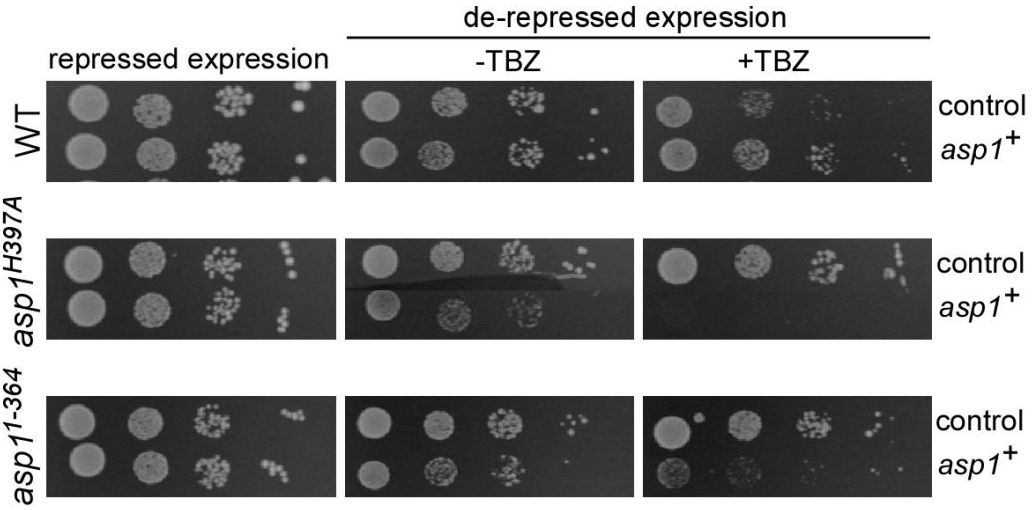

Fig20. Plasmid-borne expression of *asp1*$^{+}$ induces cell lysis in *asp1*^{H397A} *and asp1*$^{1-364}$ strains. Serial dilution patch tests (10^4 to 10^1cells) of strains transformed with vector (control) or a plasmid expressing *asp1*$^{+}$ from the thiamine-repressible promoter *nmt1*$^{+}$. Transformants were grown under plasmid selective conditions in absence or presence of thiamine and 9 µg/ ml thiabendazole (TBZ) at 25°C for 10 days.

These results proved that Asp1 protein increases the TBZ resistance of the wild-type and *asp1Δ* strain (Fig19 and 20) indicating that, as the endogenous *asp1*$^{+}$*,* the favored enzymatic activity of Asp1 is the kinase reaction. Accordingly, overexpression of Asp1 leads to cell lysis of strains asp1^{H397A} and asp1$^{1-364}$, in which IP_8 levels are higher than wild-type, suggesting that inositol pyrophosphates reached toxic levels.

3.2. Study of regulatory mechanism of Asp1 enzymatic activities

My analysis demonstrated that the cellular synthesis and dephosphorylation of IP_8 is carried out by Asp1. However, how these antagonistic activities are regulated within the same molecule is unknown. To date, there is no known modulator *in vivo* which could regulate the dual function of Asp1 or any other member of the Vip1 family. In this chapter two possible regulatory mechanisms will be presented.

3.2.1. Influence of the Asp1 interaction partner Met10 on Asp1 function.

To identify Asp1 interaction partners, a yeast-2-hybrid screen using pGBKT7-*asp1*$^{+}$ as bait and an *S.pombe* cDNA library constructed in pGAD GH was performed in our laboratory by Visnja Jakopec. One of the candidates identified was the Met10 protein, which interacted specifically with Asp1 pyrophosphatase domain.

To determine if Met10 had an effect on Asp1 pyrophosphatase function, the *met10*$^{+}$ ORF was cloned in *E.coli* expression vector pKM36 to generate recombinant GST-Met10 and tested if it had an effect on GST-Asp1$^{365\text{-}920}$ pyrophosphatase activity *in vitro*.

As also shown in the previous section, GST-Asp1$^{365\text{-}920}$ dephosphorylated IP_7 *in vitro* (Fig21, lane 2). However, addition of equimolar amounts of GST-Met10 and GST-Asp1$^{365\text{-}920}$ to the *in vitro* pyrophosphatase assay inhibited IP_7 dephosphorylation (Figure 21, lane 3). To exclude that the inhibitory effect observed was due to GST-GST interactions, the assay was repeated using His-Asp1$^{365\text{-}920}$ and GST-Met10. His-Asp1$^{365\text{-}920}$ could not dephosphorylate IP_7 in the presence of GST-Met10 (Figure 21, lane 4 and 5) proving that *in vitro* the Met10 protein is an inhibitor of the Asp1 pyrophosphatse activity.

Next, it was tested if Met10 could also inhibit other pyrophosphatases. The *S. cerevisiae* Ddp1 protein is a known unspecific inositol pyrophosphate phosphatase (Lonetti et al., 2011). Ddp1 enzymatic activity was not altered in the presence of equimolar amount of GST-Met10 (Figure 21, lanes 6 and 7). Thus, the inhibitory effect of Met10 is specific for Asp1$^{365\text{-}920}$ pyrophosphatase activity *in vitro.*

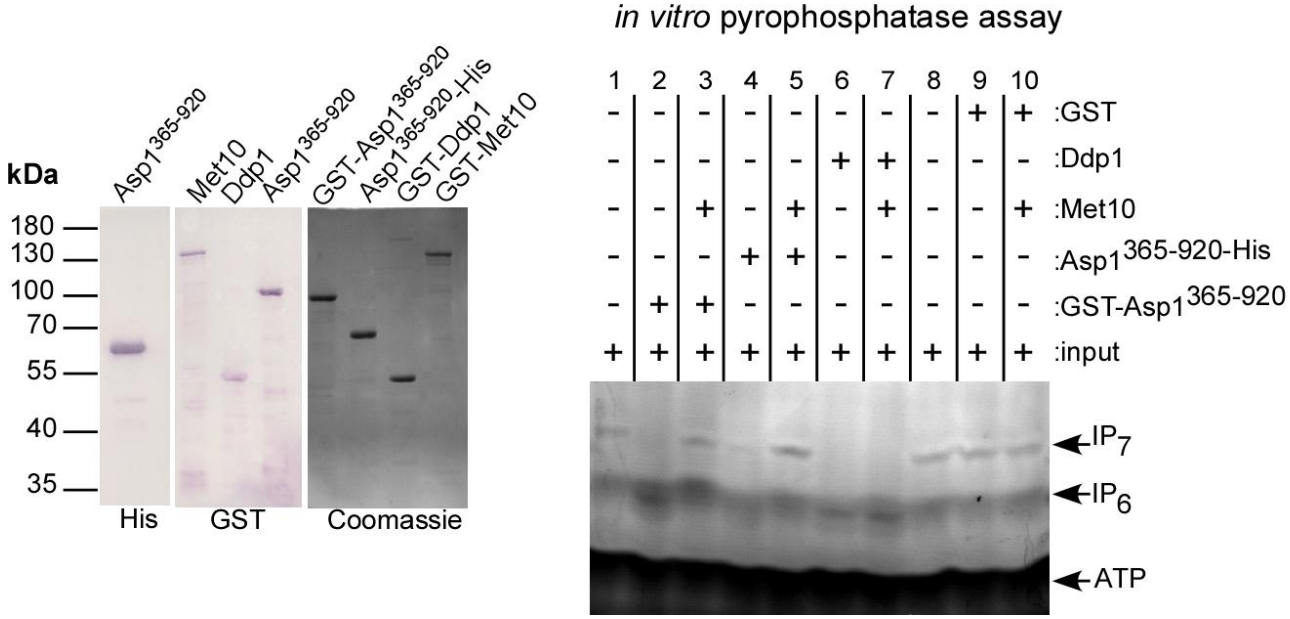

Fig21. Met10 inhibits Asp1 pyrophosphatase activity *in vitro*. Left: Western blot analysis using either GST antibody or His antibody. Proteins purified from *E. coli* were quantified (Coomassie stained gel on the right) and equal amounts loaded on a 10% PAGE. Left blots: His-tagged Asp1$^{365\text{-}920}$ and GST-tagged Asp1$^{365\text{-}920}$ run at the expected size of 66,1 kDa and 90,8 kDa respectively. GST-tagged Ddp1 and GST-tagged Met10 run at the expected size of 48 kDa and 137,8 kDa respectively. Right: *In vitro* pyrophosphatase assay using 4 µg of GST-Asp1$^{365\text{-}920}$ (lane 2) or 4 µg of GST-Asp1$^{365\text{-}920}$ in presence of 6 µg Met10 (lane 3). *In vitro* pyrophosphatase assay using 4 µg of Asp$^{365\text{-}920}$-His (lane 4) or 4 µg of Asp$^{365\text{-}920}$-His in presence of 8 µg Met10 (lane 5). *In vitro* pyrophosphatase assay using 2 µg of Ddp1-GST (lane 6) or 2 µg of Ddp1-GST in presence of 6 µg Met10 (lane7). Lanes 8 and 9 show empty assay or with addition of 2 µg GST respectively. *In vitro* pyrophosphatase assay using 6µg of GST-Met10 and 2 µg GST (lane10). All assays were incubated for 16 hours and the resulting inositol polyphosphates resolved on a 35.5% PAGE and stained with Toluidine Blue; - component not added , + component added. Assay performed by Eva Walla. Figure and figure legend modified from (Pascual-Ortiz et al., 2017 submitted manuscript).

Microscopic analysis of cells in which the endogenous *met10*$^{+}$ ORF was fused to GFP showed localization pattern similar to that observed for mitochondria. In fact, life cell imaging of Met10-GFP cells stained with the mitochondria specific dye Mitotracker showed a co-localization (Fig22)

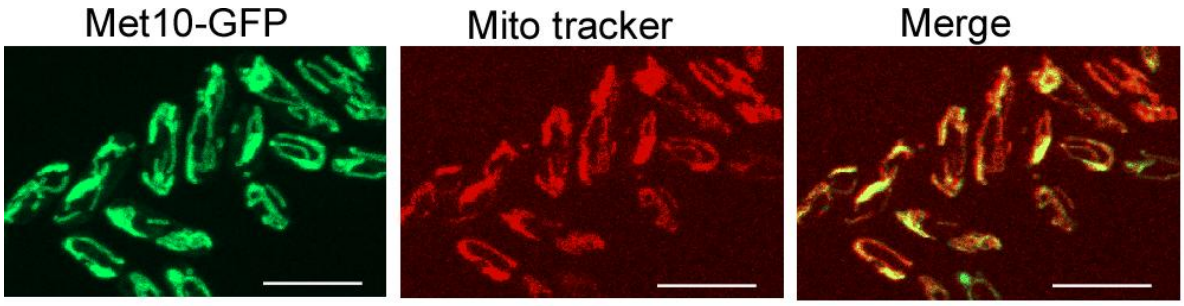

Fig22. Met10-GFP co-localizes with mitochondria. Life cell imaging of wild-type cells expressing met10-gfp (left panel). Mitochondria are visualized in red after staining with the specific dye Mitotracker (middle panel). Shown are maximum-projection images of interphase cells grown at 25°C. Bar, 10 µm. *met10-gfp* strain generated by Natascha Künzel. Image acquisition Marina Pascual Ortiz. Figure and figure legend modified from (Pascual-Ortiz et al., 2017 submitted manuscript).

To investigate a possible relevance of the inhibition of Asp1 pyrophosphatase activity by Met10 *in vivo*, the impact of Met10 on inositol polyphosphate metabolism was examined. Cells from a wild-type strain and *met10Δ* strain were radiolabeled with [^{3}H]inositol, however the *met10Δ* strain required the presence of methionine and cysteine to grow on minimal media (Fig23) and thus, the media used to radiolabel inositol polyphosphates was modified.

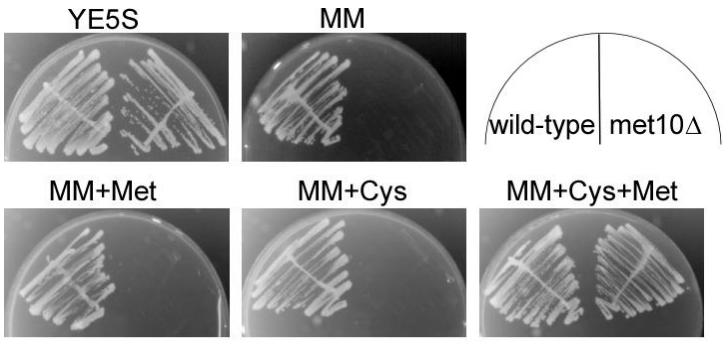

Fig23. *met10Δ* confers cysteine and methionine auxotrophy in *S. pombe*. Growth of wild-type and *met10Δ* strains on agar plates with different media; YE5S (full media), MM (minimal media), MM+methionine, MM+Cysteine and MM+Methionine+Cysteine. Plates were incubated at 25°C for 3 days. Figure and figure legend modified from (Pascual-Ortiz et al., 2017 submitted manuscript).

Wild-type and *met10Δ* cells were radiolabeled with [^{3}H]inositol in liquid minimal media containing 140μM Methionine and 330μM Cysteine. After incubation at 30°C, inositol polyphosphates were extracted and separared by HPLC. In comparison to the wild-type strain, the inositol polyphosphate profile of the *met10Δ* strain did not show any evident variation of IP_6, IP_7 or IP_8 intracellular levels in comparison to the wild-type grown under the same conditions (Fig24).

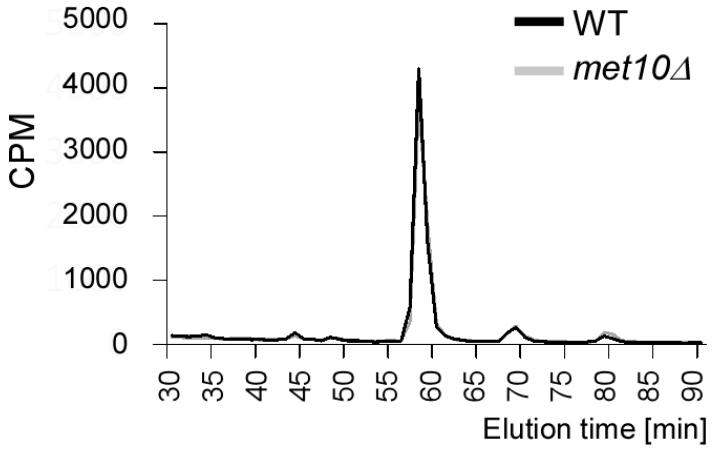

Fig24. Inositol polyphosphate profiles of wild-type and *met10Δ* strains. HPLC elution profile of inositol polyphosphates of the wild-type strain (black) and the *met10Δ* strain (grey). *S.pombe* cells were radiolabeled with [^{3}H] inositol in minimal media + 140μM Methionine and 330μM Cysteine and cell lysates were separated using anion-exchange HPLC. Figure and figure legend modified from (Pascual-Ortiz et al., 2017 submitted manuscript).

Next, the sensitivity to TBZ of the *met10Δ* strain was analyzed and compared to the wild-type. The double mutants *asp1^{D333A}met10Δ, asp1^{H397A}met10Δ* were also analyzed and compared their TBZ sensitivity to the single mutants *asp1^{D333A}* and *asp1^{H397A}*. Neither *met10Δ* nor the double mutants *asp1^{D333A} met10Δ* and *asp1^{H397A} met10Δ* showed a significant effect on TBZ sensitivity in comparison to the single *asp1* mutants (Fig25).

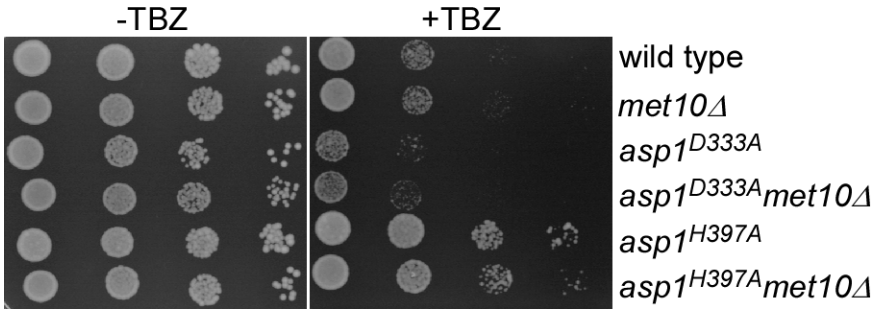

Fig25. Deletion of *met10$^+$* does not affect TBZ sensitivity. Serial dilution patch tests (10^4 to 10^1 cells) of the wild-type strain, *met10Δ*, *asp1^{D333A}, asp1^{H397,}* and the double-mutants *asp1^{D333A}met10Δ* and *asp1^{H397A}met10Δ*. Cells were grown in full media (YE5S) at 25°C for 5 days in presence of 9 μg/ml TBZ.

The results indicated that deletion of the *met10*$^{+}$ ORF does not cause an evident effect on inositol polyphosphate *in vivo* metabolism and, accordingly does not affect TBZ sensitivity under the conditions tested. To elucidate wheter overexpression of *met10*$^{+}$ would lead to measurable phenotype, *met10*$^{+}$ was expressed on a plasmid in the wild-type strain and the growth analyzed. Interestingly, high expression of *met10*$^{+}$ was lethal (Fig25).

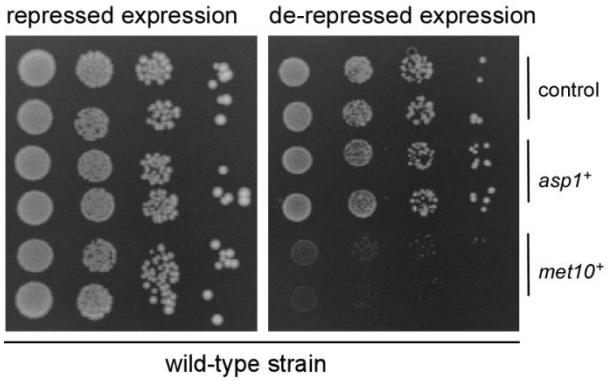

Fig25. Plasmid-borne expression of *met10*$^{+}$ reduces the growth of the wild-type strain. Serial dilution patch tests (10^{4} to 10^{1}cells) of the wild-type strain expressing *met10*$^{+}$ on a plasmid from the *nmt1*$^{+}$ promotor. Transformants were grown under plasmid selective conditions at 25°C for 8 days. Figure and figure legend modified from (Pascual-Ortiz et al., 2017 submitted manuscript).

To know if the effect caused by *met10*$^{+}$ overexpression required *asp1*$^{+}$, *met10*$^{+}$ was expressed on a plasmid in strains in which either the endogenous *asp1*$^{+}$ or the pyrophosphatase domain of *asp1*$^{+}$ was deleted; *asp1Δ* and *asp1*$^{1\text{-}364}$ strains, respectively. As in the wild-type strain, growth of the strain *asp1*$^{1\text{-}364}$ was reduced upon high expression of *met10*$^{+}$ (Fig26 top panel). Interestingly, plasmid expression of *met10*$^{+}$, although reduced growth, did not cause such a drastic effect in the *asp1Δ* strain (Fig26 bottom panel), suggesting that in absence of the complete *asp1*$^{+}$ ORF, the effect caused by Met10 is reduced.

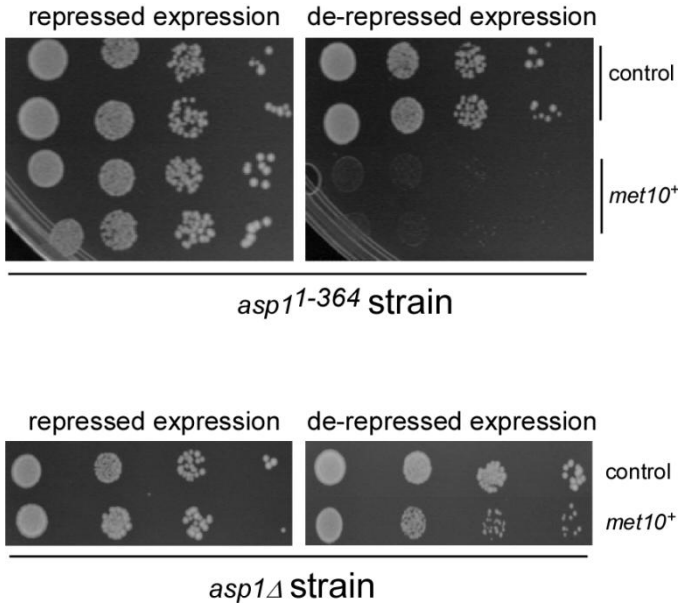

Fig26. Plasmid-borne expression of *met10*$^{+}$ reduced the growth of the *asp1*$^{1\text{-}364}$ and *asp1Δ* strains. Top: Serial dilution patch tests (10^{4} to 10^{1}cells) of the *asp1*$^{1\text{-}364}$ strain expressing *met10*$^{+}$ on a plasmid from the *nmt1*$^{+}$ promotor. Transformants were grown under plasmid selective conditions at 25°C for 8 days. Bottom: Serial dilution patch tests (10^{4} to 10^{1}cells) of the *asp1Δ* strain expressing *met10*$^{+}$ on a plasmid from the *nmt1*$^{+}$ promotor. Transformants were grown under plasmid selective conditions at 25°C for 11 days. The bottom part of the figure and figure legend are taken and modified from (Pascual-Ortiz et al., 2017 submitted manuscript).

All together these results proved that the pyrophosphatase activity of Asp1 is inhibited by Met10 *in vitro*. However, under the conditions tested *in vivo,* Met10 does not significantly influence the cellular IP_8 pools and plasmid-borne expression of *met10*$^{+}$ reduces growth independently of Asp1 pyrophosphatase function.

3.2.2. Role of cysteine 607 in Asp1 function *in vivo*

The second possible regulatory mechanism of Asp1 dual enzymatic activity is the binding to iron-sulfur clusters. It has been shown that the pyrophosphatase activity of Asp1 was inhibited upon iron-sulfur cluster binding *in vitro* (Wang et al., 2015). For the stable formation of an iron-sulfur cluster, cysteine ligands are commonly required. In Asp1, six cysteine residues have been proposed to be the likely candidates to bind the iron-sulfur cluster *in vitro (Wang et al., 2015).* However whether iron-sulfur clusters regulate the function of Asp1 *in vivo* is unknown. To that purpose, cysteine 607 was replaced by serine and the impact on Asp1 function *in vivo* analyzed.

Among the six other cysteines, C607 was chosen because it was not conserved in other members of Vip1, thus it was the possibility that an exchange of this amino acid would impact the protein structure was lower compared to the other conserved cysteines.

The *asp1Δ* strain expressing *asp1*$^{+}$ or *asp1*^{C607S} on a plasmid from the thiamine promoter was grown on plates with and without TBZ. The differences in sensitivity to TBZ were used as a read-out of Asp1 pyrophoshatase activity, i.e IP_8 levels.

As expected, in comparison to the vector control, wild-type Asp1 rescued the TBZ sensitivity of the *asp1Δ* strain (Fig28A). The same phenotype was observed upon plasmid-borne expression of *asp1*^{C607S}, which also showed higher TBZ resistance than the control (Fig28A). Since both proteins, Asp1 and Asp1^{C607S} were equally expressed (Fig28B), this results indicated that mutation of one of the cysteines involved in iron-sulfur coordination *in vitro* does not influence the pyrophosphatase activity of Asp1 *in vivo*. If cysteine 607 is required to bind the iron-sulfur cluster also *in vivo*, thus the binding of Asp1 to an iron-sulfur cluster is not the main regulatory mechanism under the conditions I tested.

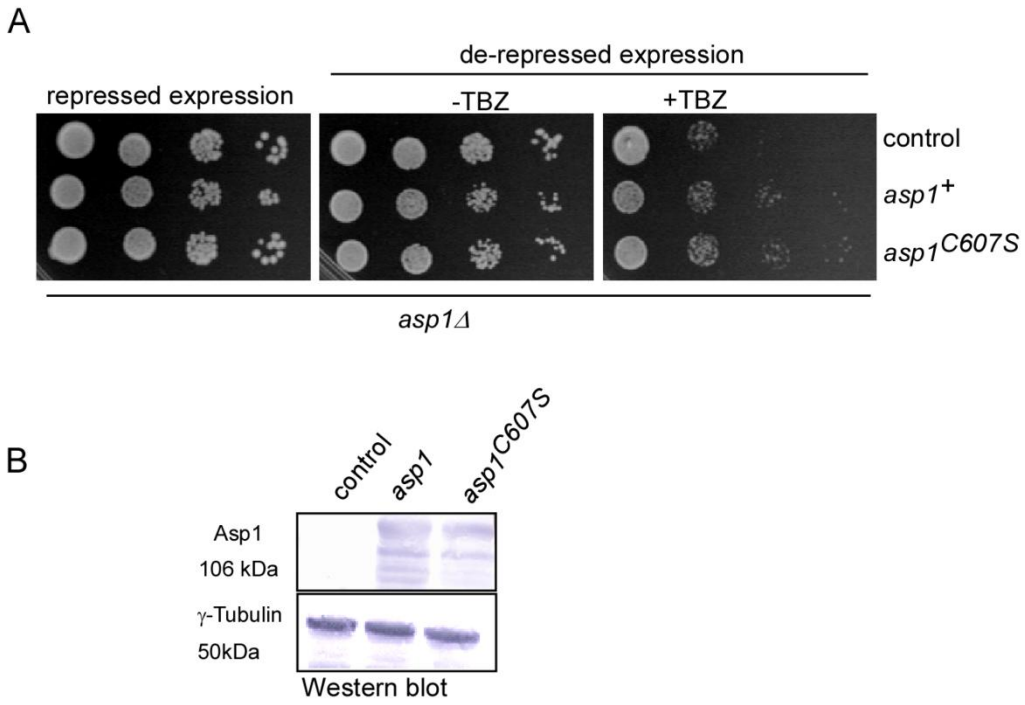

Fig28. **Expression of *asp1*^{C607S} variant in the *asp1Δ* strain.** A)Serial dilution patch tests (10^4 to 10^1cells) of the *asp1Δ* strain transformed with vector (control), *asp1*$^+$ or *asp1*^{C607S} from the thiamine-repressible promoter *nmt1*$^+$. Transformants were grown under plasmid selective conditions at 25°C for 7 days. B)Western blot analysis of Asp1 variants expressed in the *asp1Δ* strain under *nmt1*$^+$ de-repressing conditions using an Asp1 antibody (Feoktistova, McCollum et al. 1999). γ-tubulin protein was used as an internal control.

The data presented in section 3.2. demonstrate that Met10 inhibits Asp1 pyrophosphatase *in vitro.* However the contribution of Met10 in the *in vivo* regulation of Asp1 remains elusive at present. The growth reduction seen upon overexpression of Met10 depended on Asp1 function. The role of C607 in the regulation of Asp1 pyrophosphatase activity is not essential. Together, these evidences suggest that in the cellular context the regulation of Asp1 bifunctional activity might be very complex and involves the action of different components.

3.3. Asp1-generated IP_8 regulates the microtubule cytoskeleton and distribution of landmark proteins

Our laboratory has shown previously that Asp1-generated inositol pyrophosphates modulate the microtubule cytoskeleton. Absence of Asp1 kinase activity in the *asp1*^{D333A} strain resulted in highly dynamic microtubules which had an increased number of catastrophe events, faster growth rate and reduced pausing time at cell the tips. In addition *asp1*^{D333A} cells failed to undergo NETO in 84% of the cases (Pöhlmann et al., 2014). I

therefore analyzed if the failure to undergo NETO was caused by an altered distribution of landmark proteins such as Tea1 protein.

3.3.1. Localization of the landmark factor Tea1 in absence of Asp1 kinase activity

The Tea1 protein is a polarity factor which is transported in a complex with Tea4 by the polymerizing + ends of microtubules towards the cells tips where it is then anchored by the membrane protein Mod5. At the cell tips, Tea1/Tea4 promote actin assembly and polarized growth via recruitment of active Cdc42 (Kokkoris et al., 2014; Martin et al., 2007; Mata and Nurse, 1997; Snaith and Sawin, 2003). Previous studies from our laboratory showed that the bipolar distribution of Tea1-GFP was impaired in *asp1*^{D333A} strain (Pöhlmann, 2010 unpublished observations). To know more about the distribution of Tea1-GFP in the absence of Asp1 kinase activity, a strain expressing *asp1*^{D333A} and *tea1-gfp* was crossed with a strain expressing coronin1 (actin associated protein) fused to tdTomato (*crn1-tdTomato)* in order to visualize the growing zones (presence of actin) and, thus, cell polarity.

Tea1-GFP equally distributed at both cell tips in bipolar growing *asp1*$^{+}$ cells (Fig29A). In the case of bipolar growing cells, Crn1-tdTomato also shows an equal distribution at both cell tips (Fig29A). However, in *asp1*^{D333A} cells*,* less Tea1-GFP was detected and surprisingly the accumulation of Tea1-GFP was more prominent at the non-growing end of the cells than at the growing end (Fig29B, quantification in C).

Next, it was determined if the accumulation of Tea1-GFP at the non-growing cell tip was specific trait of *asp1*^{D333A} cells. In monopolar growing wild-type cells the distribution of Tea1-GFP also showed unequal distribution in 38% of the cells. However, no statistically difference between the accumulation of Tea1-GFP at the growing or at the non-growing end could be detected (Fig29C).

Total Tea1-GFP intensity was lower in *asp1*^{D333A} cells than in wild-type cells (Fig29D). Thus perhaps the amount of Tea1-GFP was not sufficient to be equally distributed and promote NETO in *asp1*^{D333A} cells. To examine this possibility, total Tea1-GFP fluorescence intensity in monopolar and bipolar cells was quantified and found to be similar in the two strains analyzed, wild-type and *asp1*^{D333A} (Fig29E). This indicates that altered levels of Tea1 protein are not the likely reason of the unequal distribution of Tea1 in monopolar cells.

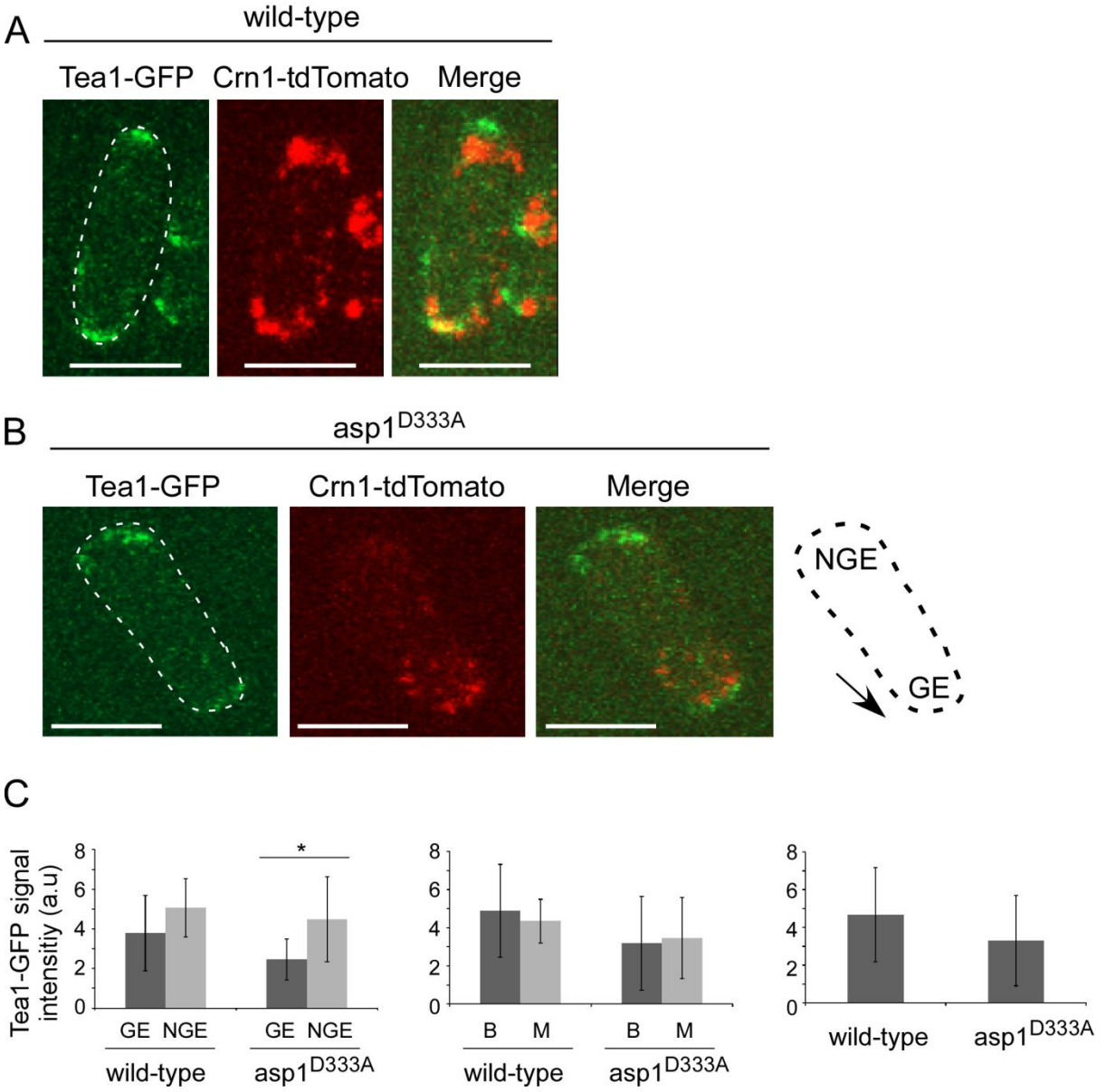

Fig29. Tea1 accumulates at the non-growing end in *asp1^{D333A}* cells. A)Live-cell imaging of wild-type cells expressing *tea1-gfp* and *crn1-tdTomato* (actin marker). B) Live-cell imaging of *asp1^{D333A}* cells expressing *tea1-gfp* and *crn1-tdTomato* (actin marker). Cells from A and B were grown at 25°C in Minimal Media, pictures shown are result of maximum-intensity projection (MIP) images from z-stack of 25 slices with a distance of 0.5 µm. Scale bar 5µm. C) Fluorescence intensity of Tea1-GFP at the growing end (GE) and non-growing end (NGE) of wild-type and *asp1^{D333A}* strains (n>20), *P>0.05 determined by t-test. D) Total Tea1-GFP intensity in wild-type (n=108) and *asp1^{D333A}* (n=88) strains. E) Tea1-GFP intensity in bipolar growing cells (B) and monopolar growing cells (M) of wild-type (n=108) and *asp1^{D333A}* (n=88) strains. Representative results of two independent experiments.

3.3.2. Analysis of microtubule dynamics at the growing and non-growing end of *asp1*^{D333A} cells.

Essential factors for the distribution of the protein Tea1 are microtubule growth and the microtubule pausing time at the cell tips. In wild-type cells microtubules grow mostly in a symmetrical way. An example is shown in Fig30. This wild-type cell has 4 interphase microtubule bundles organized along the cell axis to the cell ends. Overlapping microtubule minus ends localize close to the nucleus and microtubule plus ends grow towards the cell tips: two microtubule bundles growing towards the upper tip and the other two growing towards the bottom tip (both tips are growing as can be seen by the calcofluor staining (Fig30, left).

To explore if the unequal distribution of Tea1 could be explained by different microtubule growth behavior between growing and non-growing end of the cells, microtubule dynamics parameters of a strain expressing α-*tubulin-gfp* and *asp1*^{D333A} were analyzed (Fig30 right).

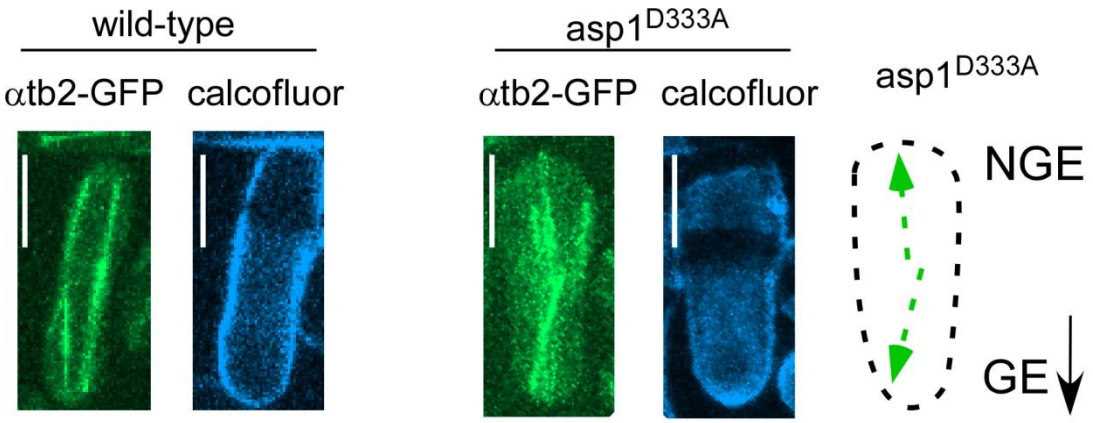

Fig30. Determination of microtubule asymmetry in *asp1*^{D333A} cells Left: Live-cell imaging of a wild-type strain expressing atb2-GFP and stained with calcofluor (marker of growth zones). Right: Live-cell imaging of the *asp1*^{D333A} strain expressing αtb2-GFP and stained with calcofluor, the scheme represents the calcofluor-stained growing end (GE) and the non-growing dark cell end (NGE) shown in the picture, the growth direction of microtubules is represented by the green arrows. Cells were grown at 25°C in Minimal Media, pictures shown are result of maximum-intensity projection (MIP) images from z-stack of 25 slices with a distance of 0.5 µm. Scale bar 5µm.

Calcofluor staining was used to discriminate between growing and non-growing end (Fig31A). The microtubule dynamics parameters analyzed were: maximal length (µm) of a microtubule before catastrophe event (Fig31B), growth rate (µm/min) (Fig31C), dwell/pausing time(s) at the cell end before depolymerization (Fig31D) and shrinkage rate (µm/min) (Fig31E). There was no significant difference for any of the parameters analyzed for microtubules growing towards the NGE (non-growing end) or the GE (growing end) of the cells (Fig31B-E).

These results showed that the unequal distribution of Tea1-GFP and NETO defects are not due to differences in microtubule dynamics between the growing end and the non-growing end of *asp1*^{D333A} cells suggesting that there must be another mechanism involved in correct deposition of Tea1 which is impaired in absence of $IP_{8.}$

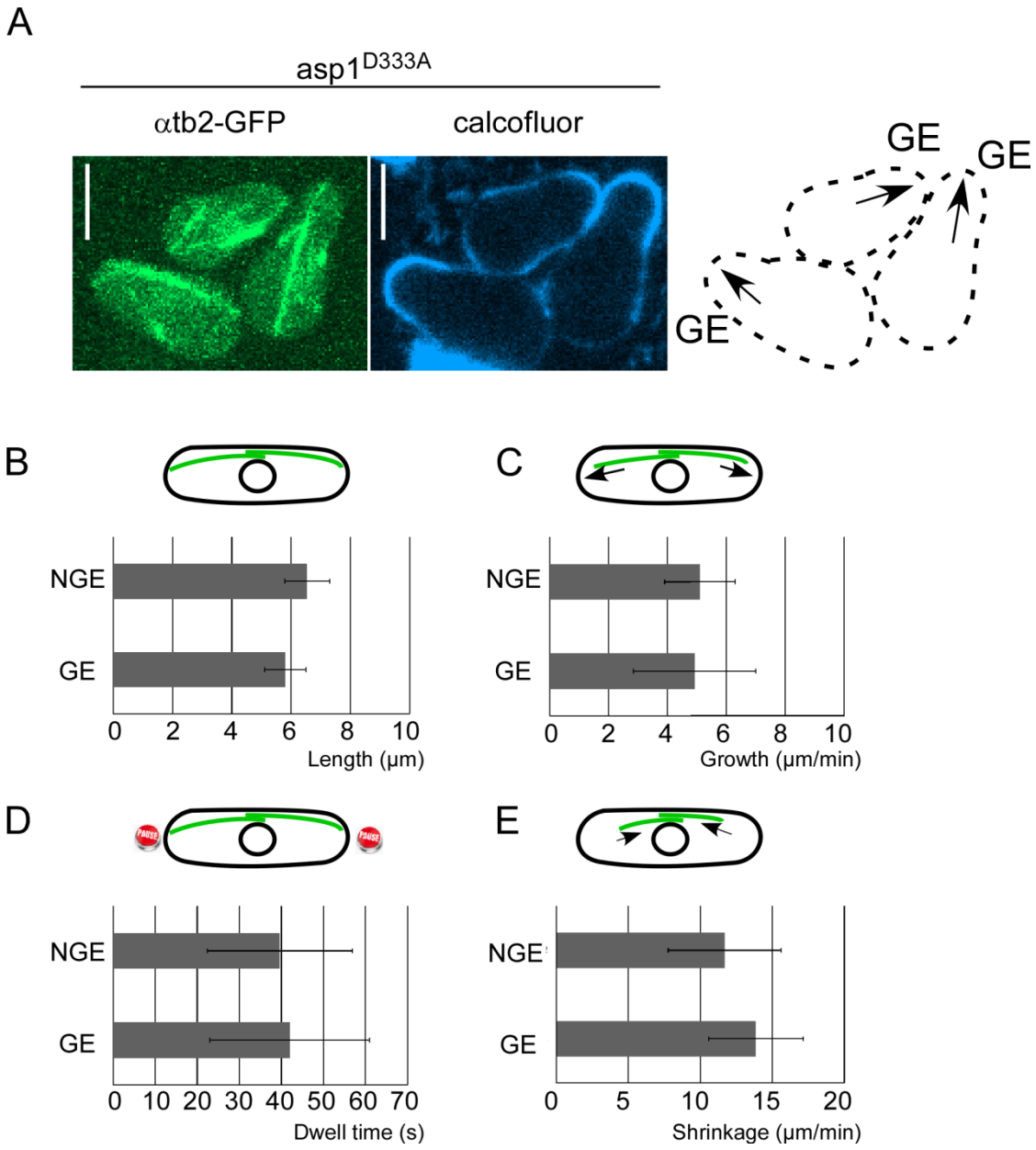

Fig31. Microtubule behavior in *asp1*^{D333A} cells. A)Left: live-cell imaging of the *asp1*^{D333A} strain expressing αtb2-GFP and stained with calcofluor. Cells were grown at 25°C in Minimal Media, pictures shown are result of maximum-intensity projection (MIP) images from z-stack of 10 slices with a distance of 0.5 μm. Scale bar 5μm. Right: scheme representing the calcofluor-stained growing end (GE) and the non-growing dark cell end (NGE). Black arrows show direction of cell growth. B) Quantification of microtubule length (μm) of microtubules growing towards the non-growing end (NGE) 6.54±0.7μm or towards the growing end (GE) 5.80±0.6μm of *asp1*^{D333A}, n=14. C) Quantification of microtubule growth rate (μm min^{-1}) of microtubules growing towards the non-growing end (NGE) 5.10±1.19 μm min^{-1}or towards the growing end (GE) 4.92±2.08 μm min^{-1} of *asp1*^{D333A} cells, n=15. D) Quantification of microtubule dwell time (s) of microtubules pausing at the non-growing end (NGE) 39.6±17.2s or at the growing end (GE) 42±18.9s of *asp1*^{D333A}, n=24. E)Quantification of microtubule

shrinkage rate (μm min^{-1}) of microtubules growing towards the non-growing end (NGE) 11.70±3.9μm min^{-1} or towards the growing end (GE) 13.86±3.2 μm min^{-1} of *asp1*^{D333A}, n=22.

3.4. Asp1 kinase enzymatic activity is required for proper mitochondrial distribution

3.4.1. Abnormal mitochondrial distribution in *asp1* mutant strains

The Asp1 interaction partner, Met10, localizes to mitochondria and inhibits Asp1 pyrophosphatase activity *in vitro* (Pascual-Ortiz, 2017 manuscript submitted). Therefore the possibility that Asp1 might be involved in mitochondrial function was investigated.

Microscopic analysis of mitochondria in the different *asp1* mutant strains was performed. A strain expressing the mitochondrial inner membrane protein Cox4 tagged with RFP (Fu et al., 2011) was crossed with *asp1*^{D333A}, *asp1*^{H397A}, *asp1Δ* or *asp1*$^{1-364}$ strains and the localization of Cox4-RFP analyzed in the resulting strains.

In *Schizosaccharomyces pombe*, mitochondria distribution is facilitated by microtubules in a motor-independent manner (Li et al., 2015). Wild-type cells display tubular mitochondrial structures which colocalize with the microtubule cytoskeleton as shown in the diagrammatic representation of Fig32A, left. Accordingly, upon treatment with microtubule depolymerizing drugs, the distribution along the cell axis is lost and mitochondria appear aggregated mainly at the cell ends (Fig32A, right).

Live-cell imaging of a wild-type strain showed the expected tubular mitochondria distributed along the cell length, only 17% of cells showing aggregation of mitochondria mainly at the cell ends (Fig32B and Fig33). A similar distribution pattern was observed in the *asp1*$^{1-364}$ strain with 20.8% of cells showing aggregated mitochondria (Fig32C and Fig33). However, in *asp1*^{D333A} and *asp1Δ* strains, the percentage of cells with abnormal distribution of mitochondria was 39.7% and 56.9% respectively (Fig32D-E and Fig33). Surprisingly, the *asp1*^{H397A} strain showed only 3.9% aberrant mitochondrial distribution (Fig32F and Fig33). These results suggest that the kinase activity of Asp1 and, consequently, IP_8, are required for proper mitochondrial distribution.

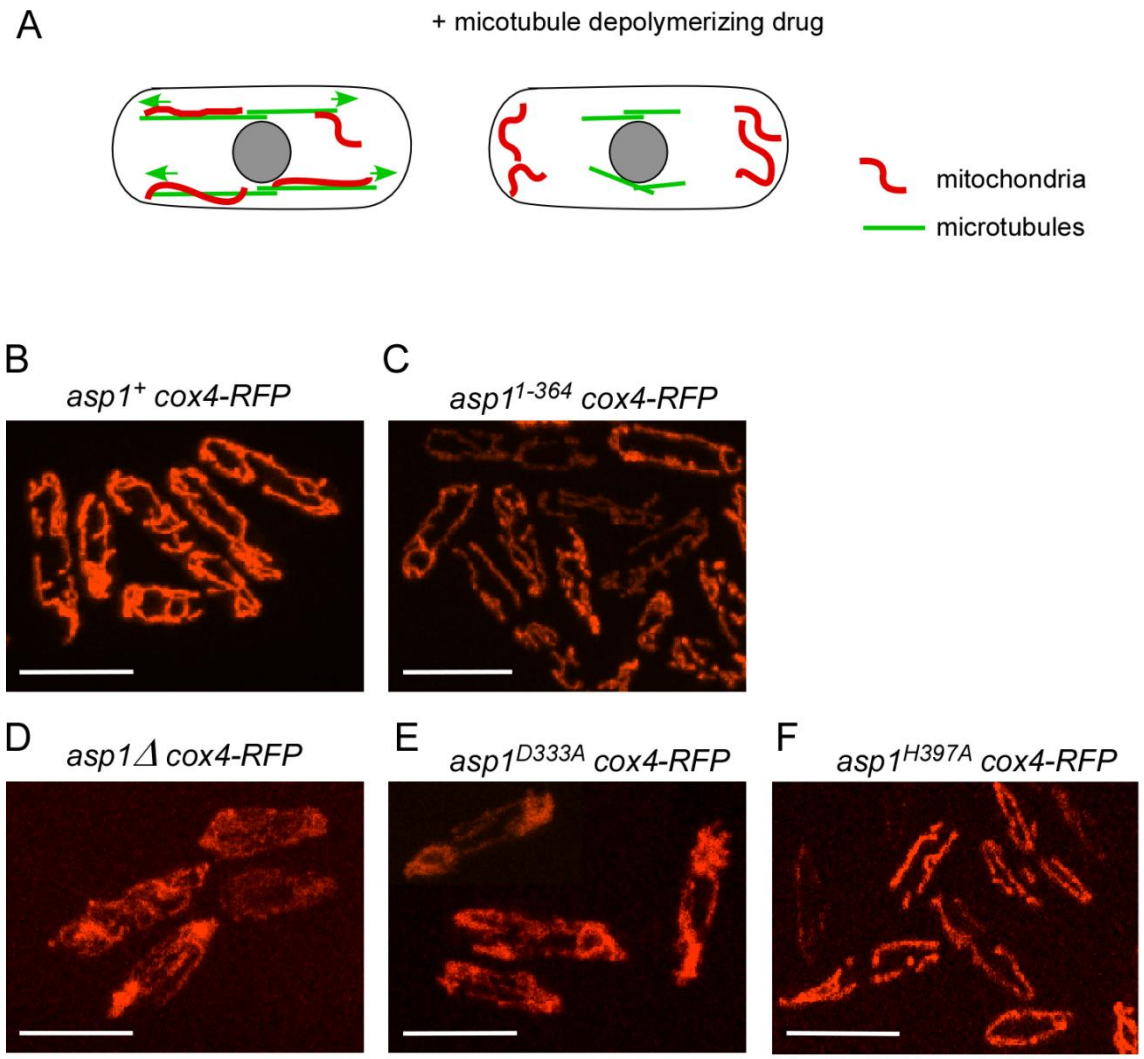

Fig32. Mitochondrial distribution is affected in asp1 mutant strains. A) Left: diagrammatic representation of mitochondria distribution (red) along interphase microtubules (green). Right: diagrammatic representation of mitochondria aggregation phenotype (red) upon treatment with microtubule depolymerizing drug resulting in aberrant short microtubules. B) Live cell imaging of the mitochondria marker Cox4-RFP in asp1^{+}, *asp1*^{D333A}, *asp1Δ*, *asp1*^{H397A} and *asp1*$^{1-364}$ cells. Shown are maximum-intensity-projection images of interphase cells grown at 25°C. Scale bar, 10 µm.

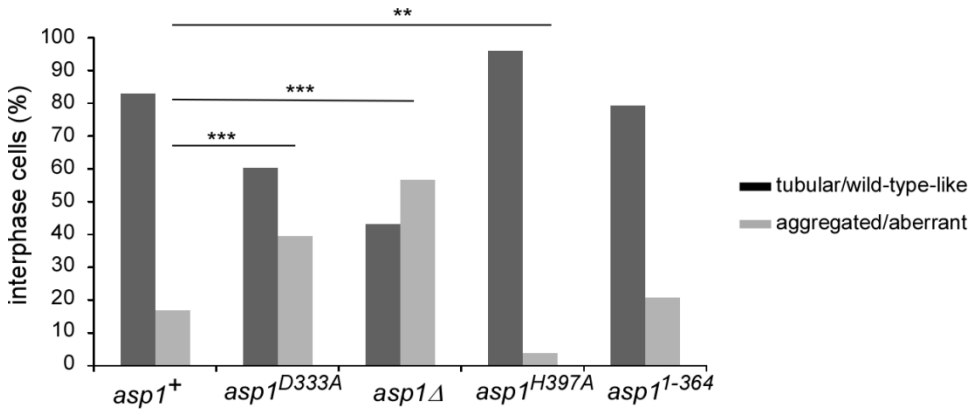

Fig33. Quantification of mitochondrial distribution phenotypes in asp1 mutant strains. Quantification of mitochondrial aggregation, asp1^{+} strain, n = 143; *asp1*^{D333A} strain, n = 63; *asp1Δ* strain, n=44; *asp1*^{H397A} strain, n = 77; *asp1*$^{1-364}$ strain, n=77, P** < 0.05, P*** < 0.005 as determined using χ2 test.

3.4.2. Asp1 pyrophosphatase activity affects the growth of *mmb1Δ* strain

Movement and proper distribution of mitochondria depends on the binding of mitochondria to the microtubule cytoskeleton via the Mmb1 protein. Loss of Mmb1 leads to increased mitochondria aggregation at one or both cells ends, resulting in 10% of cells with asymmetric mitochondria distribution between daughter cells after division (Fu et al., 2011). Daughter cells which receive no mitochondria stop growing and die eventually (Okamoto and Shaw, 2005). As Asp1 enzymatic activity influenced mitochondrial distribution, the phenotypic consequences of altering cellular Asp1-generated inositol pyrophosphate levels in a strain lacking Mmb1 protein were examined.

An *mmb1Δ* strain was transformed with either a vector control or plasmids expressing *asp1*$^{+}$, *asp1*$^{1\text{-}364}$, *asp1*$^{365\text{-}920}$ or *asp1*$^{365\text{-}920/H397A}$ under the control of the *nmt1*$^{+}$ repressible promotor and growth on solid media was examined. Under non-repressed expression conditions, plasmid-borne Asp1 reduced the growth of the *mmb1Δ* strain (Fig34) while expression of the Asp1 kinase domain (*asp1*$^{1\text{-}364}$) had no effect (Fig34 *asp1*$^{1\text{-}364}$ *vs* control). Interestingly, plasmid-borne expression of *asp1*$^{365\text{-}920}$ encoding the pyrophosphatase domain but not the enzymatically inactive variant *asp1*$^{365\text{-}920/H397A}$, massively reduced growth of the strain (Fig34). In conclusion, extra expression of a functional Asp1 pyrophosphatase domain nearly abolishes growth of the *mmb1Δ* strain. This phenotype suggests that the products of *mmb1*$^{+}$ and *asp1*$^{+}$ act in parallel pathways involved in mitochondrial distribution.

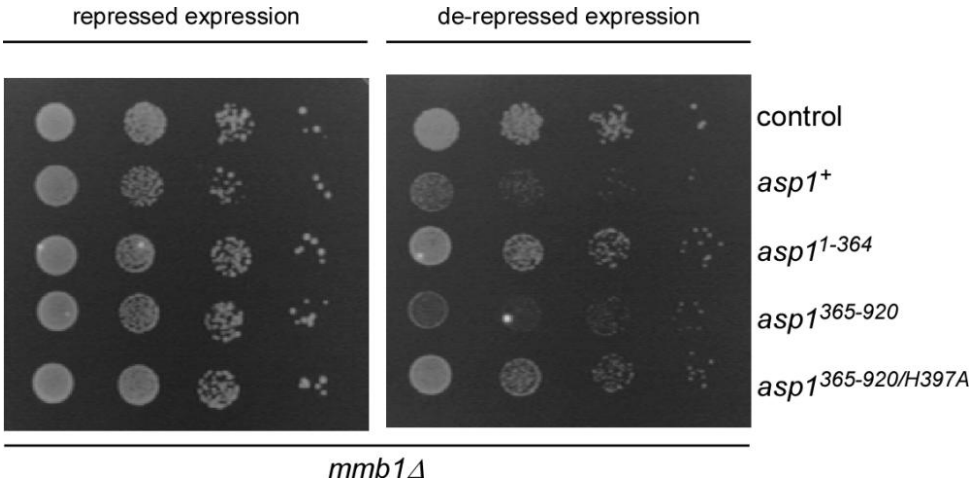

Fig34. Growth of *mmb1Δ* strain is strongly reduced by expression of extra Asp1 pyrophosphatase domain. Serial dilution patch tests (10^{4} to 10^{1}cells) of *mmb1Δ* strain transformed with either vector control or plasmids expressing *asp1*$^{+}$, *asp1*$^{1\text{-}364}$, *asp1*$^{365\text{-}920}$ or *asp1*$^{365\text{-}920/H397A}$. Transformants were grown under plasmid selective conditions in absence or presence of thiamine at 25°C for 6 days.

The Mmb1 protein binds to microtubules but preferably to mitochondria (Fu et al., 2011). To examine whether the localization of Mmb1-GFP was altered upon alteration of

inositol pyrophosphate levels, a strain endogenously expressing *mmb1-gfp* was transformed with a vector control or plasmids expressing either *asp1*$^{1-364}$ or *asp1*$^{365-920}$ and the localization of Mmb1-GFP was examined under de-repressed expression conditions. Mmb1-GFP localized along the mitochondrial tubular structures (Fig35) as described previously (Fu et al., 2011). A similar distribution was observed when either the kinase domain or the pyrophosphatase domain of Asp1 was overexpressed (Fig35). This result shows that alteration of cellular Asp1-generated inositol pyrophosphates did not affect the cellular localization of Mmb1-GFP. Thus, in conclusion, the function of Asp1 in regulating mitochondrial distribution is independent of Mmb1.

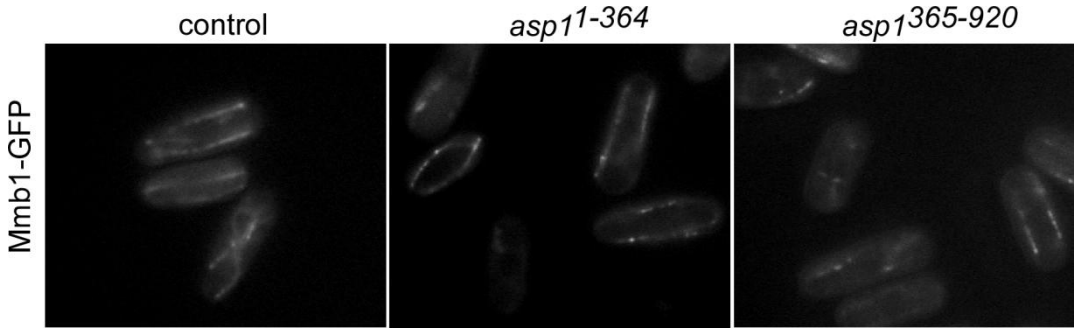

Fig35. Cellular localization of Mmb1-GFP is not dependent on Asp1 enzymatic activity. Live-cell imaging of the *mmb1-gfp* strain transformed with either vector control or plasmids expressing *asp1*$^{1-364}$ *or asp1*$^{365-920}$. Cells were grown at 25°C under plasmid selective conditions in absence of thiamine. Images were taken immediately after preparation of the slides.

3.5. Mitochondrial association of mutant Asp1 variants

3.5.1. Subcellular localization of wild-type Asp1 and mutant Asp1 variants

Under physiological conditions at 30°C, Asp1 is mainly present in the cytoplasm without a specific subcellular localization (Feoktistova et al., 1999). However, observations in our laboratory showed that Asp1 can localize to the nucleus in a temperature-dependent manner. A correlation between low temperature and nuclear localization was observed (Fig36). The presence of Asp1 in the nucleus depends on the function of another protein, Hpm1 (Patrick Fischbach master thesis, 2016), demonstrating that the cellular localization of Asp1 is regulated by interactions with other proteins.

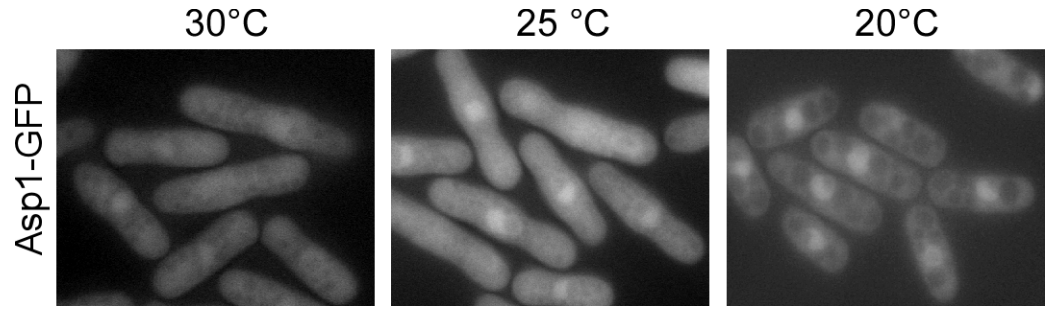

Fig36. Cellular localization of Asp1-GFP. Live-cell imaging of the *asp1-gfp* strain. Cells were grown either at 30°C, 25°C or 20°C in Minimal Media. Images were taken immediately after preparation of the slides.

The cellular localization of the different Asp1 variants fused to GFP was analyzed. Strains endogenously expressing either *asp1*$^{+}$*-gfp, asp1*^{H397A}*-gfp, asp1*^{D333A}*-gfp* or *asp1*^{D333A}*-gfp* were crossed with a strain expressing the mitochondrial inner membrane protein Cox4-RFP. The resulting strains were analyzed by using fluorescence microscopy.

As previously shown, wild-type Asp1-GFP exhibited cytoplasmic and nuclear localization which shifted to increased nuclear accumulation when the temperature was decreased (experiment performed at 25°C) (Fig37A). A similar localization was observed for Asp1^{H397A}-GFP (Fig37B). However, Asp1^{D333A}-GFP and Asp1$^{1-364}$-GFP showed a specific intracellular localization pattern which was similar to that observed for Cox4-RFP (Fig37C and D), indicating mitochondrial association of these two Asp1 variants. Furthermore, the temperature-controlled nuclear localization was lost in these variants (Fig37C-D).

Interestingly, an experiment performed in our lab in which the ability to bind lipids of different recombinant Asp1 variants was tested, showed that GST-Asp1$^{1-364}$ could bind to cardiolipin, a lipid that is unique to the mitochondrial membrane (Pascal Ramrath, master thesis 2012)(van Meer et al., 2008). These observations strongly indicate that Asp1 mutants, Asp1^{D333A} and Asp1$^{1-364}$, associate with the mitochondrial network.

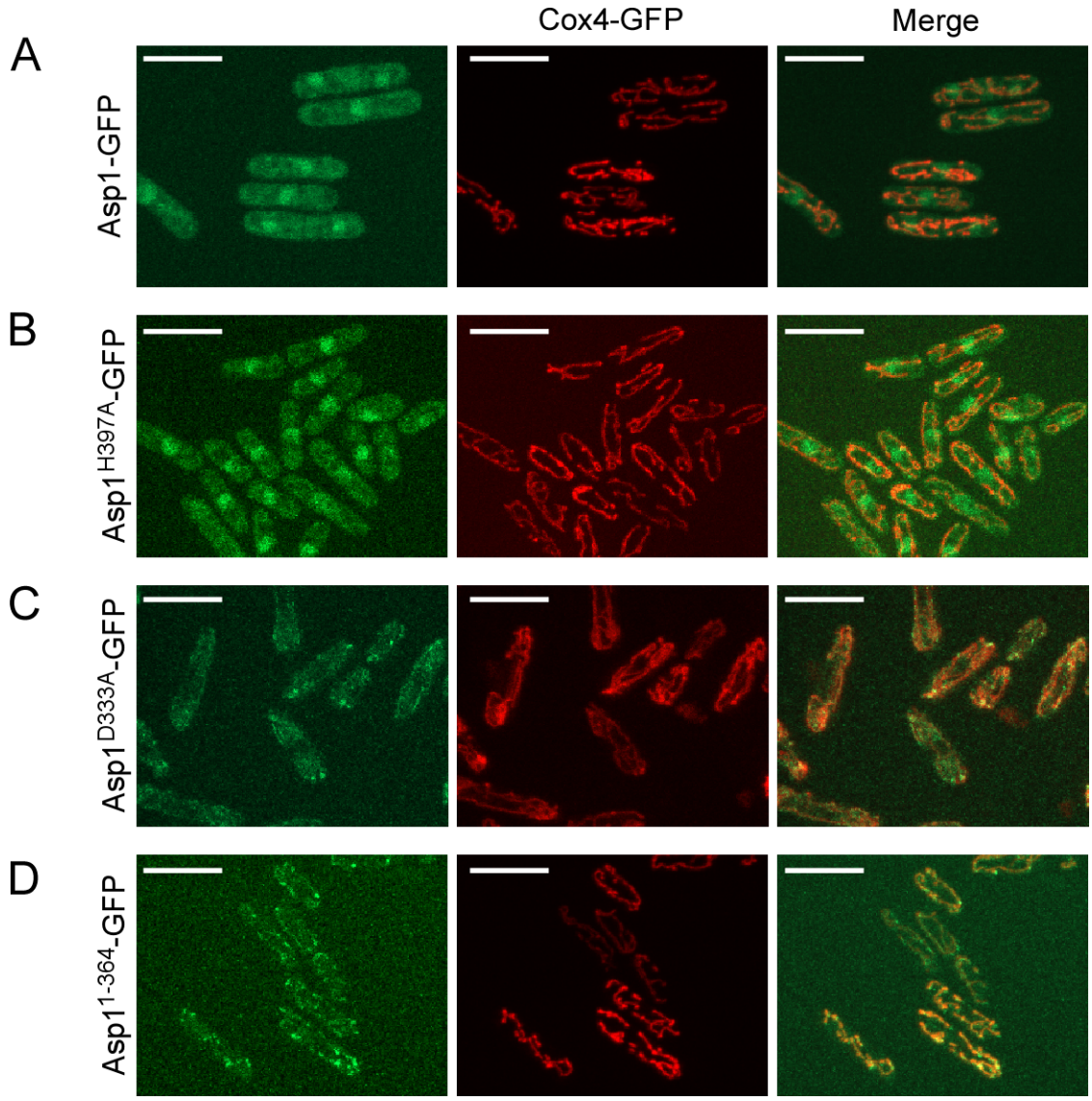

Fig37. Asp1^{D333A}-GFP and Asp1$^{1-364}$-GFP probably colocalize with the mitochondrial network. A)Live-cell imaging of the *asp1*$^{+}$*-gfp* strain expressing the mitochondrial marker *cox4-rfp*. B) Live-cell imaging of the *cox4-rfp, asp1*^{H397A}*-gfp* strain. C) Live-cell imaging of the *cox4-rfp, asp1*^{D333A}*-gfp* strain. D) Live-cell imaging of the *cox4-rfp, asp1*$^{1-364}$*-gfp* strain. Cells were grown at 25°C in Minimal Media. Pictures shown are result of maximum-intensity projection (MIP) images from z-stack of 15 slices with a distance of 0.5 µm. Scale bar 10µm.

To test whether the localization of Asp1$^{1-364}$ affected the cellular function of this Asp1 variant, I analyzed growth and resistance to TBZ (thiabendazole) of this strain. A serial dilution patch test using the wild-type, *asp1Δ*, *asp1*^{H397A}, and *asp1*$^{1-364}$ strains was performed and plates were incubated either at 25°C or 20°C and at 25°C with or without TBZ. Strains grew in a similar way at 25°C without TBZ (Fig38 left panel). However, in the presence of TBZ, *asp1*^{H397A} and *asp1*$^{1-364}$ strains showed a higher TBZ resistance than the wild type strain (Fig38 central panel), while the *asp1Δ* strain was TBZ hypersensitive. The outcome of these results can be explained by the different levels of cellular IP_8 that the strains produced as it has been shown in chapter 3.1. However, interestingly, while growth at 20°C of wild-type and

asp1^{H397A} strains were comparable, the *asp1*$^{1-364}$ strain showed a growth pattern similar to *asp1Δ* (Fig38 right panel).

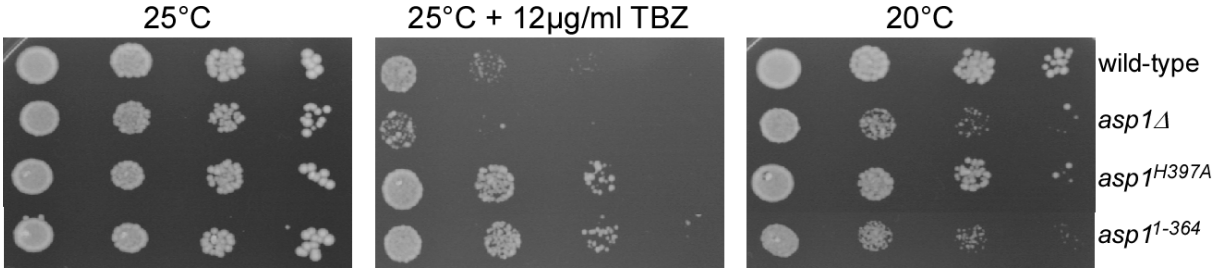

Fig38. Growth of *asp1* mutants strains at different temperatures. Serial dilution patch tests (10^4 to 10^1cells) of wild-type, *asp1Δ , asp1*^{H397A} and *asp1*$^{1-364}$ strains on YE5S full media with or without the addition of 12µg/ml TBZ at 25°C and 20°C for 5 days.

I found that Asp1$^{1-364}$-GFP colocalized with the mitochondrial marker Cox4-RFP at 30°C. Therefore I analyzed if that was also the case at 20°C. Wild-type *asp1-gfp* and *asp1*$^{1-364}$ *–gfp* strains were grown in full-media at 30°C (to increase the cytoplasmic localization of wild-type Asp1-GFP) and 20°C (to increase the nuclear localization of wild-type Asp1-GFP) overnight and analyzed microscopically. As already shown, Asp1-GFP localized to the nucleus and cytoplasm at 30°C. The nuclear fraction of Asp1-GFP was more prominent when these cells were grown at 20°C (Fig39). However, the cellular distribution of Asp1$^{1-364}$-GFP remained mitochondria-like regardless of the temperature (Fig39).

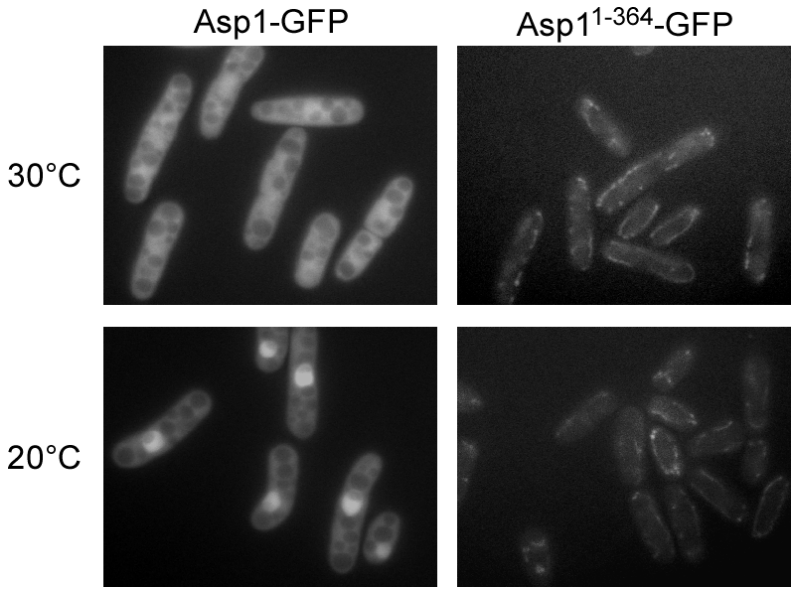

Fig39. Cellular localization of Asp1-GFP and Asp1$^{1-364}$-GFP. Live-cell imaging of the *asp1-gfp* and *asp1*$^{1-364}$*-gfp* strains. Cells were grown either at 30°C or 20°C in full media. Images were taken immediately after preparation of the slides.

These data demonstrate that Asp1 variants which showed altered cellular localization fail to accumulate in the nucleus at lower temperatures, possibly preventing Asp1 from

executing its function. Therefore Asp1 function is tightly linked to changes in its cellular distribution.

3.6. Role of Asp1 in phosphate homeostasis

3.6.1. Direct correlation between Asp1-generated IP_8 and cellular accumulation of polyP

An interconnection between the three phosphate rich molecules in the cell: ATP, inositol pyrophosphates and inorganic polyphosphate, has been proposed(Silva et al., 2017). The relative cellular pools of these molecules might be adjusted in order to regulate phosphate homeostasis (Silva et al., 2017). Previous studies in *S. cerevisiae* reported a link between inositol pyrophosphate metabolism and inorganic polyphosphate (polyP). In fact, *S. cerevisiae* cells unable to synthesize inositol pyrophosphates cannot accumulate polyP (Auesukaree et al., 2005; Lonetti et al., 2011).

As cellular IP_8 levels are regulated by Asp1 bifunctional enzymatic activity, polyP levels could also vary in the strains with altered Asp1 enzymatic activity. To investigate this, polyP was extracted from the wild-type, $asp1^{D333A}$, $asp1^{H397A}$, $asp1^{I808D}$, $asp1^{1-364}$ and *asp1Δ* strains and analyzed by PAGE.

In comparison to the extract from the wild-type strain, a massive reduction of cellular polyP accumulation was observed in extracts of $asp1^{D333A}$ and *asp1Δ* strains (Fig40 left). In contrast, strains with impaired or absent Asp1 pyrophosphatase activity; $asp1^{H397A}$, $asp1^{I808D}$, and $asp1^{1-364}$ had higher than wild-type polyP levels (Fig40 left). A quantitative malachite-green assay used to measure phosphate release after acid-treatment is shown on the right panel, Fig40. This data demonstrates a direct correlation between Asp1-generated IPPs and cellular polyP levels.

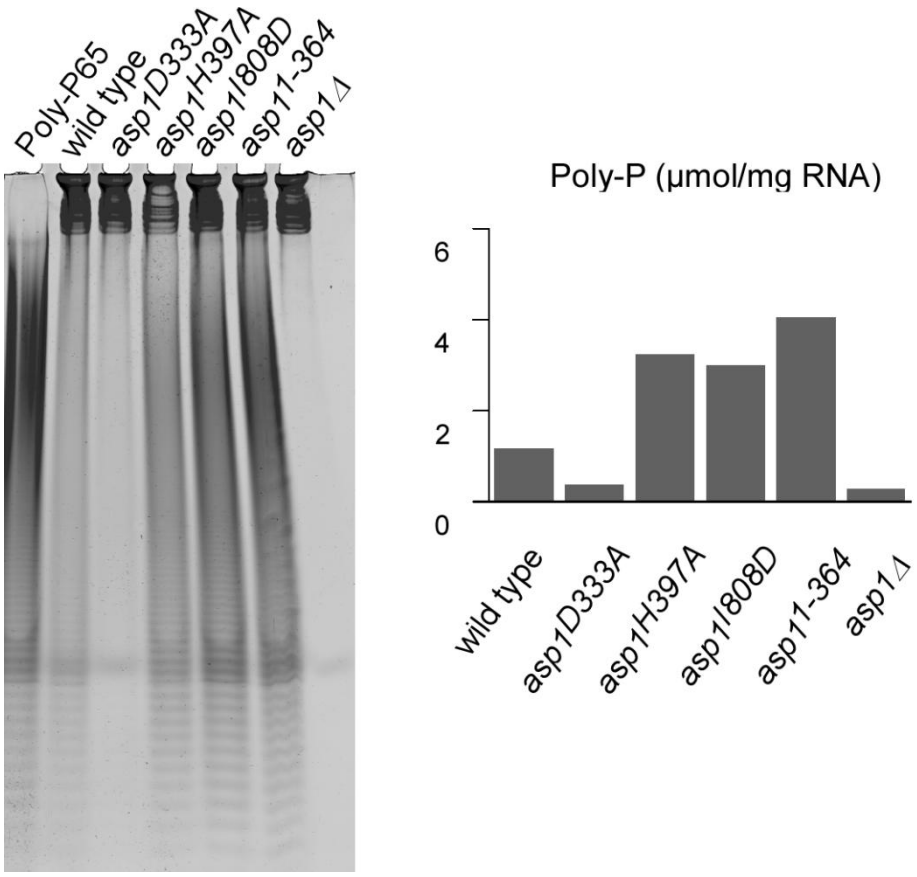

Fig40. Direct correlation between Asp1 pyrophosphate activity and cellular polyP levels. Left: *S. pombe* polyP detected as a dark smear by PAGE analysis of lysates of the wild-type, *asp1*^{D333A}, *asp1*^{H397A}, *asp1*^{I808D}, *asp1*$^{1-364}$ and *asp1Δ* strains. All yeast cultures were in exponential growth phase before harvesting and equal amounts of phenol/chloroform extract (measured as RNA content, 40µg) were loaded. Right: Quantification of polyP levels using a Malachite Green assay. Average values shown from two independent experiments. (Figure and Figure legend modified from Pascual-Ortiz, 2017 manuscript submitted)

Since cellular levels of polyP increase in strains with impaired Asp1 pyrophosphatase activity, I examined if overexpression of Asp1 pyrophosphatase domain in the wild-type strain had the opposite effect. PolyP was extracted from the wild-type strain transformed with either a vector control or plasmids expressing either *asp1*$^{365-920}$ or *asp1*$^{365-920/H397A}$ grown in minimal media under de-repressed expression conditions. PolyP was considerably reduced upon expression of *asp1*$^{365-920}$ (Fig41, *asp1*$^{365-20}$ in comparison to control) while plasmid expression of the enzymatically inactive variant, *asp1*$^{365-920/H397A}$ had no effect (Fig41, quantification on the right) on cellular polyP levels. These results demonstrate that presence of extra Asp1 pyrophosphatase activity affects the abundance of polyP.

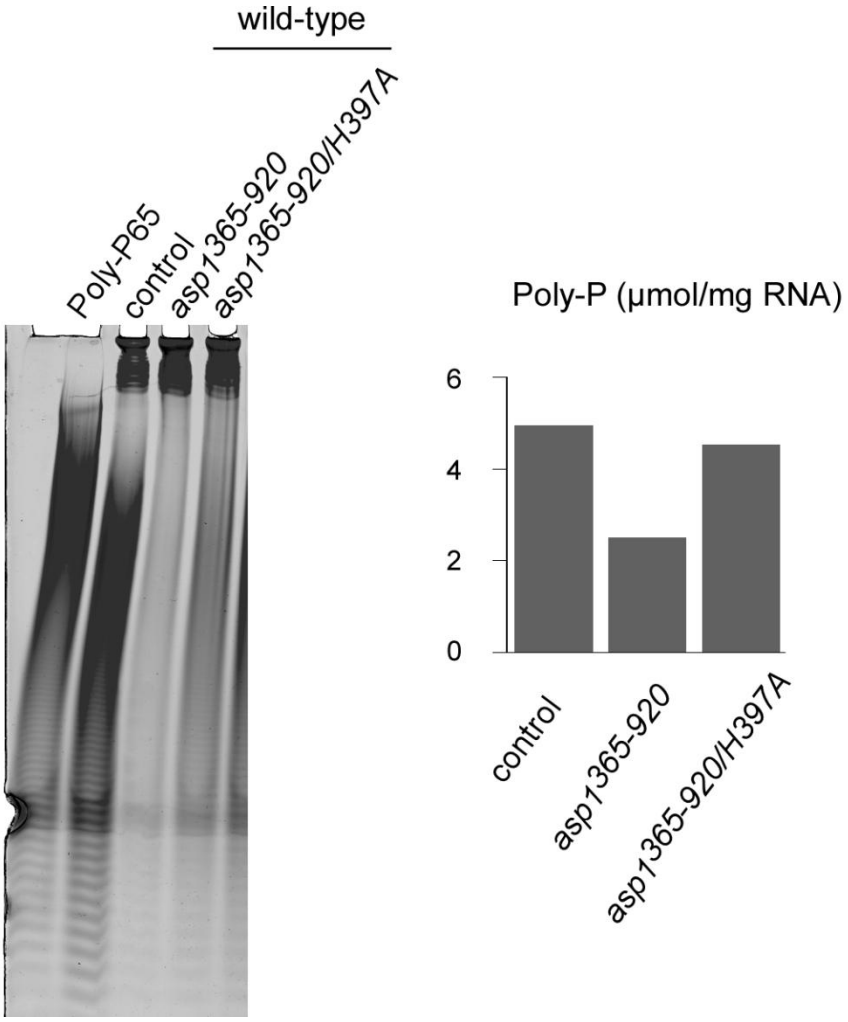

Fig41. Plasmid-borne expression of Asp1 pyrophosphatase activity leads to a reduction in cellular polyP. Left: *S. pombe* polyP detected as a dark smear by PAGE analysis of lysates of the wild-type strain transformed with either vector control or plasmids expressing *asp1*$^{365\text{-}920}$ or *asp1* $^{365\text{-}920/H397A}$. All yeast cultures were in exponential growth phase in thiamine-less minimal media before harvesting and equal amounts of phenol/chloroform extract (measured as RNA content, 40µg) were loaded. Right: Quantification of polyP levels using a Malachite Green assay. Average values shown from two independent experiments.

Next, polyP was extracted from the *asp1Δ* strain transformed with either a vector control or plasmid expressing either *asp1*$^{365\text{-}920}$ or *asp1*$^{365\text{-}920/H397A}$. Due to the scant amount of polyP that is observed in *asp1Δ* extracts (Fig40), the experiment was performed with two different sets of cultures; in the first one polyP was extracted from exponentially growing cells and in the second set, polyP was extracted from cultures which had already reached saturation in order to have a higher cell number. Almost no polyP was detected in extracts from non-saturated cultures ("NS" in Fig31). However, the amount of polyP in saturated cultures was sufficient for analysis ("S" in Fig42). No difference in polyP accumulation was observed in extracts from *asp1Δ* cells expressing either vector control, *asp1*$^{365\text{-}920}$ or *asp1*$^{365\text{-}}$

$^{920/H397A}$ plasmids ("S" in Fig42) indicating that Asp1 pyrophosphatase domain does not directly affect polyP.

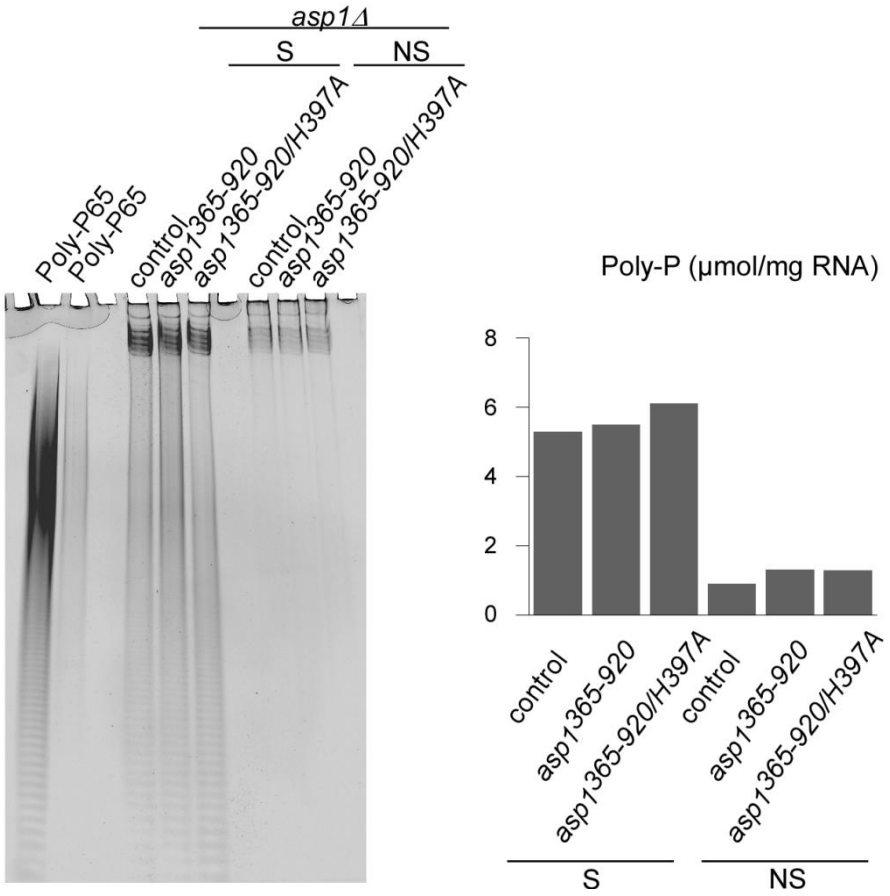

Fig42. Expression of Asp1 pyrophosphatase activity does not affect levels of polyP in the *asp1Δ* strain. Left: *S. pombe* polyP detected as a dark smear by PAGE analysis of lysates of the *asp1Δ* strain transformed with either vector control or plasmids expressing *asp1*$^{365-920}$ or *asp1* $^{365-920/H397A}$. Yeast cultures were either in exponential growth phase (NS: non-saturated) or grown until saturation (S: saturated) in thiamine-less minimal media before harvesting. Equal amounts of phenol/chloroform extract (measured as RNA content, 10µg) were loaded. Right: Quantification of polyP levels using a Malachite Green assay.

These results demonstrate that polyP is not likely an additional cellular substrate of Asp1. However, variations of IP_8 caused by Asp1 function modulate polyP levels.

3.6.2. Genetic interaction between *asp1* and *pef1*

Cellular phosphate stored as polyP is mobilized in response to phosphate fluctuations in *S. cerevisiae* (reviewed in(Tomar and Sinha, 2014). Furthermore, in *S.cerevisiae*, response to phosphate limitation by the Pho80-Pho85-Pho81 complex is inhibited by IP_7 and the transcription of genes involved in phosphates homeostasis upregulated (Lee et al., 2008). Thus, to learn more about the possible role of Asp1 in relation to phosphate

homeostasis, the function ortholog of the PHO85 in *S.pombe*, *pef1 (Tanaka and Okayama, 2000)* was analyzed.

To test if Asp1 enzymatic activity influenced the function of Pef1, the strains *asp1Δpef1Δ, asp1^{D333A}pef1Δ*, *asp1^{H397A}pef1Δ* were generated and their growth analyzed. Growth of *pef1Δ* strain was slighty reduced in comparison to the wild-type strain (Fig43). However, the double mutant *asp1Δpef1Δ* was found to be synthetically sick in comparison to both single mutants, *pef1Δ* and *asp1Δ* (Fig43). That was also the case for the double mutant *asp1^{D333A}pef1Δ* whose growth was massively reduced in comparison to either of the single mutants, *asp1^{D333A}* or *pef1Δ* (Fig43). The strain *asp1^{H397A}pef1Δ* rescued the growth deffect of the *pef1Δ* strain (Fig43). These results suggest that the kinase activity of Asp1 and Pef1 function are involved in a parallel pathway in regard to phosphate metabolism and that an excess of Asp1-generated IP_8 might bypass Pef1 function.

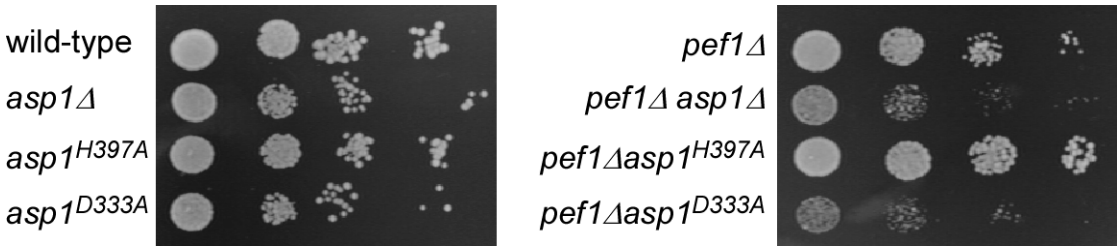

Fig43. Genetic interaction between *asp1* and *pef1*. Left: Serial dilution patch test (10^4 to 10^1cells) of wild-type, *asp1Δ, asp1^{H397A}* and *asp1^{D333A}* strains. Right: Serial dilution patch test (10^4 to 10^1cells) of *pef1Δ*, *pef1Δasp1Δ, pef1Δasp1^{H397A}* and *pef1Δasp1^{D333A}* strains. Cells were grown in full media (YE5S) at 25°C for 5 days.

3.6.3. Asp1-generated IP_8 triggers NETO in G1 arrested cells

Cell cycle progression is blocked upon phosphate limitation. In *S. cerevisiae,* lack of phosphate induces cell cycle arrest in G1 via destabilization of cyclin Cln3 in a process dependent on Pho85-Pho80 function (Menoyo et al., 2013). Interestingly, in *S. pombe* the Pho85-homolog, Pef1, also seems to play an important role in regulating the G1/S phase cyclin Pas1 (Tanaka and Okayama, 2000).

Asp1 kinase activity, and thus the generation of IP_8, is essential for NETO transition, a cell cycle-coordinated process (Mitchison and Nurse, 1985). Only cells which have completed S-phase and attained a critical cell size undergo NETO transition. Hence, I analyzed if Asp1-generated inositol pyrophosphates induce NETO in cells arrested in G1 phase (pre-NETO stage).

The *asp1* mutant strains, *asp1^{H397A}* and *asp1^{D333A}* were crossed with the temperature-sensitive cell-cycle mutant *cdc10-129*. At the restrictive temperature, 36°C, *cdc10-129* cells are arrested in G1 phase and show monopolar growth (Mitchison and Nurse, 1985). Single

mutant *cdc10-129* and double mutants *asp1*^{H397A} *cdc10-129* and *asp1*^{D333A} *cdc10-129* were grown at 36°C for 4 hours to induce the G1 arrest. Then, cells were stained with calcofluor (polarity marker) and the growth pattern was analyzed (Fig44A). As expected, 68% of *cdc10-129* cells showed monopolar growth and the similar effect was observed in *asp1*^{D333A} *cdc10-129* cells, however, the opposite phenotype was observed in *asp1*^{H397A} *cdc10-129* cultures in which 75% of cells were bipolar (Fig44B). This result indicates that the NETO delay in G1 cells depends on Asp1 pyrophosphatase activity suggesting a role of inositol pyrophosphates in cell cycle progression.

Together, these results demonstrate that alteration of cellular Asp1-generated IP_8 levels impacts the phenotype of the *pef1Δ* strain and the amount of polyP, suggesting a role of Asp1 function in phosphate homeostasis. Furthermore, and in line with the ability of phosphate to impact cell cycle, Asp1 pyrophosphatase activity is required to coordinate NETO with the cell cycle.

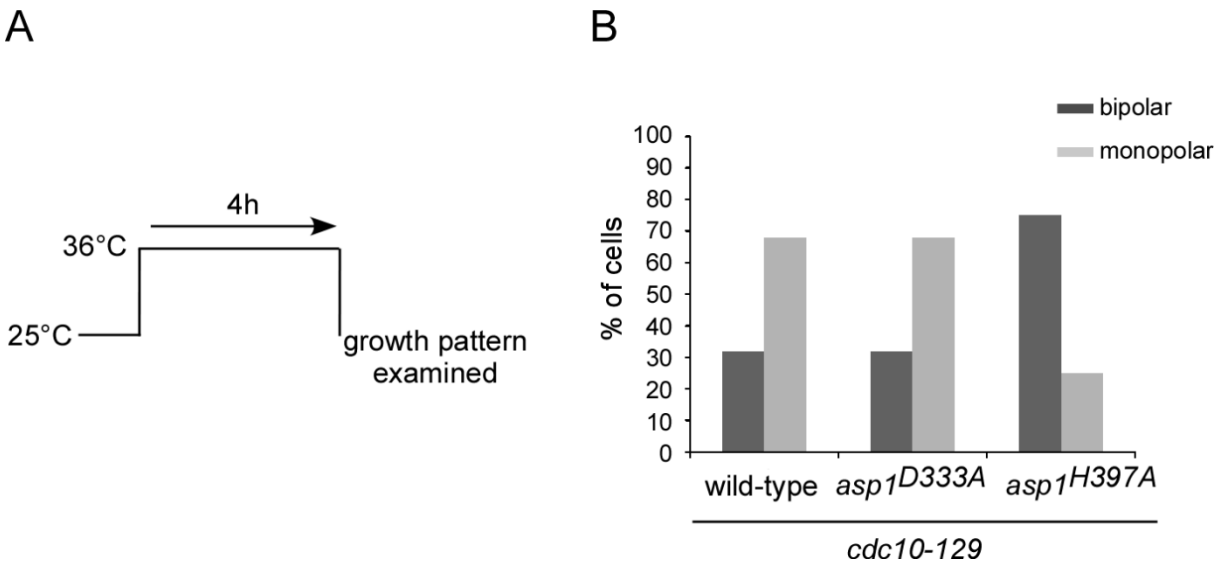

Fig44. Asp1-generated inositol pyrophosphates trigger NETO in G1 arrested cells. A) Experimental design, cells were grown in minimal media at 25°C overnight and next morning diluted to OD_{600} 0.4. After 4 hours incubation at 36°C to induce the arrest in G1, growth pattern was analyzed. B) Percentages of monopolar and bipolar growth in *cdc10-129* cells: 68% monopolar, 32% bipolar (n>100). C) Percentages of monopolar and bipolar growth in *asp1*^{D333A}*cdc10-129* cells: 68% monopolar, 32% bipolar (n>50). D) Percentages of monopolar and bipolar growth in *asp1*^{H397A}*cdc10-129* cells: 25% monopolar, 75% bipolar (n>100).

4. Discussion

4.1. Asp1 is a bifunctional enzyme

This work demonstrates that the *Schizosaccharomyces pombe* PPIP5Ks/Vip1 family member Asp1 protein is a bifunctional enzyme capable of adding and cleaving a di-phosphate group to the fully phosphorylated inositol ring. Asp1 enzymatic functions are responsible for the synthesis and hydrolysis of one specific inositol pyrophosphate molecule, IP_8. Together with our *in vivo* data concerning chromosome segregation, spindle dynamics and polarized growth (Pohlmann and Fleig, 2010; Pohlmann et al., 2014; Topolski et al., 2016) which are all regulated by IP_8, my analysis demonstrates that changes in intracellular IP_8 levels modulate these biological processes.

4.1.1. Asp1 kinase domain synthesizes IP_8 *in vivo*

When the Vip1 family was described in *S. cerevisiae* in 2007, it was proposed that this protein family only had kinase activity and phosphorylated IP_6, synthesizing an IP_7 molecule which was structurally different to that resulting from IP6Ks/Kcs1 kinase activity (Mulugu et al., 2007). It was shown later that this molecule was a different isomer of IP_7, 1-IP_7 (Lin et al., 2009; Wang et al., 2011).

Now, my results demonstrate that the kinase activity of Asp1 uses IP_7 as a substrate and therefore, its physiological function is the synthesis of IP_8 *in vivo*. Although *in vitro*, purified *S. cerevisiae* Vip1 can also function as an IP_7 kinase, Mulugu and colleagues performed the *in vivo* experiments using mutant yeast strains in which the *KCS1* gene was deleted and no 5-IP_7 was generated. thus Vip1 could not use this substrate in the cell (Mulugu et al., 2007). In this context, Vip1 will use IP_6 as a substrate and synthesize 1-IP_7 (see Fig2 page 46). Another publication reported that the human Vip1 proteins, PPIP5K1 and PPIPK2 were both, IP_6 and IP_7 kinases (Fridy et al., 2007). However in that study, the *in vivo* activity of PPIP5Ks was investigated in mammalian cells with a non-physiological increased production of IP_7, therefore unbalancing the cellular abundance of the available substrates for PPIPKs/Vip1 kinase activity. My study is the first one demonstrating that the *S. pombe* Vip1 family member, Asp1 protein, is an IP_7 kinase under physiological conditions. Only one study before proposed that Vip1 proteins might be IP_7 kinases, this publication showed that *S. cerevisiae* cells lacking Vip1 protein exhibited increased levels of IP_7 and massively reduced levels of IP_8 (Onnebo and Saiardi, 2009). In contrast *S. pombe asp1Δ* and *asp1*^{D333A}

(kinase-dead) cells, have no IP_8 (Fig2 and Fig3 pages 46 and 47), demonstrating that Asp1 is the only IP_7 kinase in this yeast.

However, Asp1 can also use IP_6 as a substrate under certain conditions. High, plasmid-borne expression of the Asp1 kinase domain not only increases cellular levels of IP_8 but also those of IP_7 (Fig4 page 47). Inositol pyrophosphate profile of *S.pombe* cells overexpressing the Asp1 kinase domain shows an IP_7 elution peak that is slightly shifted to the left in comparison to the control. Such a shift is to be expected when 1-IP_7 instead of 5-IP_7 is present indicating that the main IP_7 isomer in cells with higher-than-wild type Asp1 kinase activity is likely 1-IP_7 (Fig4 page 47). The crystal structure of the kinase domain of PPIP5K2 revealed that the active site of the enzyme would allow only one orientation of phosphates and di-phosphates around the inositol ring; a configuration that only IP_6 and 5-IP_7 have. The presence of lysine at position 214 (Asp1 numbering: K224) interacts with the 5β phosphate of 5-IP_7 which would explain the preference for this substrate over IP_6 (Wang et al., 2011). However, pyrophosphorylation of IP_6 by Asp1 kinase is possible when the natural substrate becomes scarce, which will occur when an increased amount of the kinase is present in the cell (Fig4 page 47).

4.1.2. Function of the Asp1 C-terminal pyrophosphatase domain

The function of the C-terminal domain of PPIP5Ks/Vip1 proteins has been a matter of debate for years. Several attempts failed to find a substrate which could be dephosphorylated by PPIP5Ks. A number of substrates were tested including different inositol polyphosphates and the generic substrate for acid phosphatases, *p*-nitrofenol, but none of them were dephosphorylated by PPIP5Ks (Choi et al., 2007; Gokhale et al., 2011)

Our group was the first one to demonstrate that the C-terminal domain of the Vip1 family member Asp1 was enzymatically active *in vitro* (Pohlmann et al., 2014). After that, a later publication, showed that *in vitro* PPIP5Ks/Vip1 C-terminal domain was extremely specific for the 1-diphosphate group of 1-IP_7 or 1,5-IP_8. The authors who previously had shown that PPIP5Ks were enzymatically inactive, argued that the PPIP5Ks constructs used before did not contain the necessary amino acids for phosphatase activity (Gokhale et al., 2011; Wang et al., 2015).

The data presented in this thesis, demonstrates that the *in vitro* results obtained by our group reflect the function of Asp1 *in vivo* (Pöhlmann et al., 2014). Furthermore, I have shown that the physiologically relevant substrate of the Asp1 pyrophosphatase domain is

IP_8 (Fig1). Levels of IP_8 were massively reduced in cells with higher-than-wild type Asp1 pyrophosphatase activity (Fig15 page 57). Accordingly, IP_8 was increased about two-fold in strains in which the Asp1 pyrophosphate function was abolished (Fig18 page 59). These results correlate with our previous *in vitro* observations in which the generation of pyrophosophates was increased two-fold by $Asp1^{H397A}$ (pyrophosphatase dead variant) in comparison to the wild type Asp1 protein (Pohlmann et al., 2014).

At the start of my study, exclusively non-enzymatic functions had been attributed to the C-terminal domain of PPIP5Ks/Vip1 proteins. A role in translocation to the plasma membrane was proposed for the human PPIP5K1 C-terminal domain (Gokhale et al., 2011). I did not observe membrane localization for *S. pombe* Asp1 or for Asp1 mutants under all conditions tested. Another publication showed that the PPIP5K2 C-terminal domain harboured a functional NLS sequence and the authors proposed that the function of C-terminal domain of PPIP5K2 was to generate a gradient of inositol pyrophosphates across the nuclear membrane (Yong et al., 2015). Yong and colleagues proposed that the NLS sequence of PPIP5K2 was present in a 63 amino acid sequence in the C-terminal domain (Yong et al., 2015). Sequence alignment revealed that such a sequence was not present in Asp1. However, a temperature-dependent nuclear localization was observed for Asp1 variants tagged with GFP (Fig36 page 76).

Two Asp1 variants show an altered cellular localization; $Asp1^{1-364}$-GFP and $Asp1^{D333A}$-GFP (Fig37 page 77). These variants show the same intracellular localization pattern associated with the mitochondria network (Fig37 page). They failed to accumulate in the nucleus at lower temperatures as has been observed for the other Asp1 variants. (Fig 37 and Fig39 page 78). Interestingly, growth of $asp1^{1-364}$ strain is reduced at 20ºC in comparison to the wild-type which shows an accumulation of Asp1-GFP in the nucleus at the same temperature (Fig38 page). This data suggests that, under specific conditions a nuclear accumulation of Asp1 is required, likely to create a local concentration of IP_8, as it has been observed for other inositol phosphate kinases (Brehm et al., 2007; Nalaskowski et al., 2011). Nuclear translocation of Asp1 depends on the function of another protein, Hpm1 (Patrick Fischbach master thesis, 2016). Hpm1 interacts with the kinase domain of Asp1 (Visnja Jakopec, unpublished results). These data demonstrates that the cellular localization of Asp1 is regulated by a number of mechanisms. Subcellular Asp1 localization relies on the complex interplay of (i) the C-terminal pyrophosphatase domain, (ii) the interaction between the kinase domain and Hpm1 (iii) the ability to generate IP_8.

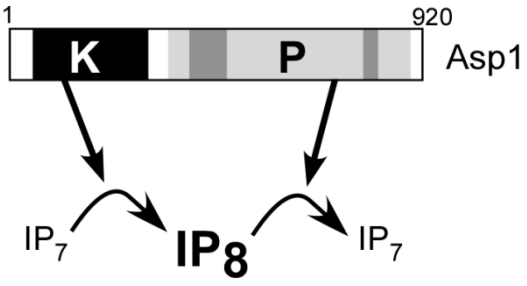

Fig1. Asp1 bifunctional activity *in vivo*. The N-terminal kinase domain of Asp1 (black box) synthesizes IP_8 from IP_7, while the C-terminal pyrophosphatase domain (light grey box) uses IP_8 as a substrate to generate IP_7 in a cyclic reaction.

4.1.3. Comparison of the phosphatase signature motifs of Asp1 pyrophosphatase and members of the histidine acid phosphatase family

Although Asp1 does not have the complete signature of histidine acid phosphatases it has pyrophosphatase activity. To date, only the crystal structure of the N-terminal kinase domain has been obtained (Wang et al., 2011). There is no crystal structure of the C-terminal domain from any of the members of the PPIP5Ks/Vip1 family, which makes it difficult to understand the catalytic mechanism.

Residues within the first conserved motif (RHxxR, positions 396-400 of the Asp1 protein) are essential for the pyrophosphatase activity (Fig8 page 50). These amino acids are completely conserved in all members of the histidine acid superfamily (Rigden, 2008) indicating that the enzymatic mechanism of Asp1 (and thus Vip1 family members) and histidine acid phosphatase share similarities. The disparity appears in the second conserved motif (HI, position 807-808 of the Asp1 protein). Histidine 807 is required but not essential for Asp1 pyrophosphatase activity. This histidine is conserved in members of the histidine acid superfamily and is essential for enzymatic function (Rigden, 2008). There is only one further example in the literature where mutation of this histidine did not abolish phosphatase activity; the rat 6-phosphofructo-2-kinase/fructose-2,6-bisphosphatase where a mutation of the corresponding histidine causes a 12% reduction of phosphatase activity (Mizuguchi et al., 1999). In other members of the histidine acid phosphatase family, the role of this histidineis to stabilize the phosphate group (Rigden, 2008). It is possible that in Asp1 another amino acid can substitute for this function.

Regarding the role of isoleucine 808 which is essential for Asp1 pyrophosphatase activity, there are some other examples of histidine acid phosphatase family members which seem to function without the proton donor. These include the *Escherichia coli* dPGM (di-phosphoglycerate mutase) (Fothergill-Gilmore and Watson, 1989) and the rat and human multiple inositol polyphosphate phosphatase (Caffrey et al., 1999). It is unclear if these proteins use a different proton donor placed at another position or if they do not require proton donation (Rigden, 2008).

Interestingly isoleucine 808 of Asp1 is essential and cannot be changed to an amino acid found at that position in other Vip1 proteins (FigS4). These results suggest that the catalytic mechanism of Asp1 pyrophosphatase activity differs from that of the histidine acid phosphatases.

4.2. Synthesis pathway of inositol pyrophosphates in *S. pombe*

Although the kinases that synthesize inositol polyphosphates are very specific, formally only unspecific phosphatases had been described to be involved in the hydrolysis of these molecules (Fisher et al., 2002; Lonetti et al., 2011; Safrany et al., 1998). This changed with the finding of Siw14. *S. cerevisiae* Siw14 is a pyrophosphatase with positional specificity towards the 5-diphosphate group of 5-IP_7 *in vitro* and *in vivo* (Steidle et al., 2016). Equivalent to what is observed in *SIW14Δ* mutants in which levels of IP_7 are increased, *asp1* pyrophosphatase dead mutants show an increase of IP_8 levels (Fig18 page 59) (Steidle et al., 2016). Hence, the discovery that *S. pombe* Asp1 has pyrophosphatase activity towards 1,5-IP_8 *in vivo* gives strength to the idea that specific pyrophosphatases as specific regulators of certain inositol pyrophosphates levels exist. My results not only support the model which proposes that the primary pathway to synthesize IP_8 occurs through the addition of a diphosphate group at position 1 of the 5-IP_7 by PPIP5Ks/Vip1 kinases (Choi et al., 2007), but also bring valuable new data to understand the catabolism of inositol pyrophosphates.

4.3. Regulatory mechanism of Asp1 bifunctional activity

The only member of the histidine acid phosphatase superfamily which shows a bifunctional activity is the enzyme involved in glycolysis: 6-phosphofructo-2-kinase/fructose-2,6-bisphosphatase. In mammals, there are four isoforms of this enzyme and two of them, the liver isoform and the heart isoform, have been shown to regulate their kinase/phosphatase functions via phosphorylation in different ways. Phosphorylation of the liver isoenzyme results in up-regulation of the phosphate activity, while phosphorylation of the heart isoenzyme up-regulates its kinase activity. (Rider et al., 2004). A phosphoproteome analysis of *S. pombe* identified 4 putative Asp1 phosphorylation sites (Wilson-Grady et al., 2008). However, our *in vivo* read-out of inositol pyrophosphate generation by wild-type Asp1 and the potential Asp1 phosphomutants did not show any differences (FigS5) (Pascal Ramrath master thesis, 2012).Thus it is at unlikely that phosphorylation regulates the two Asp1 enzymatic activities.

Other regulatory mechanisms could control Asp1 enzymatic activities. Binding to an iron-sulfur cluster inhibits Asp1 pyrophosphatase activity *in vitro* (Wang et al., 2015) Assembly of iron-sulfur clusters starts in the mitochondria and finishes in the cytoplasm where iron-sulfur clusters are inserted into apoproteins via the CIA complex (cytosolic iron-sulfur protein assembly) (Netz et al., 2014). Interestingly, the Met10 protein is an iron-sulfur-containing-protein of the CIA complex (Stehling et al., 2012). However in our *in vitro* analysis Met10 could inhibit Asp1 pyrophosphatase function in the absence of iron-sulfur clusters. (Fig21 page 62).

In vivo, under the experimental condition used, absence of *met10*$^{+}$ did not significantly change the inositol polyphosphates profile in comparison to that of the wild-type strain (Fig23 page 63). A possible reason for that could be the mitochondrial localization of Met10. Asp1 is ubiquitously present in whole cytoplasm and Met10 might only affect the Asp1 pool that is proximal to the mitochondrial network. Considering the hypothesis that a local concentration of inositol pyrophosphates would be necessary to compete with the more abundant IP_6 due to structural similarities (Burton et al., 2009), it would not be surprising that a local inhibition of Asp1 pyrophosphatase activity close the mitochondria exists. In that scenario the local concentration of IP_8 would increase raising the possibilities for IP_8 over IP_6 to bind the target molecule/s (Fig2)

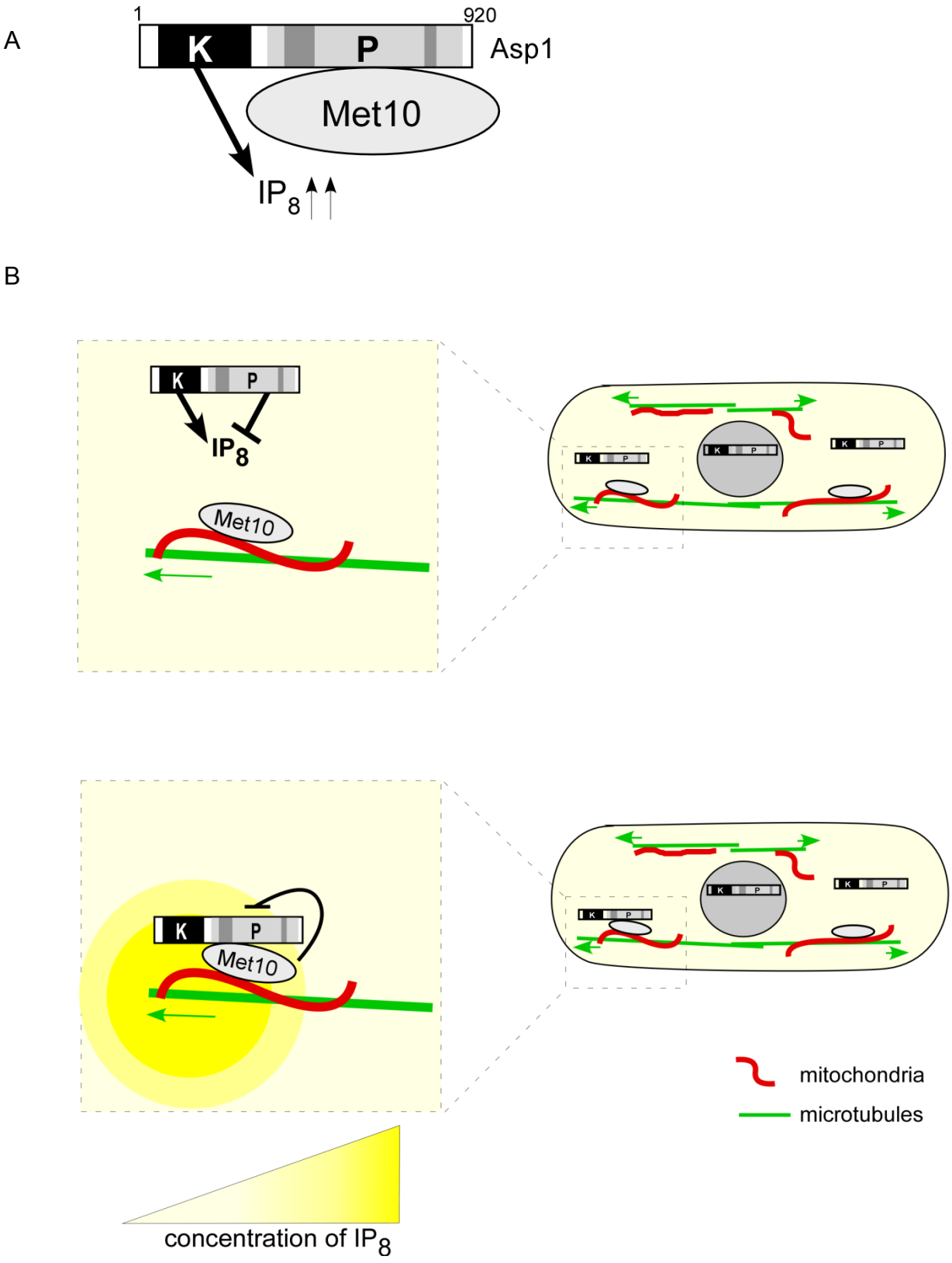

Fig2. Model for the regulatory mechanism of Asp1 bifunctional activity. A) Asp1 pyrophosphatase activity is inhibited by Met10, increasing the IP_8 output of the Asp1 kinase domain. B) A subset of cellular Asp1 molecules localizes proximal to the mitochondrial network where Met10 is localized. Upon contact, Met10 inhibits Asp1 pyrophosphatase activity and thus, local levels of IP_8 increase which can then modulate the microtubule cytoskeleton

4.4. Biological functions of Asp1

Alteration of inositol pyrophosphates leads to pleiotropic effects as these molecules are involved in several biological processes. My work presents new data to elucidate how these signalling molecules regulate polarized growth and, importantly has uncovered two new cellular processes in *S. pombe* in which inositol pyrophosphates play an important role. These are mitochondrial distribution and phosphate homeostasis.

4.4.1. Role in polarized growth

With the aim to understand how Asp1-generated inositol pyrophosphates regulate polarized growth, I focussed on the distribution of the polarity factor Tea1 and the microtubule cytoskeleton behaviour in cells with non-physiological levels of $IP_{8.}$

Tea1 modulates the microtubule cytoskeleton and it is necessary for the recruitment and retention of other polarity factors at the cell ends (Behrens and Nurse, 2002). However, different amounts of Tea1 at the cell ends did not affect the microtubule dynamics between the growing and the non-growing end in *asp1*^{D333A} cells (Fig31 page 71). Why then is Tea1 predominantly accumulated at the non-growing end? Other polarity mutants, such as *tea4Δ* cells, show an accumulation of Tea1 at the non-growing end that does not correlate with defective microtubule transport (Martin et al., 2005). Polarity factors do not only have to accumulate at the cell tips, they must be distributed into different specific clusters to ensure proper establishment of cell polarity (Dodgson et al., 2013). Interestingly, in invasively growing *S. pombe* cells, and during shmoo development i.e a mating projection, Tea1 is also enriched at the non-growing tip (Dodgson et al., 2010). Thus, proper transport, distribution and specific reorganization of Tea1 seems to be a requirement for bipolar yeast growth. Asp1 function does not only affect the pausing time of microtubules at the cell ends but also several interphase microtubule dynamics parameters (Pöhlmann et al., 2014). Furthermore, in absence of the +TIP protein, Mal3 (EB1), Asp1 can still modulate the microtubule (Pohlmann et al., 2014). Thus, Asp1 function might control microtubule cytoskeleton through mechanisms independent of Mal3.

4.4.2. Asp1 function at the mitochondria-microtubule interface?

S. pombe has tubular mitochondria that are transported and distributed by the microtubule cytoskeleton (Li et al., 2015). Therefore, as Asp1 kinase function is required for the microtubule cytoskeleton stability (Pöhlmann et al., 2014; Topolski et al., 2016), the abnormal mitochondria distribution phenotype observed in *asp1Δ* and *asp1*^{D333A} strains could

be explained by the higher microtubule instability (Fig32 and 33 page 73). The lower abnormal mitochondrial distribution in *asp1*^{H397A} cells in comparison with the wild-type suggests that, as the microtubule stability does, proper mitochondrial distribution correlates with cellular IP_8 levels (Fig32 and 33 page 73). Thus, abnormal distribution of mitochondria seems to be a consequence of altered microtubule dynamics caused by Asp1. Proper distribution of mitochondria by microtubules requires the function of Mmb1 (Fu et al., 2011). The relation between this protein and Asp1 is unclear, however, the gene products of *mmb1*$^{+}$ and *asp1*$^{+}$ might be involved in parallel pathways (Fig34 page 74). It is important to note that Mmb1 decreases microtubule dynamics and increases microtubule stability, a similar phenotype to that observed in *asp1*^{H397A} cells (Fu et al., 2011; Pohlmann et al., 2014).

4.4.3. Asp1 function is linked to phosphate homeostasis

Finally, my finding of a direct correlation between IP_8 levels and intracellular polyP levels has uncovered a new function for inositol pyrophosphates in phosphate homeostasis in *S. pombe.* This correlation is in contrast to what has been found for *S. cerevisiae*. In this yeast a *VIP1* deletion strain does not show altered polyP levels, while a deletion of the other inositol polyphosphate kinase, *KCS1* abolishes polyP accumulation (Lonetti et al., 2011). Among *ascomycetes*, the components of the PHO pathway are often not conserved (Tomar and Sinha, 2014). However, similar phosphate-response phenotypes have been observed in *S. pombe* and *S. cerevisiae* when, independently, genes involved either in inositol pyrophosphate metabolism or polyphosphate metabolism are deleted (Henry et al., 2011). This suggests that inositol pyrophosphates play equivalent roles in phosphate homeostasis in both yeasts. However, my results indicate that these roles might be organism-specific since, different to IP_7 in *S. cerevisiae*, in *S. pombe* is IP_8 which plays a major role in modulating phosphate metabolism.

PolyP is present in all organisms where it is required for a wide variety of functions (reviewed in (Silva et al., 2017). In addition to buffering phosphate, other functions have been attributed to this molecule. For instance, in *Trypanosoma brucei*, polyP is involved in cytokinesis and virulence (Fang et al., 2007; Lander et al., 2013). In human platelets, polyP is secreted to enhance blood clotting (Morrissey et al., 2012). In *S. cereveisiae*, polyP levels fluctuate during the cell cycle, being reduced prior to M phase and increased after mitosis (Neef and Kladde, 2003). Interestingly, inositol pyrophosphates have been shown to modulate cell cycle progression in *S.cerevisiae* (Banfic et al., 2013) and act in parallel with the TORC1 pathway to regulate the response to stress (Worley et al., 2013). I could show that fine-tuning of Asp1-generated inositol pyrophosphates is essential to coordinate growth with the cell cycle (Fig44 page 84) Thus, it is possible that cell-cycle specific fluctuations of

Asp1-generated inositol pyrophosphates exists and that they might control intracellular polyP levels in response to cell cycle clues and extrinsic signals such as the phosphate starvation response.

5. Appendix

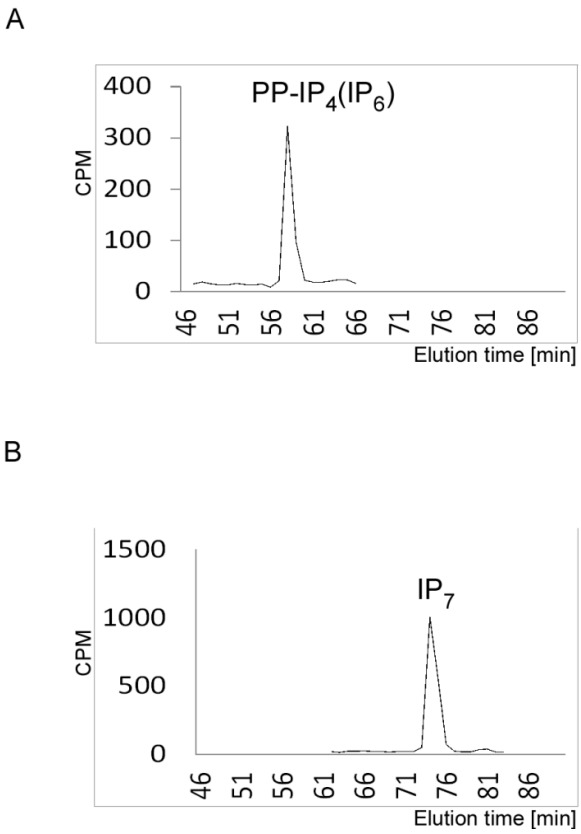

FigS1. Elution profiles of IPPs standards. A)Elution profile of (^{3}H)PP-IP$_4$ standard. B)Elution profile of (^{3}H)IP$_7$ standard. Figure and figure legend modified from (Pascual-Ortiz et al, 2017 submitted manuscript).

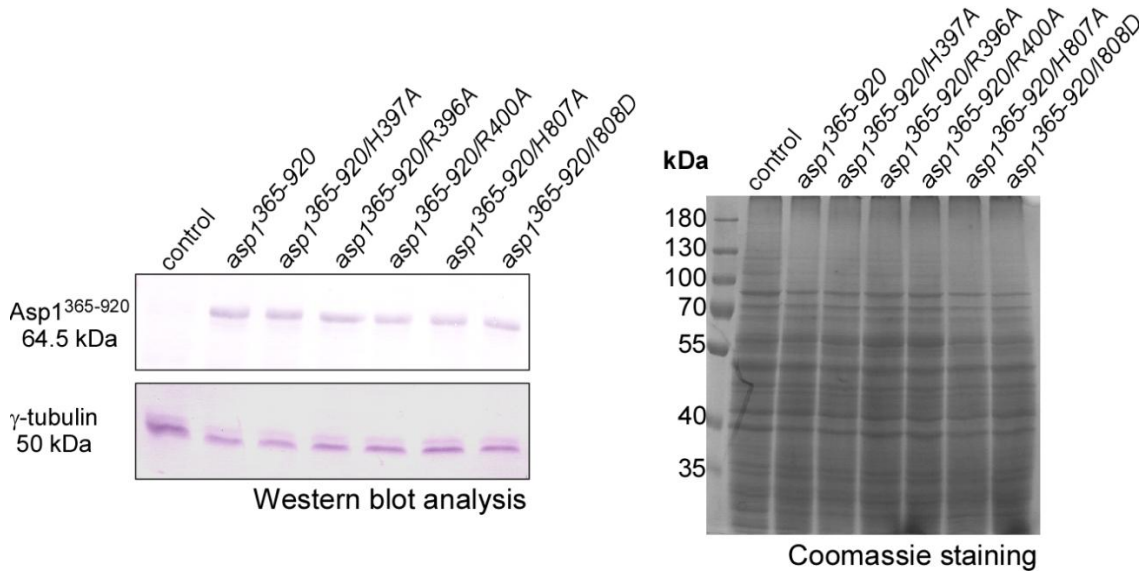

FigS2. Western blot analysis of Asp1 C-terminal variants using an Asp1 antibody (Feoktistova, McCollum et al. 1999). Transformants were grown in thiamine-less media. γ-Tubulin protein was used as an internal control. Figure and figure legend modified from (Pascual-Ortiz et al, 2017 submitted manuscript).

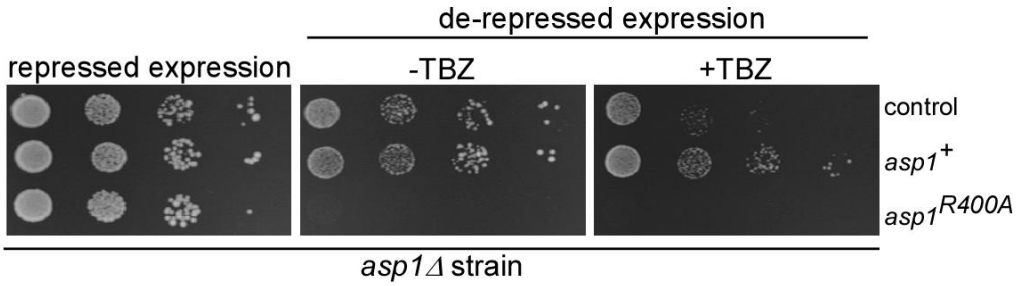

FigS3. Plasmid-borne expression of *asp1*^{R400A} leads to cell lysis. Serial dilution patch test (10^4 to 10^1cells) of an *asp1Δ* strain transformed with vector (control) or plasmids expressing *asp1*$^+$ or *asp1*^{R400A} from the *nmt1*$^+$ promoter. Transformants were grown under plasmid selective conditions in absence or presence of thiamine and with or without 7 µg/ ml TBZ at 25°C for 7 days. Figure and figure legend modified from (Pascual-Ortiz et al, 2017 submitted manuscript).

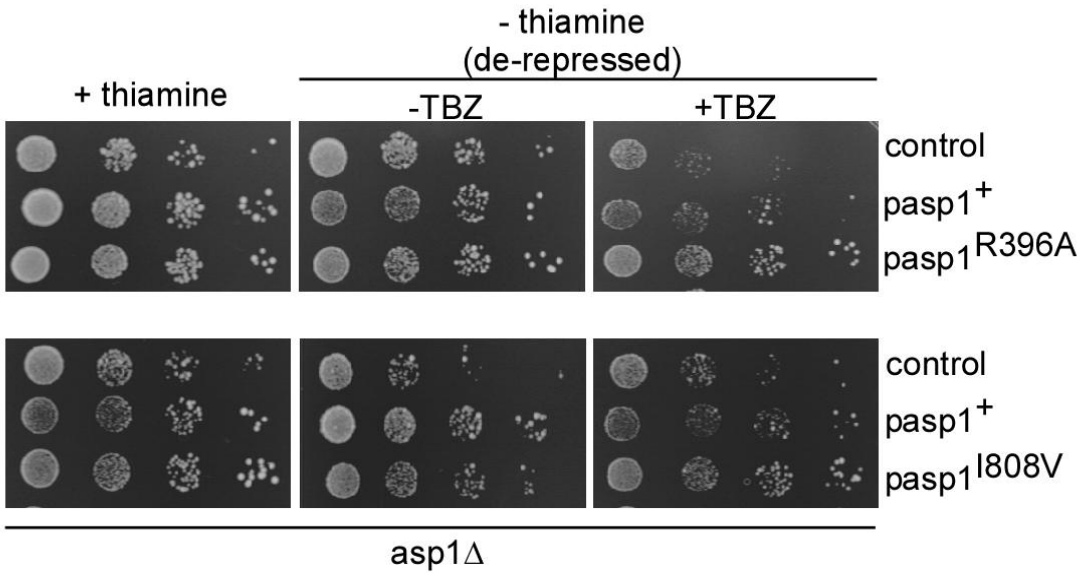

FigS4. Expression of Asp1 variants in the asp1Δ strain. Serial dilution patch tests (10^4 to 10^1cells) of the *asp1Δ* strain transformed with vector (control), *asp1*$^+$, *asp1*^{R396A}, and *asp1*^{I808V} from the thiamine-repressible promoter *nmt1*$^+$. Transformants were grown under plasmid selective conditions at 25°C for 7 days.

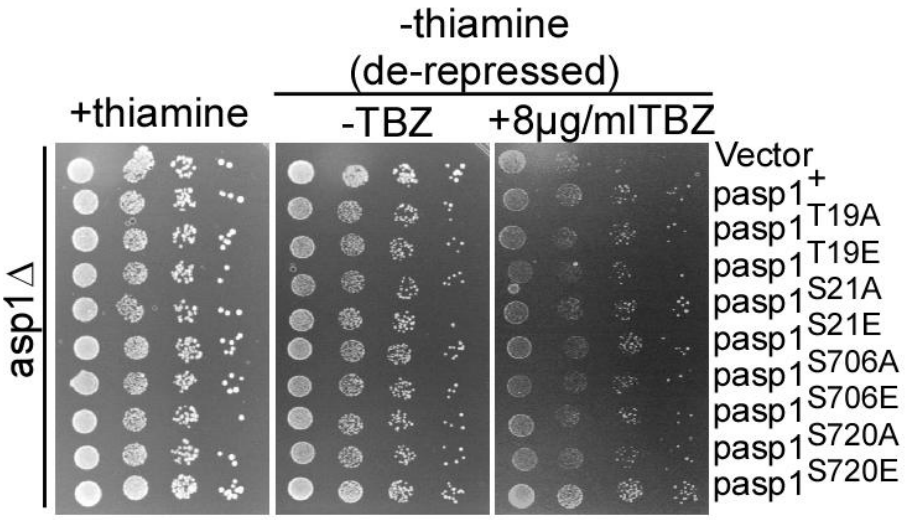

FigS5. Analysis of mapped Asp1 phosphorylation sites concerning Asp1 function. Serial dilution patch tests (10^4 to 10^1cells) of the *asp1Δ* strain transformed with vector (control), *asp1*$^{+}$, *asp1*^{T19A}, *asp1*^{T19E}, *asp1*^{S21A}, *asp1*^{S21E}, *asp1*^{S706A}, *asp1*^{S706E}, *asp1*^{S720A} or *asp1*^{S720E} from the thiamine-repressible promoter nmt1^{+}. Transformants were grown under plasmid selective conditions at 25°C for 8 days.

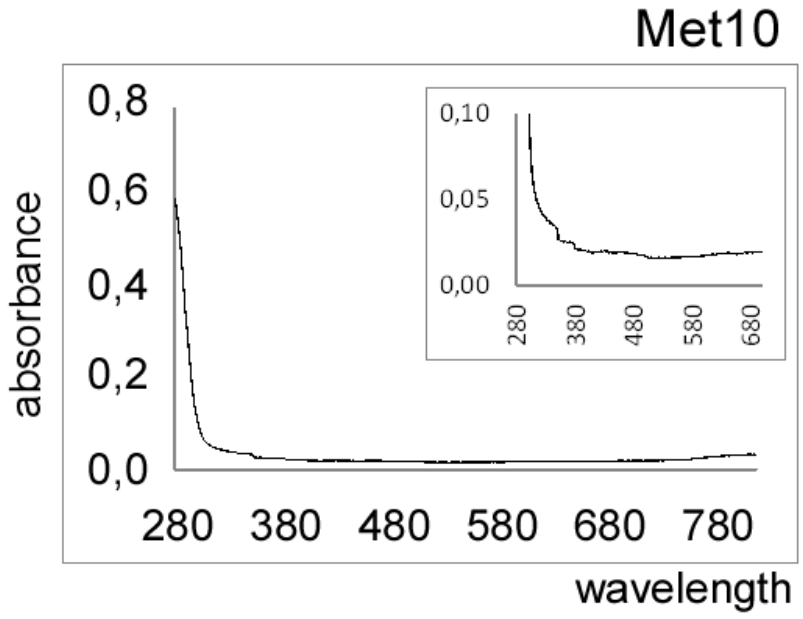

FigS6. Determination of possible iron-sulfur clusters in Asp1$^{365\text{-}920}$ variants. UV–visible absorption spectra of recombinant Met10 is shown. ~1 µg/µl protein concentration used.

6. List of figures

Introduction

Results

Discussion

7. Bibliographical references

Auesukaree, C., Tochio, H., Shirakawa, M., Kaneko, Y., and Harashima, S. (2005). Plc1p, Arg82p, and Kcs1p, enzymes involved in inositol pyrophosphate synthesis, are essential for phosphate regulation and polyphosphate accumulation in Saccharomyces cerevisiae. J Biol Chem *280*, 25127-25133.

Azevedo, C., Burton, A., Ruiz-Mateos, E., Marsh, M., and Saiardi, A. (2009). Inositol pyrophosphate mediated pyrophosphorylation of AP3B1 regulates HIV-1 Gag release. Proc Natl Acad Sci U S A *106*, 21161-21166.

Azevedo, C., and Saiardi, A. (2006). Extraction and analysis of soluble inositol polyphosphates from yeast. Nat Protoc *1*, 2416-2422.

Azevedo, C., and Saiardi, A. (2017). Eukaryotic Phosphate Homeostasis: The Inositol Pyrophosphate Perspective. Trends Biochem Sci *42*, 219-231.

Banfic, H., Bedalov, A., York, J.D., and Visnjic, D. (2013). Inositol pyrophosphates modulate S phase progression after pheromone-induced arrest in Saccharomyces cerevisiae. J Biol Chem *288*, 1717-1725.

Bedinger, P.A., Hardeman, K.J., and Loukides, C.A. (1994). Travelling in style: the cell biology of pollen. Trends Cell Biol *4*, 132-138.

Behrens, R., and Nurse, P. (2002). Roles of fission yeast tea1p in the localization of polarity factors and in organizing the microtubular cytoskeleton. J Cell Biol *157*, 783-793.

Beinhauer, J.D., Hagan, I.M., Hegemann, J.H., and Fleig, U. (1997). Mal3, the fission yeast homologue of the human APC-interacting protein EB-1 is required for microtubule integrity and the maintenance of cell form. J Cell Biol *139*, 717-728.

Bennett, M., Onnebo, S.M., Azevedo, C., and Saiardi, A. (2006). Inositol pyrophosphates: metabolism and signaling. Cell Mol Life Sci *63*, 552-564.

Berridge, M.J. (1993). Inositol trisphosphate and calcium signalling. Nature *361*, 315-325.

Bhandari, R., Juluri, K.R., Resnick, A.C., and Snyder, S.H. (2008). Gene deletion of inositol hexakisphosphate kinase 1 reveals inositol pyrophosphate regulation of insulin secretion, growth, and spermiogenesis. Proc Natl Acad Sci U S A *105*, 2349-2353.

Bhandari, R., Saiardi, A., Ahmadibeni, Y., Snowman, A.M., Resnick, A.C., Kristiansen, T.Z., Molina, H., Pandey, A., Werner, J.K., Jr., Juluri, K.R., *et al.* (2007). Protein pyrophosphorylation by inositol pyrophosphates is a posttranslational event. Proc Natl Acad Sci U S A *104*, 15305-15310.

Birnboim, H.C., and Doly, J. (1979). A rapid alkaline extraction procedure for screening recombinant plasmid DNA. Nucleic Acids Res *7*, 1513-1523.

Brehm, M.A., Schenk, T.M., Zhou, X., Fanick, W., Lin, H., Windhorst, S., Nalaskowski, M.M., Kobras, M., Shears, S.B., and Mayr, G.W. (2007). Intracellular localization of human Ins(1,3,4,5,6)P5 2-kinase. Biochem J *408*, 335-345.

Browning, H., Hayles, J., Mata, J., Aveline, L., Nurse, P., and McIntosh, J.R. (2000). Tea2p Is a Kinesin-like Protein Required to Generate Polarized Growth in Fission Yeast. J Cell Biol *151*, 15-28.

Brunner, D., and Nurse, P. (2000). CLIP170-like tip1p spatially organizes microtubular dynamics in fission yeast. Cell *102*, 695-704.

Burton, A., Hu, X., and Saiardi, A. (2009). Are inositol pyrophosphates signalling molecules? J Cell Physiol *220*, 8-15.

Caffrey, J.J., Hidaka, K., Matsuda, M., Hirata, M., and Shears, S.B. (1999). The human and rat forms of multiple inositol polyphosphate phosphatase: functional homology with a histidine acid phosphatase up-regulated during endochondral ossification. FEBS Lett *442*, 99-104.

Coradini, D., Casarsa, C., and Oriana, S. (2011). Epithelial cell polarity and tumorigenesis: new perspectives for cancer detection and treatment. Acta Pharmacol Sin *32*, 552-564.

Chakraborty, A., Koldobskiy, M.A., Bello, N.T., Maxwell, M., Potter, J.J., Juluri, K.R., Maag, D., Kim, S., Huang, A.S., Dailey, M.J.*, et al.* (2010). Inositol pyrophosphates inhibit Akt signaling, thereby regulating insulin sensitivity and weight gain. Cell *143*, 897-910.

Chanduri, M., Rai, A., Malla, A.B., Wu, M., Fiedler, D., Mallik, R., and Bhandari, R. (2016). Inositol hexakisphosphate kinase 1 (IP6K1) activity is required for cytoplasmic dynein-driven transport. Biochem J *473*, 3031-3047.

Choi, J.H., Williams, J., Cho, J., Falck, J.R., and Shears, S.B. (2007). Purification, sequencing, and molecular identification of a mammalian PP-InsP5 kinase that is activated when cells are exposed to hyperosmotic stress. J Biol Chem *282*, 30763-30775.

da Silva, J.S., and Dotti, C.G. (2002). Breaking the neuronal sphere: regulation of the actin cytoskeleton in neuritogenesis. Nat Rev Neurosci *3*, 694-704.

Dent, E.W., Gupton, S.L., and Gertler, F.B. (2011). The growth cone cytoskeleton in axon outgrowth and guidance. Cold Spring Harb Perspect Biol *3*.

Dodgson, J., Brown, W., Rosa, C.A., and Armstrong, J. (2010). Reorganization of the growth pattern of Schizosaccharomyces pombe in invasive filament formation. Eukaryot Cell *9*, 1788-1797.

Dodgson, J., Chessel, A., Yamamoto, M., Vaggi, F., Cox, S., Rosten, E., Albrecht, D., Geymonat, M., Csikasz-Nagy, A., Sato, M.*, et al.* (2013). Spatial segregation of polarity factors into distinct cortical clusters is required for cell polarity control. Nat Commun *4*, 1834.

Draskovic, P., Saiardi, A., Bhandari, R., Burton, A., Ilc, G., Kovacevic, M., Snyder, S.H., and Podobnik, M. (2008). Inositol hexakisphosphate kinase products contain diphosphate and triphosphate groups. Chem Biol *15*, 274-286.

Drummond, D.R., and Cross, R.A. (2000). Dynamics of interphase microtubules in Schizosaccharomyces pombe. Current Biology *10*, 766-775.

Europe-Finner, G.N., Gammon, B., and Newell, P.C. (1991). Accumulation of [3H]-inositol into inositol polyphosphates during development of Dictyostelium. Biochem Biophys Res Commun *181*, 191-196.

Fang, J., Rohloff, P., Miranda, K., and Docampo, R. (2007). Ablation of a small transmembrane protein of Trypanosoma brucei (TbVTC1) involved in the synthesis of polyphosphate alters acidocalcisome biogenesis and function, and leads to a cytokinesis defect. Biochem J *407*, 161-170.

Fawaz, M.V., Topper, M.E., and Firestine, S.M. (2011). The ATP-grasp enzymes. Bioorg Chem *39*, 185-191.

Fennessy, D., Grallert, A., Krapp, A., Cokoja, A., Bridge, A.J., Petersen, J., Patel, A., Tallada, V.A., Boke, E., Hodgson, B.*, et al.* (2014). Extending the Schizosaccharomyces pombe molecular genetic toolbox. PLoS One *9*, e97683.

Feoktistova, A., McCollum, D., Ohi, R., and Gould, K.L. (1999). Identification and characterization of Schizosaccharomyces pombe asp1(+), a gene that interacts with mutations in the Arp2/3 complex and actin. Genetics *152*, 895-908.

Fernandez, S., Homann, M.J., Henry, S.A., and Carman, G.M. (1986). Metabolism of the phospholipid precursor inositol and its relationship to growth and viability in the natural auxotroph Schizosaccharomyces pombe. J Bacteriol *166*, 779-786.

Fischer, R., Zekert, N., and Takeshita, N. (2008). Polarized growth in fungi--interplay between the cytoskeleton, positional markers and membrane domains. Mol Microbiol *68*, 813-826.

Fisher, D.I., Safrany, S.T., Strike, P., McLennan, A.G., and Cartwright, J.L. (2002). Nudix hydrolases that degrade dinucleoside and diphosphoinositol polyphosphates also have 5-phosphoribosyl 1-pyrophosphate (PRPP) pyrophosphatase activity that generates the glycolytic activator ribose 1,5-bisphosphate. J Biol Chem *277*, 47313-47317.

Fothergill-Gilmore, L.A., and Watson, H.C. (1989). The phosphoglycerate mutases. Adv Enzymol Relat Areas Mol Biol *62*, 227-313.

Fridy, P.C., Otto, J.C., Dollins, D.E., and York, J.D. (2007). Cloning and characterization of two human VIP1-like inositol hexakisphosphate and diphosphoinositol pentakisphosphate kinases. J Biol Chem *282*, 30754-30762.

Fu, C., Jain, D., Costa, J., Velve-Casquillas, G., and Tran, P.T. (2011). mmb1p binds mitochondria to dynamic microtubules. Curr Biol *21*, 1431-1439.

Gerasimaite, R., Pavlovic, I., Capolicchio, S., Hofer, A., Schmidt, A., Jessen, H.J., and Mayer, A. (2017). Inositol Pyrophosphate Specificity of the SPX-Dependent Polyphosphate Polymerase VTC. ACS Chem Biol *12*, 648-653.

Gietz R.D., W.R.A. (2006). Yeast Transformation by the LiAc/SS Carrier DNA/PEG Method. In Methods in Molecular Biology 313: Yeast Protocols, 2nd edition

W. Xiao, ed. (Totowa, New Jersey: Humana Press), pp. p. 107-120.

Gokhale, N.A., Zaremba, A., and Shears, S.B. (2011). Receptor-dependent compartmentalization of PPIP5K1, a kinase with a cryptic polyphosphoinositide binding domain. Biochem J *434*, 415-426.

Gu, C., Nguyen, H.N., Hofer, A., Jessen, H.J., Dai, X., Wang, H., and Shears, S.B. (2017). The Significance of the Bifunctional Kinase/Phosphatase Activities of Diphosphoinositol Pentakisphosphate Kinases (PPIP5Ks) for Coupling Inositol Pyrophosphate Cell Signaling to Cellular Phosphate Homeostasis. J Biol Chem *292*, 4544-4555.

Gu, C., Wilson, M.S., Jessen, H.J., Saiardi, A., and Shears, S.B. (2016). Inositol Pyrophosphate Profiling of Two HCT116 Cell Lines Uncovers Variation in InsP8 Levels. PLoS One *11*, e0165286.

Henry, T.C., Power, J.E., Kerwin, C.L., Mohammed, A., Weissman, J.S., Cameron, D.M., and Wykoff, D.D. (2011). Systematic screen of Schizosaccharomyces pombe deletion collection uncovers parallel evolution of the phosphate signal transduction pathway in yeasts. Eukaryot Cell *10*, 198-206.

Hoffman, C.S., and Winston, F. (1987). A ten-minute DNA preparation from yeast efficiently releases autonomous plasmids for transformation of Escherichia coli. Gene *57*, 267-272.

Hothorn, M., Neumann, H., Lenherr, E.D., Wehner, M., Rybin, V., Hassa, P.O., Uttenweiler, A., Reinhardt, M., Schmidt, A., Seiler, J.*, et al.* (2009). Catalytic core of a membrane-associated eukaryotic polyphosphate polymerase. Science *324*, 513-516.

Jakopec, V., Walla, E., and Fleig, U. (2011). Versatile use of Schizosaccharomyces pombe plasmids in Saccharomyces cerevisiae. FEMS Yeast Res *11*, 653-655.

Kokkoris, K., Gallo Castro, D., and Martin, S.G. (2014). The Tea4-PP1 landmark promotes local growth by dual Cdc42 GEF recruitment and GAP exclusion. J Cell Sci *127*, 2005-2016.

Kornberg, A., Rao, N.N., and Ault-Riche, D. (1999). Inorganic polyphosphate: a molecule of many functions. Annu Rev Biochem *68*, 89-125.

Laha, D., Johnen, P., Azevedo, C., Dynowski, M., Weiss, M., Capolicchio, S., Mao, H., Iven, T., Steenbergen, M., Freyer, M.*, et al.* (2015). VIH2 Regulates the Synthesis of Inositol Pyrophosphate InsP8 and Jasmonate-Dependent Defenses in Arabidopsis. Plant Cell *27*, 1082-1097.

Lander, N., Ulrich, P.N., and Docampo, R. (2013). Trypanosoma brucei vacuolar transporter chaperone 4 (TbVtc4) is an acidocalcisome polyphosphate kinase required for in vivo infection. J Biol Chem *288*, 34205-34216.

Laussmann, T., Eujen, R., Weisshuhn, C.M., Thiel, U., and Vogel, G. (1996). Structures of diphospho-myo-inositol pentakisphosphate and bisdiphospho-myo-inositol tetrakisphosphate from Dictyostelium resolved by NMR analysis. Biochem J *315 (Pt 3)*, 715-720.

Lee, Y.S., Huang, K., Quiocho, F.A., and O'Shea, E.K. (2008). Molecular basis of cyclin-CDK-CKI regulation by reversible binding of an inositol pyrophosphate. Nat Chem Biol *4*, 25-32.

Lee, Y.S., Mulugu, S., York, J.D., and O'Shea, E.K. (2007). Regulation of a cyclin-CDK-CDK inhibitor complex by inositol pyrophosphates. Science *316*, 109-112.

Lev, S., Li, C., Desmarini, D., Saiardi, A., Fewings, N.L., Schibeci, S.D., Sharma, R., Sorrell, T.C., and Djordjevic, J.T. (2015). Fungal Inositol Pyrophosphate IP7 Is Crucial for Metabolic Adaptation to the Host Environment and Pathogenicity. MBio *6*, e00531-00515.

Li, T., Zheng, F., Cheung, M., Wang, F., and Fu, C. (2015). Fission yeast mitochondria are distributed by dynamic microtubules in a motor-independent manner. Sci Rep *5*, 11023.

Lin, H., Fridy, P.C., Ribeiro, A.A., Choi, J.H., Barma, D.K., Vogel, G., Falck, J.R., Shears, S.B., York, J.D., and Mayr, G.W. (2009). Structural analysis and detection of biological inositol pyrophosphates reveal that the family of VIP/diphosphoinositol pentakisphosphate kinases are 1/3-kinases. J Biol Chem *284*, 1863-1872.

Lonetti, A., Szijgyarto, Z., Bosch, D., Loss, O., Azevedo, C., and Saiardi, A. (2011). Identification of an evolutionarily conserved family of inorganic polyphosphate endopolyphosphatases. J Biol Chem *286*, 31966-31974.

Losito, O., Szijgyarto, Z., Resnick, A.C., and Saiardi, A. (2009). Inositol pyrophosphates and their unique metabolic complexity: analysis by gel electrophoresis. PLoS One *4*, e5580.

Loss, O., Azevedo, C., Szijgyarto, Z., Bosch, D., and Saiardi, A. (2011). Preparation of quality inositol pyrophosphates. J Vis Exp, e3027.

Luo, H.R., Huang, Y.E., Chen, J.C., Saiardi, A., Iijima, M., Ye, K., Huang, Y., Nagata, E., Devreotes, P., and Snyder, S.H. (2003). Inositol pyrophosphates mediate chemotaxis in Dictyostelium via pleckstrin homology domain-PtdIns(3,4,5)P3 interactions. Cell *114*, 559-572.

Luo, H.R., Saiardi, A., Yu, H., Nagata, E., Ye, K., and Snyder, S.H. (2002). Inositol pyrophosphates are required for DNA hyperrecombination in protein kinase c1 mutant yeast. Biochemistry *41*, 2509-2515.

Maniatis, T., Fritsch, E.F., and Sambrook, J. (1989). "Molecular cloning. A laboratory manual." (Cold Spring Harbor, New York: Cold Spring Habor Laboratory Press).

Marks, J., Hagan, I.M., and Hyams, J.S. (1986). Growth polarity and cytokinesis in fission yeast: the role of the cytoskeleton. J Cell Sci Suppl *5*, 229-241.

Martin, S.G. (2009). Microtubule-dependent cell morphogenesis in the fission yeast. Trends Cell Biol *19*, 447-454.

Martin, S.G., McDonald, W.H., Yates, J.R., 3rd, and Chang, F. (2005). Tea4p links microtubule plus ends with the formin for3p in the establishment of cell polarity. Dev Cell *8*, 479-491.

Martin, S.G., Rincon, S.A., Basu, R., Perez, P., and Chang, F. (2007). Regulation of the formin for3p by cdc42p and bud6p. Mol Biol Cell *18*, 4155-4167.

Mata, J., and Nurse, P. (1997). tea1 and the microtubular cytoskeleton are important for generating global spatial order within the fission yeast cell. Cell *89*, 939-949.

Menniti, F.S., Miller, R.N., Putney, J.W., Jr., and Shears, S.B. (1993). Turnover of inositol polyphosphate pyrophosphates in pancreatoma cells. J Biol Chem *268*, 3850-3856.

Menoyo, S., Ricco, N., Bru, S., Hernandez-Ortega, S., Escote, X., Aldea, M., and Clotet, J. (2013). Phosphate-activated cyclin-dependent kinase stabilizes G1 cyclin to trigger cell cycle entry. Mol Cell Biol *33*, 1273-1284.

Mitchison, J.M., and Nurse, P. (1985). Growth in cell length in the fission yeast Schizosaccharomyces pombe. J Cell Sci *75*, 357-376.

Mizuguchi, H., Cook, P.F., Tai, C.H., Hasemann, C.A., and Uyeda, K. (1999). Reaction mechanism of fructose-2,6-bisphosphatase. A mutation of nucleophilic catalyst, histidine 256, induces an alteration in the reaction pathway. J Biol Chem *274*, 2166-2175.

Morrissey, J.H., Choi, S.H., and Smith, S.A. (2012). Polyphosphate: an ancient molecule that links platelets, coagulation, and inflammation. Blood *119*, 5972-5979.

Mulugu, S., Bai, W., Fridy, P.C., Bastidas, R.J., Otto, J.C., Dollins, D.E., Haystead, T.A., Ribeiro, A.A., and York, J.D. (2007). A conserved family of enzymes that phosphorylate inositol hexakisphosphate. Science *316*, 106-109.

Nalaskowski, M.M., Fliegert, R., Ernst, O., Brehm, M.A., Fanick, W., Windhorst, S., Lin, H., Giehler, S., Hein, J., Lin, Y.N.*, et al.* (2011). Human inositol 1,4,5-trisphosphate 3-kinase isoform B (IP3KB) is a nucleocytoplasmic shuttling protein specifically enriched at cortical actin filaments and at invaginations of the nuclear envelope. J Biol Chem *286*, 4500-4510.

Neef, D.W., and Kladde, M.P. (2003). Polyphosphate loss promotes SNF/SWI- and Gcn5-dependent mitotic induction of PHO5. Mol Cell Biol *23*, 3788-3797.

Netz, D.J., Mascarenhas, J., Stehling, O., Pierik, A.J., and Lill, R. (2014). Maturation of cytosolic and nuclear iron-sulfur proteins. Trends Cell Biol *24*, 303-312.

O'Neill, E.M., Kaffman, A., Jolly, E.R., and O'Shea, E.K. (1996). Regulation of PHO4 nuclear localization by the PHO80-PHO85 cyclin-CDK complex. Science *271*, 209-212.

Odom, A.R., Stahlberg, A., Wente, S.R., and York, J.D. (2000). A role for nuclear inositol 1,4,5-trisphosphate kinase in transcriptional control. Science *287*, 2026-2029.

Okamoto, K., and Shaw, J.M. (2005). Mitochondrial morphology and dynamics in yeast and multicellular eukaryotes. Annu Rev Genet *39*, 503-536.

Okazaki, K., Okazaki, N., Kume, K., Jinno, S., Tanaka, K., and Okayama, H. (1990). High-frequency transformation method and library transducing vectors for cloning mammalian cDNAs by trans-complementation of Schizosaccharomyces pombe. Nucleic Acids Res *18*, 6485-6489.

Onnebo, S.M., and Saiardi, A. (2009). Inositol pyrophosphates modulate hydrogen peroxide signalling. Biochem J *423*, 109-118.

Pesesse, X., Choi, K., Zhang, T., and Shears, S.B. (2004). Signaling by higher inositol polyphosphates. Synthesis of bisdiphosphoinositol tetrakisphosphate ("InsP8") is selectively activated by hyperosmotic stress. J Biol Chem *279*, 43378-43381.

Pohlmann, J., and Fleig, U. (2010). Asp1, a conserved 1/3 inositol polyphosphate kinase, regulates the dimorphic switch in Schizosaccharomyces pombe. Mol Cell Biol *30*, 4535-4547.

Pohlmann, J., Risse, C., Seidel, C., Pohlmann, T., Jakopec, V., Walla, E., Ramrath, P., Takeshita, N., Baumann, S., Feldbrugge, M.*, et al.* (2014). The Vip1 inositol polyphosphate kinase family regulates polarized growth and modulates the microtubule cytoskeleton in fungi. PLoS Genet *10*, e1004586.

Pulloor, N.K., Nair, S., Kostic, A.D., Bist, P., Weaver, J.D., Riley, A.M., Tyagi, R., Uchil, P.D., York, J.D., Snyder, S.H.*, et al.* (2014). Human genome-wide RNAi screen identifies an essential role for inositol pyrophosphates in Type-I interferon response. PLoS Pathog *10*, e1003981.

Rider, M.H., Bertrand, L., Vertommen, D., Michels, P.A., Rousseau, G.G., and Hue, L. (2004). 6-phosphofructo-2-kinase/fructose-2,6-bisphosphatase: head-to-head with a bifunctional enzyme that controls glycolysis. Biochem J *381*, 561-579.

Ridgway, G.J., and Douglas, H.C. (1958). Unbalanced growth of yeast due to inositol deficiency. J Bacteriol *76*, 163-166.

Rigden, D.J. (2008). The histidine phosphatase superfamily: structure and function. Biochem J *409*, 333-348.

Safrany, S.T., Caffrey, J.J., Yang, X., Bembenek, M.E., Moyer, M.B., Burkhart, W.A., and Shears, S.B. (1998). A novel context for the 'MutT' module, a guardian of cell integrity, in a diphosphoinositol polyphosphate phosphohydrolase. Embo J *17*, 6599-6607.

Saiardi, A., Bhandari, R., Resnick, A.C., Snowman, A.M., and Snyder, S.H. (2004). Phosphorylation of proteins by inositol pyrophosphates. Science *306*, 2101-2105.

Saiardi, A., Erdjument-Bromage, H., Snowman, A.M., Tempst, P., and Snyder, S.H. (1999). Synthesis of diphosphoinositol pentakisphosphate by a newly identified family of higher inositol polyphosphate kinases. Curr Biol *9*, 1323-1326.

Saiardi, A., Nagata, E., Luo, H.R., Sawa, A., Luo, X., Snowman, A.M., and Snyder, S.H. (2001). Mammalian inositol polyphosphate multikinase synthesizes inositol 1,4,5-trisphosphate and an inositol pyrophosphate. Proc Natl Acad Sci U S A *98*, 2306-2311.

Saiardi, A., Resnick, A.C., Snowman, A.M., Wendland, B., and Snyder, S.H. (2005). Inositol pyrophosphates regulate cell death and telomere length through phosphoinositide 3-kinase-related protein kinases. Proc Natl Acad Sci U S A *102*, 1911-1914.

Sethuraman, A., Rao, N.N., and Kornberg, A. (2001). The endopolyphosphatase gene: essential in Saccharomyces cerevisiae. Proc Natl Acad Sci U S A *98*, 8542-8547.

Silva, R.C., Liebel, S., de Oliveira, H.H., Ramsdorf, W.A., Garcia, J.R., Azevedo, S.M., Magalhaes, V.F., Oliveira Ribeiro, C.A., and Filipak Neto, F. (2017). Cylindrospermopsin effects on cell viability and redox milieu of Neotropical fish Hoplias malabaricus hepatocytes. Fish Physiol Biochem.

Snaith, H.A., Samejima, I., and Sawin, K.E. (2005). Multistep and multimode cortical anchoring of tea1p at cell tips in fission yeast. Embo J *24*, 3690-3699.

Snaith, H.A., and Sawin, K.E. (2003). Fission yeast mod5p regulates polarized growth through anchoring of tea1p at cell tips. Nature *423*, 647-651.

Stehling, O., Vashisht, A.A., Mascarenhas, J., Jonsson, Z.O., Sharma, T., Netz, D.J., Pierik, A.J., Wohlschlegel, J.A., and Lill, R. (2012). MMS19 assembles iron-sulfur proteins required for DNA metabolism and genomic integrity. Science *337*, 195-199.

Steidle, E.A., Chong, L.S., Wu, M., Crooke, E., Fiedler, D., Resnick, A.C., and Rolfes, R.J. (2016). A Novel Inositol Pyrophosphate Phosphatase in Saccharomyces cerevisiae: Siw14 PROTEIN SELECTIVELY CLEAVES THE beta-PHOSPHATE FROM 5-DIPHOSPHOINOSITOL PENTAKISPHOSPHATE (5PP-IP5). J Biol Chem *291*, 6772-6783.

Tanaka, K., and Okayama, H. (2000). A pcl-like cyclin activates the Res2p-Cdc10p cell cycle "start" transcriptional factor complex in fission yeast. Mol Biol Cell *11*, 2845-2862.

Thota, S.G., Unnikannan, C.P., Thampatty, S.R., Manorama, R., and Bhandari, R. (2015). Inositol pyrophosphates regulate RNA polymerase I-mediated rRNA transcription in Saccharomyces cerevisiae. Biochem J *466*, 105-114.

Tomar, P., and Sinha, H. (2014). Conservation of PHO pathway in ascomycetes and the role of Pho84. J Biosci *39*, 525-536.

Topolski, B., Jakopec, V., Kunzel, N.A., and Fleig, U. (2016). Inositol Pyrophosphate Kinase Asp1 Modulates Chromosome Segregation Fidelity and Spindle Function in Schizosaccharomyces pombe. Mol Cell Biol *36*, 3128-3140.

van Meer, G., Voelker, D.R., and Feigenson, G.W. (2008). Membrane lipids: where they are and how they behave. Nat Rev Mol Cell Biol *9*, 112-124.

Van Veldhoven, P.P., and Mannaerts, G.P. (1987). Inorganic and organic phosphate measurements in the nanomolar range. Anal Biochem *161*, 45-48.

Vollmeister, E., Schipper, K., Baumann, S., Haag, C., Pohlmann, T., Stock, J., and Feldbrugge, M. (2012). Fungal development of the plant pathogen Ustilago maydis. FEMS Microbiol Rev *36*, 59-77.

Wang, H., Falck, J.R., Hall, T.M., and Shears, S.B. (2011). Structural basis for an inositol pyrophosphate kinase surmounting phosphate crowding. Nat Chem Biol *8*, 111-116.

Wang, H., Nair, V.S., Holland, A.A., Capolicchio, S., Jessen, H.J., Johnson, M.K., and Shears, S.B. (2015). Asp1 from Schizosaccharomyces pombe binds a [2Fe-2S](2+) cluster which inhibits inositol pyrophosphate 1-phosphatase activity. Biochemistry *54*, 6462-6474.

Wilson-Grady, J.T., Villen, J., and Gygi, S.P. (2008). Phosphoproteome analysis of fission yeast. J Proteome Res *7*, 1088-1097.

Worley, J., Luo, X., and Capaldi, A.P. (2013). Inositol pyrophosphates regulate cell growth and the environmental stress response by activating the HDAC Rpd3L. Cell Rep *3*, 1476-1482.

Wu, M., Chong, L.S., Perlman, D.H., Resnick, A.C., and Fiedler, D. (2016). Inositol polyphosphates intersect with signaling and metabolic networks via two distinct mechanisms. Proc Natl Acad Sci U S A *113*, E6757-E6765.

Wurst, H., Shiba, T., and Kornberg, A. (1995). The gene for a major exopolyphosphatase of Saccharomyces cerevisiae. J Bacteriol *177*, 898-906.

Yong, S.T., Nguyen, H.N., Choi, J.H., Bortner, C.D., Williams, J., Pulloor, N.K., Krishnan, M.N., and Shears, S.B. (2015). Identification of a functional nuclear translocation sequence in hPPIP5K2. BMC Cell Biol *16*, 17.

York, J.D., Odom, A.R., Murphy, R., Ives, E.B., and Wente, S.R. (1999). A phospholipase C-dependent inositol polyphosphate kinase pathway required for efficient messenger RNA export. Science *285*, 96-100.

York, S.J., Armbruster, B.N., Greenwell, P., Petes, T.D., and York, J.D. (2005). Inositol diphosphate signaling regulates telomere length. J Biol Chem *280*, 4264-4269.

8. Articles under review

Some of the results described in this thesis are part of the following submitted manuscripts:

Marina Pascual-Ortiz, Eva Walla, Adolfo Saiardi, Visnja Jakopec, Ingrid Span, Natascha Künzel, Anand Vangala and Ursula Fleig. The *Schizosaccharomyces pombe* PPIP5Ks/Vip1 pyrophosphatase domain regulates cellular inositol pyrophosphate levels. (PLOS Genetics, July 2017)

Marina Pascual-Ortiz, Eva Walla, Adolfo Saiardi, Visnja Jakopec, Ingrid Span, Natascha Künzel, Anand Vangala and Ursula Fleig. Asp1 bi-functional activity modulates spindle function via controlling cellular inositol pyrophosphate levels in *Schizosaccharomyces pombe*. (Molecular and Cellular Biology, November 2017)

9. Acknowledgements

There are many people I want to thank after these four years...

In first place, Prof. Dr. Fleig. Ursula, I have learned a lot from you during my time in the lab. Thanks for your enthusiasm during our discussions, your advice and patience and, I didn't forget, thanks for giving me a second chance when I needed it, and a third, a fourth... I think I lost count!

I want to thank my co-supervisor Prof. Dr. Michael Feldbrügge for the advice and comments during the seminars and Prof. Dr. Johannes Hegemann, for the always helpful input. Furthermore I want to thank Dr. Ingrid Span and Prof. Dr. Adolfo Saiardi for their help and contribution to this project.

All people from the Hegemann lab. Old and new members, thanks for the kindness, help and advice and also all the fun during barbecues and Christmas parties! Special thanks to Corinna, the master student and a good friend who also became my life-coach in the last months! And, of course, to my Alison, although you abandoned me at the end.., I forgive you because I can't even imagine how infinitely difficult this would have been without you. Grazie mille amiga!

Eva, thanks for your hard work, your help with the project and your support in this last crazy year and Visnja, your advice and understanding have been very important to me, thanks for all the challenges you helped me to beat and all our late talks!

Caro, Quynh, Mamina... thanks for this injection of energy that your arrival brought. I am so happy that I met you! Also, the new promises! Melanie, Anna-Lisa and Anna-Lene. Although for a short time, it has been a pleasure to work with all of you.

Special thanks to Anand, my bench-mate, I will miss our endless philosophical conversations but mostly, our crazy dinners at your flat! And to Natascha, it is very difficult to choose among thousand reasons. I will only mention your immense generosity from the first moment we met, for being always there for me and for this friendship that, I am sure, will get past many more crisis! Get ready.

A todos lo que han estado peleando conmigo desde la distancia, en especial a mis dos guerreros favoritos, siempre apoyándome y confiando en mí ¡aún cuando ni siquiera yo sabía muy bien lo que hacía! Papá y mamá, ya no quedan más aeropuertos. Os quiero muchísimo.

Ana y Alicia, siempre en primera línea de batalla. Nada de esto habría sido posible sin vosotras. Gracias por enseñarme todo lo que sé y por hacerme sentir capaz de todo, sin importar el obstáculo. Aunque no lo sepáis, cada paso que doy, lo doy para parecerme más a vosotras.

Gracias a mi yaya Mayte, la mejor yaya del mundo, por cuidarme y quererme tanto y por todos y cada uno de tus abrazos, que encierran más sabiduría que mil tesis doctorales. A Markel, por recibirme siempre como si no hubiera pasado el tiempo, por ser tan valiente y haber cuidado de todos mientras yo no estaba. Te quiero pitufo.

También a mis amigas, Sandra, MJ, Aida y Patry. Por ese primer empujón, por echarme de menos tanto como yo a vosotras y por todas las noches de risas que me hacían olvidar todo y recordar lo bueno que es estar en casa.

A Fran, ni siquiera sé por dónde empezar, podría escribir mil renglones y nunca agradecerte todo lo que has hecho por mí. Gracias por hacer que todo fuera fácil, o que al menos lo pareciera. Por no haber tirado la toalla, ni permitir que yo lo hiciera. Por creer en mí, en nosotros y en todo lo que nos espera. Te quiero.

10. Statutory Declaration

I declare under oath that I have compiled my dissertation independently and without any undue assistance by third parties under consideration of the 'Principles for the Safeguarding of Good Scientific Practice at Heinrich Heine University Düsseldorf'.
I declare that I have not used sources or means without declaration in the text. All the passages taken from other works in the wording or in the meaning have been clearly indicated with sources. This thesis has not been used in the same or similar version to achieve an academic grading or is being published elsewhere.

Düsseldorf, 03.10.2017

Marina Pascual Ortiz